An Experimental Investigation of Human/Bicycle Dynamics and Rider Skill in Children and Adults

by

Stephen Matthew Cain

A dissertation submitted in partial fulfillment
of the requirements for the degree of
Doctor of Philosophy
(Biomedical Engineering)
in the University of Michigan
2013

Doctoral Committee:

Professor Noel C. Perkins, Chair
Research Professor James A. Ashton-Miller
Professor Karl Grosh
Professor Dale A. Ulrich

DEDICATION

To my parents, who in so many ways have inspired and supported me

and

In memory of my friend, Pablo

ACKNOWLEDGEMENTS

I could not have completed the work herein without the help, friendship, mentorship, and love of many. My journey to this point has been a great experience, thanks mainly to the people that I have had the opportunity to interact with along the way. It was incredibly difficult to write these acknowledgements because it is so difficult to communicate just exactly what I am thankful for and how much and I have appreciated everything when I am limited by words and space. I hope that the words I have written sufficiently express my gratitude. I am sure I forgot someone, so if that person is you I hope I get a chance to thank you in person.

First I thank my advisor, Professor Noel Perkins, who in so many ways made my dissertation work possible. From the beginning, you encouraged me to be the driving force behind the research and provided me with the resources and support to accomplish everything I aimed to complete. As a result, I can truly call the work I completed my own. You also taught me, by example, what it means to be a good advisor, professor, and colleague. You are an extraordinary person and I am thankful to have the opportunity to work with you.

I had amazing committee members who helped significantly improve the quality of my work. Professor James Ashton-Miller: Thank you for the use of your lab and the resources needed to complete the work in Chapter 5, the many discussions that helped to

improve the quality of my work, your kind words at the defense, and the post-defense advice—I look forward to our future interactions. Professor Dale Ulrich: Thank you for giving me the opportunity to collect data during the bicycle camps—I learned so much from watching and working with the children. Moreover, thank you for your non-engineering perspective and your careful review of my work. Professor Karl Grosh: Thanks for your careful review of my work, your interest in my work, your feedback, and your positive attitude—I have enjoyed working with you.

Thank you to all the subjects that made the studies possible—it was a pleasure working with all of you.

Thank you to *Lose the Training Wheels* for providing access to the adapted bicycles and training program and the National Institute on Disability and Rehabilitation Research for a grant to Professor Dale Ulrich that made the work in Chapter 4 possible.

Thank you to the National Science Foundation's Graduate Research Fellowship Program, the Department of Mechanical Engineering, the School of Kinesiology, and the Department of Biomedical Engineering for supporting my research and education with fellowships and teaching appointments.

I have had some amazing lab mates throughout the completion of my dissertation work. Kevin King: Thanks for getting me started in the lab and thanks for the friendship. Ryan McGinnis and Andrew Hirsh: Thank you for your friendship and many research and non-research conversations.

Leah Ketcheson, Janet Hauck, Andy Pitchford, and Vince Irully Jeong: Thank you for accommodating me at the bicycle camps and making me feel welcome as part of your research team. Leah, Janet, and Andy: Thanks for tracking down subject details.

Thanks to Nicholas Groeneweg and Aliaksandra Kapshai for helping me get started collecting data in the Biomechanics Research Laboratory.

Thank you to the bicycle and motorcycle research community: Arend Schwab, Jodi Kooijman, Jason Moore, Luke Peterson, Mont Hubbard, Andrew Dressel, Matteo Massaro, Adrian Cooke, and Anthony Doyle. It has been so wonderful to interact with everyone. Your kindness and friendship has made working in this field incredibly enjoyable and rewarding; our conversations and your feedback have greatly influenced and improved the quality of my work.

I appreciate the time I spent working in the Human Neuromechanics Laboratory, under the direction of Professor Daniel Ferris. During that time, I had meaningful scientific interactions with many people (especially during the weekly neuromechanics meetings) that helped shape me as a scientist. I also formed many important friendships. Keith Gordon: Thank you for getting me started in the lab and for your mentorship through the years—I'll never forget many of your jokes. Greg Sawicki: Thanks for being a great office mate, friend, and mentor. You helped me become more social and have really helped me expand my scientific network. Antoinette Domingo: Thanks for your friendship, all the nights of watching television, and for trusting me to take care of Cherry (especially during one special afternoon in the summer of 2008!). Monica Daley: Your

friendship and mentorship was incredibly important to me—you were a large part of helping me establish my scientific confidence.

Rachael Schmedlen: I am thankful I had the opportunity to work with you—I appreciate your friendship and the support along the way.

The excellent staff at the University of Michigan made many tasks significantly more enjoyable. Specifically, I'd like to thank Kelly Chantelois and Maria Steele: Your consistent friendly demeanor, smiling faces, and seemingly always happy moods brightened my day many times.

Jeffrey and Denise Turck, *Dexter Bike and Sport*: Thanks for providing some of the essential parts for my experimental setups and thank you for the opportunity to work at the shop. Thanks for the friendship and for providing me something important along my journey.

Professor Stephen Piazza: I am glad I had the opportunity to work with you and look forward to talking with you at future meetings. The advice and insights you have given me at various times along my journey have been priceless.

Thank you to all my friends—you made Ann Arbor my home and helped ensure that I stayed balanced. To those that have moved away—you've created many places around the country that I now feel welcome. I cannot list everyone, but I would specifically like to thank Nick Boswell, Mike Bartlett, Neal Blatt, Sean Murphy, Kris Potzmann, Annie Mathias, Joaquin Anguera, Christine Walsh, and Mr. and Mrs. Bartlett. Nick, Mike, Neal, and Sean: Thanks for making it easy to take a break from science and always being up for a ride, a beer, or just hanging out—I could write on and on but I would rather thank you

in person. Kris: Thanks for the good times and great skiing. Annie: Your friendship has been invaluable throughout my entire journey—thanks for always being there. Joaquin and Christine: Thanks for the advice and the place to stay in San Francisco in 2009—I have enjoyed watching your relationship grow. Mr. and Mrs. Bartlett: Thank you for making me part of your family and thanks for all the great times up north.

Jen and Dan: I am glad you are part of my family—I can't ask for a better sister-in-law and brother-in-law; it is comforting knowing that that you care a lot about me.

To my sister, Emily: Thank you for your love and inspiration. I am so glad you are my sister and I look forward to future hootenannies with you.

To my brother, Greg: Thanks for being my best friend and making sure I take time to get into the mountains. I am sure we will have many more trips and adventures together.

To my parents (Mum and Dad): It is impossible to communicate how much I appreciate what you have done for me in only a short paragraph. You gave me an amazing childhood and helped me get the tools that I needed to start this journey. I appreciate all the sacrifices you made through the years. I am most thankful for all the time we got to (and still get to) spend together—you truly shaped who I am today. You have always given the support I needed to succeed, and as a result, I never question whether or not you are proud of me—I clearly know you are proud of me.

To my love, Melissa: I am so lucky to have met you. You help make me a better person and bring so much happiness into my life. I am not sure I would have completed this journey without your love. I look forward to a sharing a lifetime with you.

TABLE OF CONTENTS

LIST OF FIGURES

LIST OF TABLES

ABSTRACT

An Experimental Investigation of Human/Bicycle Dynamics and Rider Skill in Children and Adults

by Stephen Matthew Cain

Chair: Noel C. Perkins

While humans have been riding bicycles for nearly 200 years, the dynamics of how exactly they achieve this are not well understood. The overall goals of this dissertation were to identify the major control strategies that humans use to balance and steer bicycles, as well as to identify performance metrics that reliably distinguish rider skill level. To achieve these goals, we introduced: a) a novel instrumented bicycle to measure rider control inputs and bicycle response outputs, b) an experimental design and analytical approach for tracking and quantifying rider learning, and c) an experimental design and analytical approaches to measure the dynamics of human/bicycle balance and quantify rider balance performance. We employed variations of the instrumented bicycle in three studies that focused on: 1) how adult riders control bicycle kinematics during steady-state turning, 2) the initial learning of steering and balance control as children learn to ride bicycles, and 3) the balance skill of adult expert and novice riders.

The findings from these studies advance our understanding of the types of control used by human riders, and simultaneously, quantify rider learning and skill. During steady-state turning, rider lean strongly influences steering torque, suggesting that rider lean plays an important role in bicycle control. Children learned to ride after successfully learning how to steer in the direction of bicycle roll, thereby increasing the correlation between steer and bicycle roll angular velocities (coefficient of determination increased from 0.22 to 0.75 during the learning process). In adults, the superior balance performance of skilled versus novice riders is revealed by highly correlated lateral positions of the center of pressure and center of mass (coefficients of determination of 0.97 versus 0.89, respectively). In achieving their superior balance performance, skilled riders employed more rider lean control, less steer control, and used less control effort than novice riders. We conclude that rider lean (i.e., any lateral movements of the rider) plays a dominant role in both steering and balancing a bicycle, and that achieving balance requires coordinating both steer and rider lean (the two rider control inputs) with bicycle roll (the bicycle response).

CHAPTER 1: MOTIVATION, LITERATURE REVIEW, AND RESEARCH OBJECTIVES

1.1 Motivation

Humans have ridden bicycles (two-wheeled, single track vehicles) since the early 1800's [1], yet human/bicycle dynamics are far from well understood. Recent work [2] has established the so-called Whipple bicycle model [3] as the simplest model of a bicycle that can predict the self-stability of an uncontrolled bicycle. By contrast, there is still little understanding of the fundamental characteristics of human riders, the types of control that humans use, and the skills that distinguish riders of different ability levels. Understanding rider learning and skill could help to improve programs that teach affected populations to ride, such as *Programs to Educate All Cyclists*[1] (PEAC) and *Lose the Training Wheels*[2] and provide a way to objectively measure whether a specific bicycle is better or worse for a particular rider.

1.2 Background

1.2.1 *Stability of an Uncontrolled Bicycle and the Whipple Model*

The dynamics of an uncontrolled bicycle, either without a rider or with a rigid but non-actuating rider, are well understood. The relatively recent work by Meijaard et al. [2] presents complete equations of motion for what is referred to as the Whipple bicycle model. The authors also present bicycle parameters that can be used for benchmarking

[1] www.bikeprogram.org
[2] www.losethetrainingwheels.org

and a thorough review of the bicycle dynamics literature, arguing that no prior journal publication in English presents complete and correct equations for the Whipple model. The Whipple bicycle model consists of four rigid bodies: a rear wheel, a rear frame with a rider rigidly attached to it, a front frame consisting of the front handlebar and fork assembly, and a front wheel. The model assumes that all bodies are laterally (left-right) symmetric and that the wheels have circular symmetry. Motion of the rider relative to the frame, structural compliance and damping, joint friction, and tire compliance and slip are neglected. Tire contacts with the ground are approximated by knife-edge rolling point-contacts. The model is described by seven generalized coordinates. As noted in [2], only three of the generalized coordinates are independent upon accounting for four non-holonomic rolling constraints. After linearizing the model about upright, straight-line motion and treating forward speed as a parameter, the model is reduced to two generalized coordinates; namely the steer angle and the lean (or roll) angle. The model successfully explains the observed self-stability of an uncontrolled bicycle (within a specific speed range) and the coupling between lean and steer.

Extensions of the Whipple model have been proposed to investigate added complexities for an uncontrolled bicycle. Meijaard and Schwab [4] expanded the Whipple model to include the effects of tire shape, a linear tire model, road gradient, and driving and braking torques. Sharp [5] investigated acceleration, finite cross-section tires, tires as force and moment generators, tire dynamics, frame compliance, and rider compliance. Peterson and Hubbard [6] and Schwab et al. [7], among others, added an additional degree of freedom to allow rider lean relative to the bicycle. Schwab and Kooijman [8] investigated the effects of coupling between the passive rider and the bicycle. All of these

additional effects lead to different open-loop dynamics—however, these differences are also relatively minor.

The Whipple bicycle model is useful for predicting the stability of real bicycles. Kooijman et al. demonstrated that the eigenvalues predicted by the Whipple model are in good agreement with the experimentally measured eigenvalues for a riderless bicycle both overground [9] and on a treadmill [10]. In [11], Kooijman et al. used the Whipple bicycle model to design a self-stable bicycle with no gyroscopic effects or trail (also known as caster [11]), which are two properties of typical bicycles that were thought to be essential for a bicycle to be self-stable. These studies demonstrate that the Whipple model is sufficient for understanding the stability and open-loop dynamics of bicycles.

Under the assumption that the open-loop dynamics of a bicycle relate to "rideability" or maneuverability of the bicycle, a number of studies investigated how changes in parameters affect bicycle stability. Moore and Hubbard [12] investigated the effects of front wheel diameter, steer axis tilt (or head tube angle), trail, and wheelbase on the range of stable speeds predicted by the Whipple model. Tak et al. [13] performed a sensitivity analysis on the range of stable speeds with respect to changes in all 25 bicycle parameters and found that head tube angle had the greatest effect on stability. Not surprisingly, real bicycles are not designed to be as stable as possible—they must also be easily maneuverable [14].

1.2.2 *Human Control of Bicycles*

Sheridan and Ferrell in their book about man-machine systems [15] state that "…the quality of performance of either the human or the machine component by itself does not

determine the quality of system performance." The quality of a bicycle cannot be determined from only looking at the bicycle's open loop dynamics. Throughout the history of the bicycle, humans have demonstrated that they are capable of successfully riding a wide range of bicycle designs, including bicycles that have no self-stability. In fact, early bicycles likely had very little self-stability, as they had vertical steering axes and little to no trail [1]. Researchers also set out to design bicycles with no self-stability [16] and bicycles that are "unrideable" [17, 18]; however, such bicycles have proven to be easily rideable [16, 17] or rideable after practice. In addition, even bicycles that are self-stable are only self-stable for a limited range of speeds; outside of the limited speed range the bicycles must be stabilized by human control. Therefore, understanding the human rider and the control that a rider uses are important for understanding bicycles and bicycle design.

Researchers have modeled human control of bicycles as a steering torque (applied by a rider through the handlebars) and a leaning torque (applied by a rider by leaning relative to the bicycle) [6, 7, 19]. These control inputs are similar to those considered in the study of motorcycles [20-22]. However, the ratio of rider mass to vehicle mass is much greater for a bicycle rider than for a motorcycle rider, which makes other and more subtle control possible. For example, experimental observations of human control reveal that human riders may use lateral knee movements and more complex upper body movements, especially at lower speeds [23, 24]. A number of studies have investigated automatic or robot control of a bicycle [25-29], and reveal that human-like control (steering angle and simulated rider lean) as well as control schemes not accessible to humans (gyroscopic stabilization) can successfully keep a bicycle upright. These studies highlight the fact that

a human rider (or robot rider) has many ways of controlling and balancing a bicycle—yet not all of these control movements are easy to model or measure.

As expected, a wide range of controllers successfully stabilize and steer bicycle models. These controllers include: steer-into-the-lean (intuitive) model [7], linear quadratic regulator [7], cross-over control model [30], optimal linear preview [19], among others [6, 31, 32]. However, the primary goal of these controllers has been to evaluate bicycle design. For example, Schwab et al. [7] investigate the gains that must be used by the controller; Sharp [19] quantifies the preview time necessary to achieve certain levels of performance with a given bicycle design; and, Hess et al. [30] quantify the handling qualities of bicycles using a handling qualities metric originally proposed for evaluating aircraft. However, none of these controllers were developed with the idea of investigating the performance of the human rider.

Researchers used various forms of system identification to solve for parameters of modeled controllers. Work by van Lunteren and Stassen [33] utilized a bicycle simulator instead of a real bicycle and revealed that controller parameters can be quite variable both for different trials with the same rider and between different riders. Preliminary work by Moore [34] demonstrates similar findings. Therefore, it is not clear how control parameters might be correlated with rider skill or performance.

1.2.3 *Assessing Rider Skill/Performance*

Bicycle riding skill or performance has previously been assessed by instructing subjects to ride around a prescribed course or to perform a prescribed task. In general, the time to complete a course/task and the number of errors committed are used to quantify

performance. In the majority of studies that use these techniques, the goal has been to evaluate the performance or safety of a particular bicycle or bicycle configuration [35-40]. In a study investigating the maneuverability of children's bicycles [40], Lewis noted that there was more variation between subjects than between the use of different bicycles. The time to complete a course and number of errors were used to investigate the correlation between physical and perceptual-motor abilities and riding performance [41, 42] and to evaluate the effect of alcohol consumption on the ability to safely ride a bicycle [43]. While quantifying performance by time to complete a course/task and the number of errors is useful for the questions posed in the previously mentioned studies, the results from these studies are task specific and do not translate to new tasks. In addition, the methods of quantifying performance do not allow continuous monitoring of skill because the methods rely on completion of specific courses/tasks. The methodology is also not useful if it is not possible for a rider to complete a task; for example, a child that has not yet learned to ride a bicycle would not be able to successfully ride around a course.

Some motorcycle research suggests that riders of different skill levels use different body lean relative to the motorcycle and steering torque. For example, Rice [44] found that riders of different skill levels phased body lean and steering torque differently when executing a lane change maneuver. Similarly, Prem [45] found that novice riders in an evasive maneuver used lean torque and steering torque differently from expert riders. Prem also used skill tests to differentiate rider ability, similar to the bicycle studies mentioned above. However, these studies also provide little insight on how to continuously monitor skill or motor learning for bicycle riders.

In the absence of quantitative tools to evaluate rider learning and rider skill, researchers and programs that teach children how to ride must resort to qualitative assessments. For example, the *Lose the Training Wheels*[3] program uses specially trained floor managers to observe riders who determine if the rider is learning. The floor manager observes the speed of pedaling, whether a rider leans into turns, relaxes his/her arms and uses the handlebars to turn and control the bicycle [46]. However, it is unclear how these qualitative assessments correlate to riding skill. A quantitative measure of skill would allow bicycle programs to monitor rider progress more effectively and potentially create better methods to teach bicycle riding.

1.2.4 ***Human Balance Skill***

The ability to balance the bicycle is necessary to successfully complete any riding task. Therefore, it seems logical to investigate possible ways to quantitatively evaluate the skill or ability of a rider to balance. Other fields of research have investigated human balancing skills and performance and these provide insight into how bicycle balancing skill could be quantified. Two such fields are human postural control and human walking.

1.2.4.1 Human standing balance

The tools used to evaluate human postural control are an essential part of both clinical evaluation of patients and research into how humans maintain upright posture. Some of the most basic methods used to evaluate human postural control involve monitoring the location of the center of pressure (COP) and the center of mass (COM) [47]. By using an ideal inverted pendulum model of standing balance, Winter [47] explains that the (COP-COM) signal is directly related to the horizontal acceleration of the COM and can be

[3] www.losethetrainingwheels.org

considered to be the error signal detected by the balance control system. The assumption is that the goal of the balance control system is to maintain an upright posture and to control postural sway. While it is assumed that human standing balance can be modeled effectively as an inverted pendulum, it is important to note that more complex balancing tasks cannot be explained by this simple approach and require a more complex model of the body [48]. Researchers have used COP measurements to investigate standing balance using a wide range of statistics, including: root mean square (RMS) distance from the mean COP [49, 50], excursions of the COP [51-53], COP sway amplitude [54], velocity of the COP [55, 56], and the area enclosed by the COP trajectory [55, 57], among others.

More advanced methods of quantifying balance performance have investigated the frequency content of the COP movement [56], the relationship of the COP to the COM movement [47], and the relationship of the COP and/or COM movement to muscle activation patterns [52, 58]. Researchers have also used system identification techniques to identify various transfer functions for standing balance [59, 60]. Depending on the experimental protocol, identified system parameters or attributes can be used to understand the controller or plant during standing balance [61, 62]. However, there is not yet a clear way to use these measures for diagnosing balance disorders [63, 64].

Basic quantitative measures of postural control identify at risk populations and differences in balance performance. Maki et al. [49] demonstrated that postural sway, as measured by COP displacement, is correlated with future falling risk. Prieto et al. [57] found that the mean velocity of the COP signals differences between healthy young and elderly adults and differences between eyes-open and eyes-closed standing balance conditions. Pellecchia [50] demonstrated that postural sway, as measured by movement

of the COP, increases when subjects performed difficult cognitive tasks. Jeka and Lackner [54] demonstrated that the addition of fingertip contact could reduce postural sway, as measured by movement of the COP. These studies represent a small sample of the extensive literature in the field of human postural control that utilize measures of body sway, usually movement of the COP, to quantify balance performance. As a result, these types of measures are utilized by clinicians to identify patients with balance disorders [47, 63, 65].

1.2.4.2 Human balance during walking

Similar to human postural control is the study of human balance during walking. Like standing balance, simple models have proven to be useful. Passive dynamic walking models suggest that the sagittal plane motion of walking is passively stable [66, 67], whereas the lateral motion is unstable [67]. Kuo [67] demonstrated through the use of a walking model that medial-lateral foot placement can effectively stabilize the lateral dynamics of passive walking models. When humans walk with reduced visual information the variability of medial-lateral foot placement increases [68], suggesting that this variation is related to decreased performance. Similarly, passive walking models suggest that wider step widths are more stable than narrow step widths [67], and therefore may also be useful for quantifying balance during walking. The work of Donelan et al. [69] demonstrated that providing external lateral stabilization to human subjects during walking resulted in decreased step width variability and narrower step width, which supports the idea that step width measurements can be useful for quantifying human balance during walking.

The basic methods of quantifying the lateral dynamics of human walking are useful for assessing balance during human walking. Variability of step width remains a good predictor of falling in the elderly [70-72] that can be used in a clinical setting. Applying external lateral stabilization to subjects with myelomeningocele allows them to walk with decreased step width and decreased medial-lateral motion of the COM [73]. Given the ability to quantify balance skill, researchers investigated the use of physical guidance and error augmentation to affect the motor learning of human subjects walking on a narrow beam [74, 75].

1.3 Relationship of bicycle riding to other human balancing tasks

Both standing and walking require maintaining a specific relationship between the center of mass of the body and the base of support. In static situations, the vertical projection of the center of mass should fall within the base of support. However for dynamic situations, this description is insufficient [76, 77]. In dynamic balancing tasks, both center of mass position and velocity must be considered to understand balance limits [76-78].

Riding a bicycle is similar to standing and walking in that it requires the human to maintain balance. Instead of maintaining the center of mass of the body within some margin of the base of support, a bicycle rider must maintain the center of mass of the bicycle/rider system within some limits of the base of support defined by the contact of the bicycle tires with the ground. Most likely these limits are a function of the bicycle speed and yaw rate, which are important for understanding the lateral acceleration and thus the roll angle of a single track vehicle [79]. As discussed in Sections 1.2.4.1 and 1.2.4.2, dynamic measurements such as the center of pressure position/velocity, center of mass position/velocity, and step width can be useful for evaluating stability or balance

performance during standing and walking tasks. Unlike standing and walking, it is unclear how dynamic measures of the bicycle/rider system might be related to stability or balance performance. Bicycle riding is also unlike standing and walking in that the rider must control more than just his/her body. In addition to applying joint torques to alter body posture (as in standing balance [48, 80]), a bicycle rider can also steer the bicycle to maintain balance. Analyses of rider motion reveal that riders use both lateral body movements and steering while riding [24], but it remains unclear which rider motions are essential for balance.

1.4 Research Objective and Specific Aims

Following the above review of human/bicycle dynamics and rider skill, the overall objectives of this dissertation are to: 1) understand how humans balance and steer bicycles, and 2) quantify the skill of human riders. To meet these objectives, the following specific aims are pursued:

1. Design and build an instrumented bicycle that is capable of measuring the primary human control inputs (steer torque and rider lean) and fundamental bicycle kinematics.
2. Investigate human/bicycle dynamics and control during steady-state turning using experimental and analytical approaches.
3. Quantify the changes that occur as learners transition from non-riders to riders.
4. Quantify the differences between skilled and novice riders when balancing a bicycle.

In Chapter 2 (specific aim 1) we describe and document the instrumented bicycle. In Chapter 3 (specific aim 2) we discuss our investigation of steady-state turning, in which we employ the instrumented bicycle to make experimental measurements and present a steady-state turning model to interpret our results. Specific aim 3 is addressed by Chapter 4, in which we describe results from our study that uses measured bicycle kinematics to quantify rider learning as novice riders with disabilities progress through a specialized bicycle camp. Differences between skilled and novice riders (specific aim 4) are quantified in Chapter 5.

CHAPTER 2: DEVELOPMENT OF AN INSTRUMENTED BICYCLE

2.1 Chapter Summary

In this chapter we describe the design of an instrumented bicycle. The instrumented bicycle is capable of measuring steering torque (the primary human control), bicycle speed, steering angle, acceleration of the bicycle frame, and angular velocity of the bicycle frame. Using the methodology discussed in Chapter 3 Section 3.3.2, it is possible to resolve the bicycle roll angle and the additional roll of the bicycle caused by rider lean relative to the bicycle frame for steady turning of a bicycle. As later discussed in Chapter 5, the instrumented bicycle can also be used to resolve the roll and yaw rates of the bicycle frame and to quantify the amount of work done by a rider to balance a bicycle. We begin this chapter with a brief review of other instrumented bicycles, and then describe the instrumentation and data acquisition system. The content of this chapter also appears in a published conference paper [81] and a published journal article [82].

2.2 Brief review of instrumented bicycles

Instrumented bicycles have been used to investigate the human control and dynamic behavior of bicycles. Roland [31] instrumented a bicycle to measure the rider lean angle and the steering angle, roll angle and speed of the bicycle in order to verify simulation results of a riderless bicycle and to analyze the steer and lean control used by a human rider. Jackson and Dragovan [83] instrumented a bicycle to measure the steering angle, speed and angular velocity of the bicycle during no-hands riding in conjunction with

simplified equations of motion to understand the torque applied to the front wheel by the ground reaction force and the gyroscopic moment. Cheng et al. [84] instrumented a bicycle to measure steering torque and confirm that larger torques are required to initiate turns with larger steering angles. Kooijman et al. [9] instrumented a riderless bicycle for angular rates, steering angle, and speed to validate a model of an uncontrolled bicycle at low speeds. More recently, Kooijman and Schwab [23] instrumented a bicycle for roll, yaw, and steering rates, steering angle, rear wheel speed, pedaling cadence as well as video capture of rider motion. They conclude that during normal cycling, most rider control is imparted through steering as opposed to upper body lean.

2.3 Description of the instrumented bicycle

An instrumented bicycle was constructed to measure the primary human control used by a human rider (steer torque) and the most relevant bicycle kinematics. In the following, we describe the bicycle, the sensors, the power supplies, and the data acquisition system.

2.3.1 *Bicycle*

The bicycle shown in Figure 2.1 is a standard geometry (steer axis tilt = 18.95 degrees, trail = 64 mm, wheel base = 1.060 m), rigid (unsuspended) mountain bike (1996 Schwinn Moab 3, size 19 inch frame) equipped with 660.4 mm x 49.5 mm (26 in x 1.95 in) slick tires (Tioga City Slicker 26 x 1.95, ETRTO 48-559). The wheel bearings were properly adjusted and the wheels were trued by a professional bicycle mechanic prior to testing. To accommodate the torque sensor, the stock fork was replaced with an aftermarket rigid (unsuspended) fork (Surly 1x1, 413 mm axle-to-crown length, 45 mm rake/offset).

Figure 2.1. The instrumented bicycle. The instrumented bicycle is a standard geometry mountain bike equipped to measure: steering torque, steering angle, bicycle speed, bicycle angular velocity about three axes, and acceleration along three axes. A laptop computer, A/D boards, battery, and circuitry are supported in a box at the rear.

2.3.2 *Instrumentation*

The instrumentation selected for this study enables the simultaneous measurement of the steering torque, the steering angle, the bicycle speed, and the acceleration and angular velocity of the bicycle frame as described below.

Steering torque. We constructed the custom instrumented fork shown in Figure 2.2 to measure the steering torque. The placement of a torque sensor (Transducer Techniques SWS-20) within the steerer tube permitted the measurement of the torque transmitted between the handlebars and the front wheel. We isolated the torque sensor from unwanted bending moments and axial loading by using angular contact bearings (Enduro 7901) in conjunction with the pair of angular contact bearings in the bicycle headset; the bearings were preloaded prior to testing, similar to the way that a threadless headset is adjusted. Following installation, we calibrated the torque sensor *in situ* by orienting the

bicycle such that the steering axis was parallel to the ground, securing a long length of threaded rod in the fork dropouts, and then placing known masses at measured distances from the steering axis to create known torques. Following calibration, we measured the stiffness of the torque sensor to be 4.97 Nm/deg. The signal from the torque sensor was amplified using a load cell signal conditioner (Transducer Techniques TMO-1) and was sampled at 1000 Hz in the experiments described below. The range and resolution of the torque measurements are +/- 7.512 Nm and 0.005 Nm, respectively.

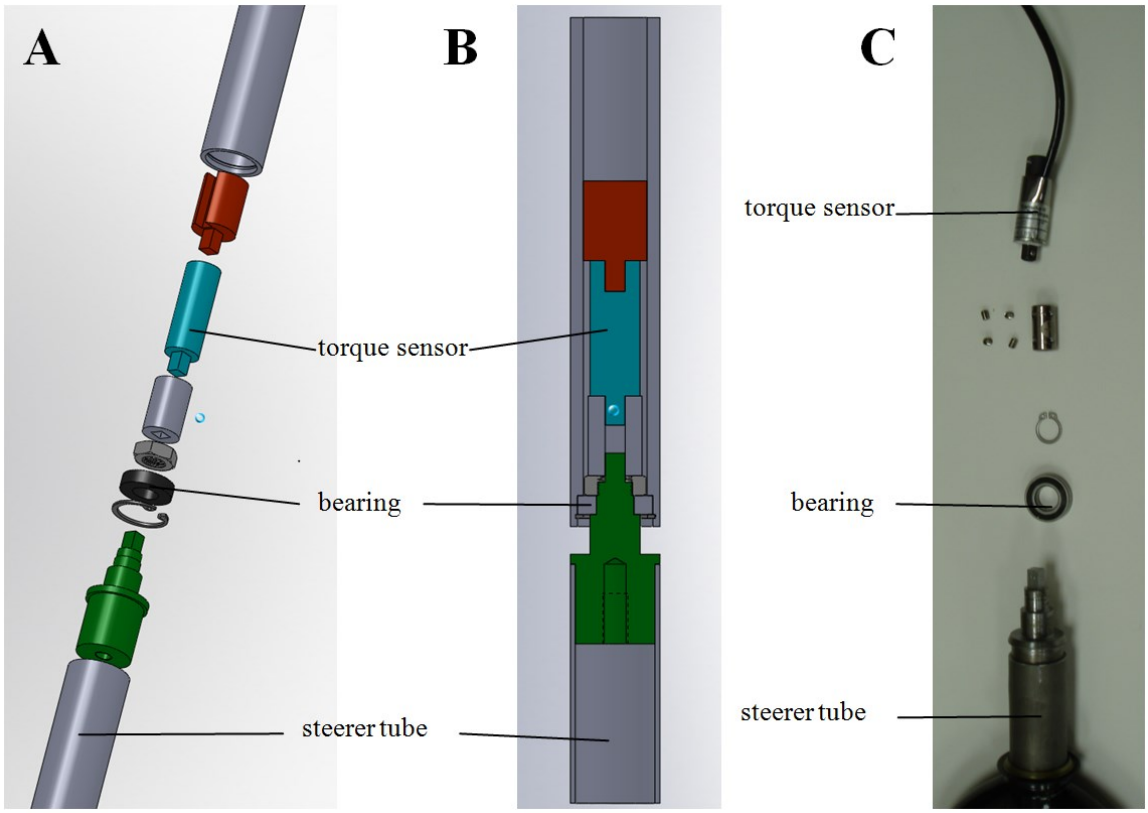

Figure 2.2. The instrumented fork. We constructed a custom instrumented fork to measure steering torque. (A) An exploded view of the steerer tube of the instrumented fork. (B) A section view of the assembled instrumented fork. (C) A photograph of the disassembled instrumented fork.

Steering angle. We employed an optical encoder to measure the steering angle. We secured a custom encoder disk (US Digital HUBDISK-2-1800-1125-I) to the bicycle fork similar to a headset spacer as illustrated in Figure 2.3. We attached the encoder module

(US Digital EM1-2-1800) to a custom aluminum plate, which was secured to the bicycle frame by using the top headset race as shown in Figure 2.3. An encoder chip (LSI/CSI LS7183 in $\times 2$ resolution mode) was used to convert the raw signal from the encoder module to up and down counts and was sampled at 200 Hz, which is the maximum sampling rate for a digital input to the data acquisition board. Due to the flexibility of the steering assembly caused by the torque sensor, the steering angle is corrected as described in Chapter 3 Section 3.3.2. The optical encoder measures the steering angle with a resolution of 0.1 degrees.

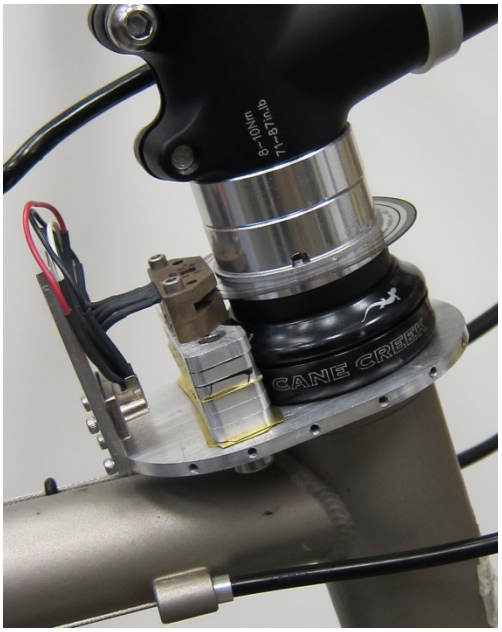

Figure 2.3. The encoder and encoder disk used to measure the steering angle. The encoder module was fastened to a custom aluminum plate secured to the bicycle frame using the upper headset cup. The encoder disk was secured to the steerer tube of the fork, similar to a headset spacer.

Bicycle speed. We calculated the average bicycle speed for each revolution of the front wheel by dividing the circumference of the front wheel by the time required for each revolution. The circumference of the front wheel was calculated from the rolling radius of the front wheel, which was measured as described in Section A.2 of Appendix A. Wheel revolutions were measured using a magnetic reed switch (Cateye 169-9772) and a single

wheel mounted magnet (Cateye 169-9691). We sampled the signal from the magnetic reed switch at 1000 Hz. Speed updates, obtained once per wheel revolution, translate to update rates from 0.5 to 4.7 Hz for the bicycle speeds in our experiments. Assuming resolutions of 0.001 seconds and 0.001 meters for the measured time for a wheel rotation and wheel circumference, respectively, we estimate that the maximum error occurs at the fastest speed (+/- 0.049 m/s or +/- 0.5%) and the minimum error occurs at the lowest speed (+/- 0.001 m/s or +/- 0.1%).

Acceleration and angular velocity. A custom inertial measurement unit (IMU) shown in Figure 2.4 was constructed using a three-axis accelerometer (Analog Devices ADXL335) and three single-axis angular rate gyros (Murata ENC-03M). We secured the IMU to a custom aluminum plate which is fastened to the seat tube of the bicycle frame utilizing the water bottle cage mounting holes (Figure 2.4). The angular velocity measurements were used to calculate the turn radius and the acceleration measurements were used to calculate the bicycle roll angle as further described in Section 3.3.2. The signals from the accelerometer and three angular rate gyros were sampled at 1000 Hz. The IMU, calibrated using the technique described by King [85], yields acceleration measurements with a range and resolution of +/- 29.43 m/s^2 and 0.067 m/s^2, respectively, and angular velocity measurements with a range and resolution of +/- 300 deg/s and 3.04 deg/s, respectively.

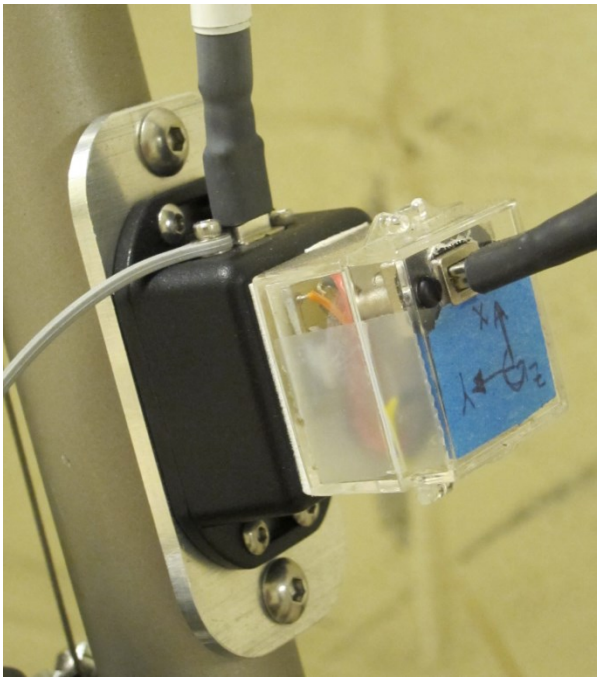

Figure 2.4. A custom inertial measurement unit (IMU). The IMU was secured to a custom aluminum plate which was fastened to the bicycle by utilizing the water bottle cage mounting holes.

Data acquisition. We used a small laptop computer (Dell Inspiron mini) running a custom LabVIEW (National Instruments) program and two data acquisition boards (National Instruments USB-6008) to convert analog signals to digital and to log data collected during each trial. The laptop and data acquisition boards were carried in a foam-padded wooden box mounted to the rear of the bicycle (Figure 2.1).

Power Supplies. Four 3.7 volt, 900 mAh polymer lithium ion batteries (Sparkfun PRT-00341) were used to supply power to the instrumentation. We created the required voltage for each sensor by wiring the required number of batteries in series. Voltage inputs for each sensor were regulated by a step-up / step-down switching DC-DC converter (All-Battery.com, AnyVolt Micro).

CHAPTER 3: MEASUREMENT AND ANALYSIS OF STEADY STATE TURNING

3.1 Chapter Summary

The steady-state turning of a bicycle arises when the bicycle/rider system negotiates a constant radius turn with constant speed and roll angle. This chapter explores steady-state turning by employing the previously described bicycle instrumented to measure steering torque, steering angle, and bicycle speed, acceleration, and angular velocity. We report data obtained from 134 trials using two subjects executing steady turns defined by nine different radii, three speeds, and three rider lean conditions. A model for steady-state turning, based on the Whipple bicycle model, is used to interpret the experimental results. Overall, the model explains 95.6% of the variability in the estimated bicycle roll angle, 99.4% of the variability in the measured steering angle, and 6.5% of the variability in the measured steering torque. However, the model explains 56.6% of the variability in steering torque for the subset of trials without exaggerated rider lean relative to the bicycle frame. Thus, the model, which assumes a rigid and non-leaning rider, reasonably predicts bicycle/rider roll and steering angles for all rider lean conditions and steering torque without exaggerated rider lean. The findings demonstrate that lateral shifting of the bicycle/rider center of mass strongly influences the steering torque, suggesting that rider lean plays an important role in bicycle control during steady-state turning. By contrast, the required steering angle is largely insensitive to rider lean, suggesting that the steering angle serves as a superior cue for bicycle control relative to steering torque. The experimental data presented in this chapter also appears in a published conference paper

[81] and a published journal paper [82]. The journal paper contains the same steady-state model presented herein, whereas the conference paper presents a simplified model that accounts for rider lean.

3.2 Background and organization of chapter

The design of the modern bicycle is the result of almost two centuries of trial and error. Recent research has helped us understand the stability of a bicycle [2, 11] and has shown that the current bicycle configuration could be made more stable with relatively small adjustments to standard bicycle geometry [12]. While much is known about bicycle stability based on models of riderless bicycles [9, 11], less is known about the dynamics and control of the entire bicycle/rider system.

One step towards this understanding is to consider the bicycle/rider system during steady-state turning. Steady-state turning of a bicycle arises when the bicycle/rider system negotiates a constant radius turn with constant speed and roll angle. Steady-state turning has been investigated most recently by Basu-Mandal et al. [86] and Peterson and Hubbard [87]. Basu-Mandal et al. [86] employ the nonlinear equations of motion for an idealized benchmark bicycle to identify hands-free (zero applied steer torque) steady-state turning motions. Doing so provides evidence that a rider need not impart large steering torques during steady-state turning. Peterson and Hubbard [87] also employ the benchmark bicycle model to identify all kinematically feasible steady-state turns and the associated steering torque and bicycle speed. Their results reveal that the steering torque can reverse sign depending on the bicycle steer and roll angles and bicycle speed. Franke et al. [88] investigate the stability of steady-state turning using a nonlinear bicycle model that includes lateral displacement of the rider center of mass. They report that stability is

extremely sensitive to rider lean. Rider lean was also considered in the steady-state turning analysis of Man and Kane [89] who employ bicycle parameters from Roland [31]. They conclude that rider lean alters the bicycle roll angle and consequently alters the maximum speed to negotiate a steady turn. In addition, a rider may use a wide range of steer angles to negotiate a turn, depending on the bicycle roll angle and speed. These findings, however, have also been questioned [86].

Related to the steady-state behavior of bicycles are numerous theoretical and experimental studies of the steady-state turning of motorcycles. Fu [90] developed a model for steady-state turning, and tested this model using a motorcycle equipped with steering angle and roll angle sensors. Experimental measurements of the motorcycle roll angle matched those predicted by the model and confirmed the importance of gyroscopic effects. The measured steering angles were somewhat less than theoretical predictions, which led Fu to suggest that the lateral tire force develops mainly from tire camber as opposed to tire side slip. Prem [45] used an instrumented motorcycle to measure the speed, steering torque, roll rate, yaw rate, steer angle, lateral acceleration, rider lean, and rider pitch for a wide range of steady turns in order to identify motorcycle steady-state control gains. Results demonstrated substantially different steady-state response parameters for motorcycles with 'acceptable' handling characteristics. Cossalter et al. [79] developed a mathematical model of the steering torque as a function of speed, turn radius, tire properties, and motorcycle geometry/mass distribution. The sign of the "acceleration index" [79, 91, 92] indicates whether steering torque must be applied in the same direction as the turn (positive) or in the opposite direction (negative). Bortoluzzi et al. [92] constructed an instrumented motorcycle capable of measuring steering torque,

steering angle, roll angle, velocity, roll rate, and yaw rate for the purpose of testing a steady-state model similar to that of [79]. The measured acceleration index remained in good agreement with theoretical predictions and was relatively insensitive to changes in tire properties and rider mass distribution. By contrast, the lateral displacement (i.e., the lean) of the rider relative to the bicycle frame had a pronounced effect on the acceleration index, especially at smaller lateral accelerations.

While bicycles and motorcycles share common features as two-wheeled single track vehicles, there are also key distinctions. For a bicycle, a rider may comprise 85-95% of the total mass, whereas for a motorcycle, a rider may only account for 15-30% of the total mass [6]. When the ratio of vehicle to rider mass is large (i.e., for motorcycles), the rider steering torque is the dominant control input [79]. By contrast, when the vehicle/rider mass ratio is small (i.e., for bicycles), other control mechanisms arise, such as upper body lean and knee movement [93].

The aim of this chapter is to report experimental measurements on steady-state turning using a novel instrumented bicycle. Secondarily, we employ a model for steady-state turning to interpret measured bicycle roll angle, steer angle, and steer torque over a wide range of steady-state turning conditions. We open the Methods Section by describing the experimental protocol and data analysis used to evaluate steady turning on a bicycle. Starting from the Whipple bicycle model presented in [2], we derive a model governing the steady-state turning of the bicycle/rider system. The Results and Discussion Sections summarize statistical comparisons of experimental and theoretical results for the bicycle roll angle, steering angle, and steering torque.

3.3 Methods

3.3.1 *Experimental protocol*

Two subjects rode the instrumented bicycle around a course containing nine curves of constant radius (radii of magnitude 9.14, 12.19, 18.29, 22.86, 27.74, 28.35, 32.31, 32.61, and 32.92 meters). All of the curves, located outdoors on smooth and level pavement, were clearly marked with chalk. Each subject selected his/her seat height and remained seated during each trial. We instructed the subjects to ride the course three times and at constant speeds that the subjects considered slow, medium, and fast. A bicycle computer with a visual display (Cateye Velo 8) allowed subjects to monitor their speed if desired. It is important to note that subjects were required to pedal the bicycle to maintain speed; no motors were used to remove the task of pedaling. Allowing the subjects to select approximate slow, medium, and fast speeds eliminated the additional mental task associated with maintaining a prescribed speed. As a result, each subject chose speeds corresponding to his/her preferred pedaling frequency. Furthermore, for a given curve and speed, the subjects were instructed to complete three trials distinguished by the degree of rider lean relative to the bicycle frame (lateral shifting of the bicycle/rider center of mass): natural rider lean (**normal riding**), exaggerated rider lean into the turn (**leaning body into turn**), and exaggerated rider lean out of the turn (**leaning body out of turn**). In summary, 81 trials were recorded for each subject: 9 curves x 3 speeds x 3 rider lean conditions. Prior to these trials, the tire pressure was set to 2.76 bar (40 psi).

3.3.2 *Data analysis*

We first reviewed the data for each trial to identify time periods of steady-state turning as seen in the example of Figure 3.1. During steady-state turning, the bicycle speed, roll rate, steering angle, and turn radius remain nearly constant. Through visual inspection of bicycle speed, roll rate, steering angle, and turn radius, we selected areas of potential steady-state turning from each trial. We then analyzed each period of steady-turning by parsing this data into five-second blocks that were also shifted by 0.5 seconds. As a result, the first block of data began at the beginning of the period of steady turning, the second block of data began 0.5 seconds after the beginning of the period, and so on. The data for each five-second block was then averaged (to filter any modest transients) and this averaged data was used for all subsequent calculations described in the following. We used the following criteria to determine whether or not a block of data was considered steady-state:

- The magnitude of the forward acceleration of the bicycle during a five-second block, as calculated from the measured bicycle speed, must be less than or equal to 0.1 m/s^2.
- The standard deviation of the measured steering angle for a five-second block must not exceed three degrees.

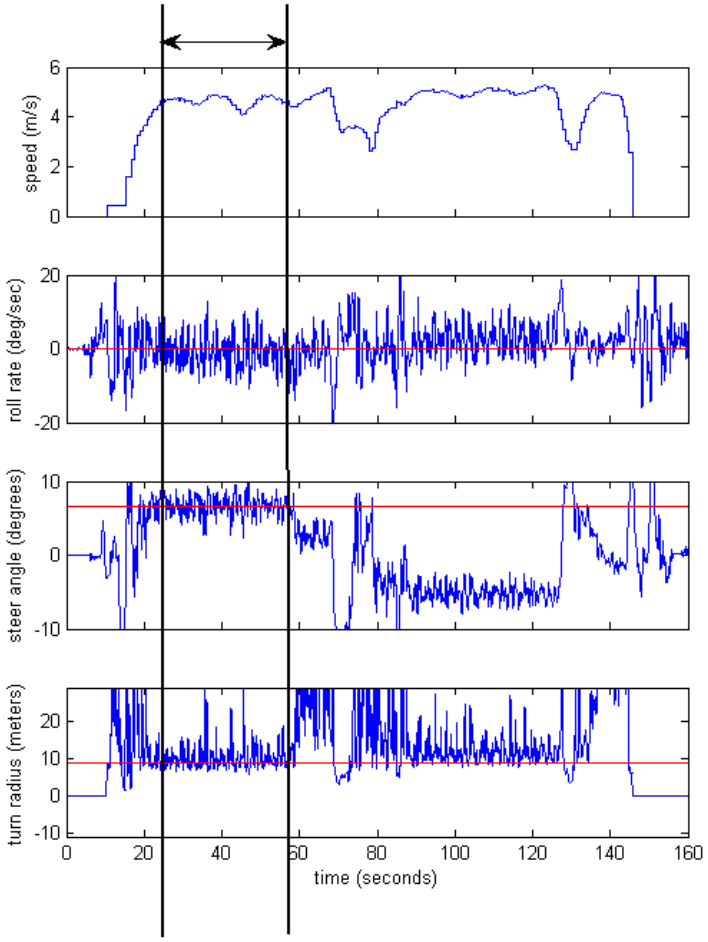

Figure 3.1. Identification of a region of steady-state turning. Bicycle speed, roll rate, steering angle, and instantaneous turn radius were used to identify a region of steady-state turning for processing. The region of steady turning for the example trial shown (a medium speed, clockwise turn with a turn radius of 9.14 meters) lies within the two vertical (black) lines. Another large region of steady-state turning begins around 90 seconds and ends at approximately 125 seconds. The turn radius data has been truncated to highlight the steady-state turning region of interest.

The inertial measurement unit defines a sensor frame of reference $(\hat{e}_1, \hat{e}_2, \hat{e}_3)$ which differs from the bicycle-fixed frame $(\hat{e}_i, \hat{e}_j, \hat{e}_k)$ illustrated in Figure 3.2A. The orientation of the sensor frame of reference relative to the conventional vehicle dynamics axes [94] for a bicycle is illustrated in Figure 3.2C. The acceleration and angular velocity components measured in the sensor-fixed frame ($\overrightarrow{a_{123}}$ and $\overrightarrow{\omega_{123}}$) must be transformed into components measured in the bicycle-fixed frame ($\overrightarrow{a_{ijk}}$ and $\overrightarrow{\omega_{ijk}}$) for subsequent data reduction. This is achieved using, for example,

$$\overrightarrow{a_{ijk}} = \begin{bmatrix} \cos\rho & 0 & -\sin\rho \\ 0 & 1 & 0 \\ \sin\rho & 0 & \cos\rho \end{bmatrix} \overrightarrow{a_{123}} \tag{3.1}$$

where ρ denotes the seat tube angle relative to vertical. For the instrumented bicycle used in this study, $\rho = -15.3$ degrees.

The average radius of the turn for each five-second block was then determined from

$$R = \frac{v}{\sqrt{\left((\omega_i)^2 + \left(\omega_j\right)^2\right)}} \tag{3.2}$$

where v denotes the corresponding bicycle speed and ω_i and ω_j denote the angular velocities about the axes defined by $\hat{e}_i$ and $\hat{e}_j$ illustrated in Figure 3.2B. The angular velocities ω_i and ω_j were determined using the outputs from the three sampled single-axis angular rate gyros. Note that upon assuming the pitch rate of the bicycle is negligible, the denominator of (3.2) represents the yaw rate; in a steady turn, the angular velocity is vertical (i.e., the $\hat{e}_k$ component is zero).

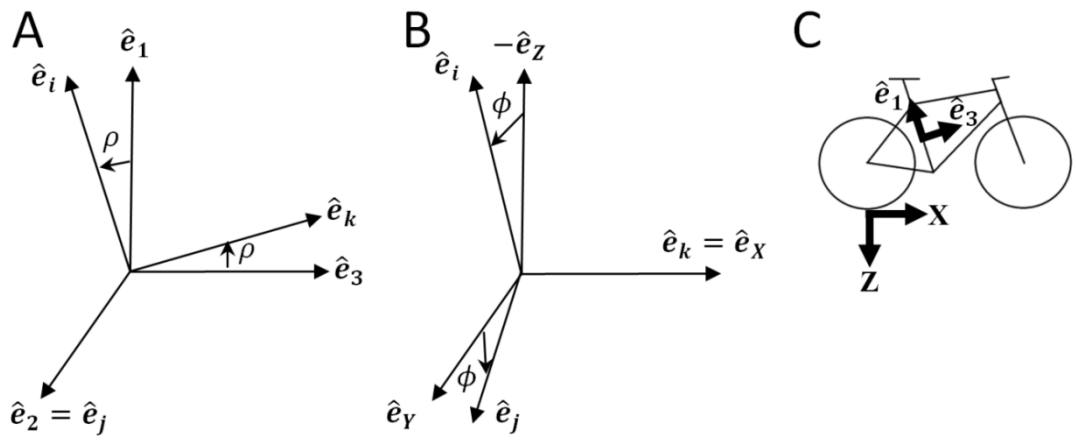

Figure 3.2. (A) The rotation of the bicycle-fixed frame $(\hat{e}_i, \hat{e}_j, \hat{e}_k)$ relative to the sensor-fixed frame $(\hat{e}_1, \hat{e}_2, \hat{e}_3)$. (B) The rotation of the bicycle-fixed frame relative to the inertial frame $(\hat{e}_X, \hat{e}_Y, \hat{e}_Z)$. (C) A sketch of a bicycle showing the relationship of the sensor-fixed frame $(\hat{e}_1, \hat{e}_2, \hat{e}_3)$ to the conventional vehicle dynamics coordinate system (X, Y, Z) when the bicycle is in the upright position. Note that $(\hat{e}_X, \hat{e}_Y, \hat{e}_Z)$ is aligned with (X, Y, Z).

The bicycle roll angle (ϕ), which we define as the roll angle of the rear of the bicycle frame relative to vertical as in [2], follows from the measured bicycle-fixed frame acceleration, $\overrightarrow{a_{ijk}}$ by exploiting the fact that the accelerometer functions as an inclinometer during steady-state turning. In particular, the IMU measures the acceleration at the location of the sensor plus the acceleration of gravity. Therefore, $\overrightarrow{a_{ijk}}$ includes the centripetal acceleration for steady turning (directed in the horizontal plane) and the acceleration due to gravity (directed along the vertical):

$$\overrightarrow{a_{ijk}} = a_i \hat{e}_i + a_j \hat{e}_j + a_k \hat{e}_k = 0\hat{e}_X + \frac{v^2}{R}\hat{e}_Y - g\hat{e}_Z \tag{3.3}$$

where v is the forward bicycle speed and R is the turn radius; positive values of R correspond to clockwise turns whereas negative values correspond to counter-clockwise turns. The frame $(\hat{e}_i, \hat{e}_j, \hat{e}_k)$ is related to the frame $(\hat{e}_X, \hat{e}_Y, \hat{e}_Z)$ through:

$$\begin{bmatrix} \hat{e}_X \\ \hat{e}_Y \\ \hat{e}_Z \end{bmatrix} = \begin{bmatrix} 0 & 0 & 1 \\ \sin\phi & \cos\phi & 0 \\ -\cos\phi & \sin\phi & 0 \end{bmatrix} \begin{bmatrix} \hat{e}_i \\ \hat{e}_j \\ \hat{e}_k \end{bmatrix} \tag{3.4}$$

Substituting (3.4) into (3.3) and solving for the bicycle roll angle (ϕ) yields:

$$\phi = \tan^{-1}\left(\frac{v^2}{Rg}\right) - \tan^{-1}\left(\frac{a_j}{a_i}\right) \tag{3.5}$$

where a_i and a_j are the (average) values of the measured acceleration along the $\hat{e}_i$ and $\hat{e}_j$ axes in Figure 3.2. The results (3.3) and (3.5) also assume that the distance between the accelerometer and the center of mass of the bicycle/rider system is negligible compared to the radius of the turn and that the bicycle-fixed axis defined by $\hat{e}_k$ is the heading direction.

We confirmed the accuracy of the above technique to estimate the bicycle roll angle by comparing the roll angle estimated from (3.5) to independently measured simulated roll angles. We created simulated roll angles by installing the IMU on a jig fastened to a two-wheeled bicycle trailer (Figure 3.3) that allows us to set and measure the simulated roll angle of the IMU using a high-precision inclinometer (resolves the pre-set roll angles to within $\pm$ 0.01 degrees). Assuming that the roll of the trailer remains negligible, the simulated roll angle of the inertial measurement unit remains constant at a pre-set and measured value when the bicycle pulls the trailer around a constant radius turn on level pavement. We conducted 20 trials, in which we varied the turn radius (9.14, 27.73, and 32.31 meters), the bicycle speed (slow, medium, and fast), and the jig roll angle (-17.34, 11.49, 1.63, and -30.51 degrees). The difference between the estimated roll angle and the

independently measured simulated roll angle was 1.10 ± 0.78 degrees (mean ± standard deviation) confirming that the acceleration-based measurement technique successfully estimates the roll angle during steady-state turning.

Figure 3.3. A jig was used to validate our method of estimating the bicycle roll angle by allowing us to orient the inertial measurement (IMU) at a fixed simulated roll angle. The simulated roll angle was independently measured using an inclinometer that can resolve the roll angle to within ± 0.01 degrees (inset photograph). The jig was secured to a bicycle trailer and pulled behind the instrumented bicycle on level pavement. The white rectangle indicates the location of the IMU on the jig secured to the trailer.

Theoretically, the bicycle roll angle could also be estimated by using the measured angular velocities:

$$\phi = -\tan^{-1}\left(\frac{\omega_j}{\omega_i}\right) \tag{3.6}$$

However, this method yields poor estimates for roll angles less than four degrees due to the limited resolution of the rate gyros. The estimate provided by (3.5) does not suffer from this limitation and yields superior estimates.

Due to the placement of the steering angle optical encoder relative to the steering torque sensor, the angular displacement of the handlebar and stem about the steering axis ($\delta_{measured}$) was recorded instead of the angular displacement of the front wheel about the steering axis (δ_{true}). However, these values differ by a small but measurable twist of the assembly. The true steering angle, or angular displacement of the front wheel about the steering axis, is given by

$$\delta_{true} = \delta_{measured} - \frac{T_\delta}{4.97} \tag{3.7}$$

where T_δ is the measured steer torque and 4.97 Nm/deg is the aforementioned stiffness of the torque sensor assembly. For all our analyses and figures we use δ_{true} per (3.7).

For statistical analysis and for plotting, we averaged the results from the five-second blocks for each trial (one combination of subject, lean condition, speed and radius), which yields one set of values per trial. The total number of trials used for analysis is 134 instead of the total measured (2 x 81 = 162) because data for 28 trials failed the aforementioned criteria for steady-state.

3.3.3 *Theoretical model for steady-state turning*

We employ the Whipple bicycle model [3] as presented by Meijaard et al. [2] to derive a model for steady-state turning similar to that for a vehicle [95-97]. The Whipple bicycle model consists of four rigid bodies: a rear wheel, a rear frame with a rider rigidly attached to it, a front frame consisting of the front handlebar and fork assembly, and a front wheel. The model assumes that all bodies are laterally (left-right) symmetric and that the wheels have circular symmetry. Motion of the rider relative to the frame,

structural compliance and damping, joint friction, and tire compliance and slip are neglected. The tire contacts with the ground are modeled as knife-edge rolling point-contacts. The model is configured with seven generalized coordinates: the location of the rear-wheel contact with the ground (x_P, y_P), the rotation of the front and rear wheels (θ_F, θ_R), the yaw rotation (ψ), the roll or lean angle (ϕ) of the bicycle frame, and the steering angle (δ). As noted in [2], only three of the generalized coordinates are independent upon accounting for four non-holonomic rolling constraints. After linearizing the model about upright, straight-line motion and treating forward speed as a parameter, only two independent generalized coordinates remain: steer (δ) and lean or roll (ϕ).

The resulting linearized equations of motion, as presented in [2] (Equation 5.3 therein), are:

$$\mathbf{M}\ddot{\mathbf{q}} + v\mathbf{C_1}\dot{\mathbf{q}} + [g\mathbf{K_0} + v^2\mathbf{K_2}]\mathbf{q} = \mathbf{f} \tag{3.8}$$

where $\mathbf{q} = [\phi, \delta]^T$ are the remaining generalized coordinates for the roll (lean) and steer angles and $\mathbf{f} = \left[T_\phi, T_\delta\right]^T$ are the associated generalized forces representing the lean and steer torques. The first and the second equation of (3.8) are referred to as the lean equation and the steer equation, respectively [2]. The other quantities appearing in (3.8) include the forward speed v , gravity g, and the matrices $\mathbf{M}, \mathbf{C_1}, \mathbf{K_0}$, and $\mathbf{K_2}$ as defined in Appendix A of [2].

During a steady turn, the steering angle (δ) and the lean or roll angle (ϕ) remain constant, reducing (3.8) to the equilibrium equation

$$[g\mathbf{K_0} + v^2\mathbf{K_2}]\mathbf{q} = \mathbf{f} \tag{3.9}$$

Assuming that the lean torque in a steady-state turn vanishes ($T_\phi = 0$), the lean and steer equations become

$$gK_{0\phi\phi}\phi + \left(v^2K_{2\phi\delta} + gK_{0\phi\delta}\right)\delta = 0 \tag{3.10}$$

$$gK_{0\phi\delta}\phi + (v^2K_{2\delta\delta} + gK_{0\delta\delta})\delta = T_\delta \tag{3.11}$$

where $K_{0\phi\phi}, K_{0\phi\delta}, K_{0\phi\phi}, K_{2\phi\delta}$, and $K_{2\delta\delta}$ are constants defined by Equations (A.14)-(A.19) in Appendix A. Note that Equation (3.11) yields the steering torque (T_δ) in terms of the bicycle configuration (ϕ, δ) and forward speed v . Under the same conditions, the yaw rate ($\dot{\psi}$) given by Equation B6 in [2] reduces to

$$\dot{\psi} = \frac{v\delta\cos\lambda}{w} = \frac{v}{R} \tag{3.12}$$

where λ is the steer axis tilt, w is the bicycle wheel base, and R is the radius of the steady turn. (Note that $\dot{\psi}$ and R are positive for clockwise turns and negative for counter-clockwise turns and that R is measured from the center of the turn to the rear wheel ground contact point.) The required steer angle is therefore

$$\delta = \frac{w}{R\cos\lambda} \tag{3.13}$$

and substitution of this result into (3.10) yields the required lean angle

$$\phi = \frac{-w\left(v^2 K_{2\phi\delta} + g K_{0\phi\delta}\right)}{Rg\cos(\lambda)\, K_{0\phi\phi}} \tag{3.14}$$

Finally, substitution of (3.13) and (3.14) into (3.11) yields the required steering torque

$$T_\delta = \frac{-w\left(g\left(K_{0\phi\delta}^2 - K_{0\delta\delta}K_{0\phi\phi}\right) + v^2\left(K_{2\phi\delta}K_{0\phi\delta} - K_{0\phi\phi}K_{2\delta\delta}\right)\right)}{R\cos(\lambda)\, K_{0\phi\phi}} \tag{3.15}$$

3.3.4 *Comparison of the model to experimental data*

In the following, we compare the measured roll angle, steer angle and steer torque to those predicted by the model above. In particular, we use the measured bicycle speed (v) and nominal turn radius (R) in the following sequence of calculations.

(1) The bicycle roll angle (ϕ), or roll of the bicycle frame, is calculated using Equation (3.14).
(2) The steer angle (δ) is calculated using Equation (3.13).
(3) The steering torque (T_δ) is calculated using Equation (3.15).

We also compute the steering torque/steer angle ratio and the roll angle/steer angle ratio. The calculations require knowledge of the bicycle parameters described in Appendix A and summarized in Table A.2 for both subjects.

The statistical fit of the experimental data to the model predictions is determined by calculating the correlation coefficient between the experimental and theoretical results and the linear least squares fit of the experimental to theoretical results. Where the model

predicts linear relationships, we compared the linear least squares fits of the experimental data to the linear relationships predicted by the model. We used t-tests with an alpha level of 0.05 to determine statistical significance.

3.4 Results

Roll angle. The estimated bicycle roll angle, calculated from Equation (3.5), is plotted versus normalized lateral acceleration in Figure 3.4 together with the roll angle predicted by the model, calculated from Equation (3.14). Due to the fact that the magnitude of $K_{0\phi\delta}$ is only about 2.5% of the magnitude of $K_{2\phi\delta}$, the model predicted roll angle is nearly linear in lateral acceleration, as shown in Figure 3.4. The non-linear effects for the experimental conditions are contained within the width of the plotted line. The model predicts 99.8% of the variation of the measured bicycle roll angle for the normal riding trials, i.e. trials without exaggerated rider lean relative to the bicycle frame. Moreover, the model predicts 95.6% of the variation of the estimated bicycle roll angle, regardless of rider posture (normal riding or leaning body into or out of the turn relative to the bicycle frame). The linear fit of measured versus predicted bicycle roll angle for all lean conditions has a slope that is not statistically significantly different from 1.0 (Table 3.2), which further confirms that this model closely predicts the measured lean angle.

A rider leaning into or out of a turn relative to the bicycle frame can significantly alter the slope of the linear fit by approximately ±13%. This arises from the additional roll of the bicycle caused by the lateral offset of the center of mass of the bicycle/rider system. For example, a rider leaning into a clockwise turn will cause the bicycle roll angle to decrease, resulting in a bicycle roll angle slightly less than that predicted by the model.

Both subjects clearly exhibit this trend, as shown by the dark gray '+' symbols in Figure 3.4. The opposite trend arises for a rider leaning out of a clockwise turn, as shown by the light gray '×' symbols in Figure 3.4. If we assume that the estimated bicycle roll angle is accurate, we can then also estimate the additional roll of the bicycle caused by a lateral shift in the center of mass as the difference between the estimated and the model predicted roll angles. The mean values for the estimated additional roll are reported in Table 3.1. Both riders were able to create significant additional roll of the bicycle by leaning; on average, the estimated additional roll angle of the bicycle was -2.5 degrees and 2.0 degrees when the riders leaned into and out of the turn, respectively. During normal riding, riders tended to lean slightly into the turn relative to the bicycle frame, generating an estimated additional roll angle of -0.2 degrees. The very small deviations between the normal riding data and the model could derive from small lateral shifts in the center of mass, asymmetric stance on the bicycle, errors in the estimated bicycle roll angle (see Section 3.3.2), and transient as opposed to steady-state conditions.

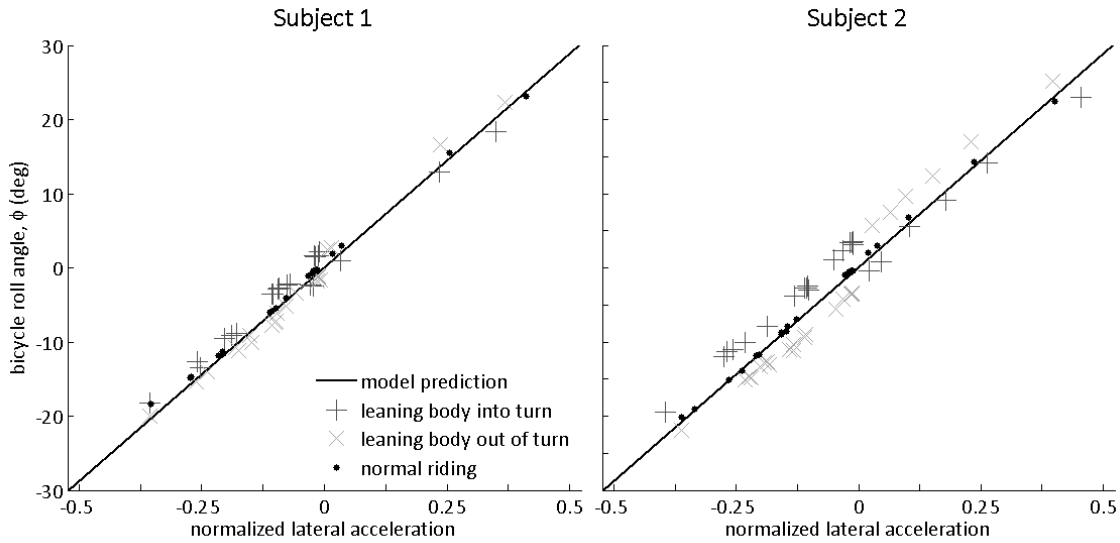

Figure 3.4. Bicycle roll angle versus normalized lateral acceleration. The experimental data are predicted well by the model (slope = 1.00, R^2 = 0.956). Deviation from the model prediction can be interpreted as additional roll of the bicycle caused by a lateral shift in the bicycle/rider system center of mass. Positive values of lateral acceleration correspond to clockwise turns; negative values correspond to counter-clockwise turns. Note that the model predicted bicycle roll angle is nearly linear in lateral acceleration; the non-linear effects for the experimental conditions are contained within the width of the plotted line.

Table 3.1. Differences between the estimated bicycle roll angle and the model predicted roll angle for different lean conditions. A positive value indicates that a rider can increase the magnitude of the bicycle roll angle by leaning, whereas a negative value indicates that rider can decrease the magnitude.

Subject	normal riding	leaning body into turn	leaning body out of turn
1	-0.4°	-1.7° *	1.0° *
2	-0.1°	-3.1° *	2.7° *
1 & 2	-0.2°	-2.5° *	2.0° *

Note: * indicates that the mean value is significantly different than the 'normal riding' lean condition (α = 0.05).

Steering angle. The measured steering angle (δ_{true}) shown in Figure 3.5 is also predicted well by the model, as evidenced by the linear fit and R^2 values reported in Table 3.2. The model predicts 99.5% of the variation in the measured steering angle for all lean conditions. Linear fits to the measured steering angle for specific lean conditions were not significantly different than the fit to all trials. However, all linear fits had slopes significantly less than 1.0, indicating that the model slightly over-predicts the measured steering angle. Measured steady turning steering angles ranged in magnitude from approximately zero to 7.5 degrees. Some deviations of the experimental data from the

model can likely be attributed to the transient dynamics that arise when the human rider makes steering corrections to remain upright and to follow the desired path. For example, the data point located far below the model prediction (predicted steering angle ≈ 7 degrees, measured steering angle ≈ 5 degrees) is from a trial where the subject was required to ride around the smallest radius curve at the slowest speed while leaning his or her body into the turn, which was the most challenging riding condition. While the data from this trial formally met our criteria for steady-state (see Section 3.3.2), closer inspection of the trial revealed that the subject used small steering angles for the majority of the trial and used occasional larger steering corrections to stay on the prescribed path.

Table 3.2. Summary of the linear fit $(y = mx + b)$ of measured values to model predicted values.

Lean condition	**Predictor, from model (x)**	**Predicted variable (y)**	**Slope (m)**	**y-intercept (b)**	**R^2**
all	bicycle roll angle	estimated bicycle roll angle	1.00	† 0.56°	0.956
normal	bicycle roll angle	estimated bicycle roll angle	0.99	† 0.47°	* 0.998
rider lean into turn	bicycle roll angle	estimated bicycle roll angle	†* 0.87	†* 1.45°	0.968
rider lean out of turn	bicycle roll angle	estimated bicycle roll angle	†* 1.14	* -0.11°	0.971
all	steering angle	measured steering angle	† 0.96	† -0.28°	0.995
normal	steering angle	measured steering angle	† 0.97	† -0.26°	0.995
rider lean into turn	steering angle	measured steering angle	† 0.94	† -0.26°	0.994
rider lean out of turn	steering angle	measured steering angle	† 0.98	† -0.32°	0.998
all	steering torque	measured steering torque	1.04	-0.07 Nm	0.065
normal	steering torque	measured steering torque	0.86	† -0.07 Nm	* 0.566
rider lean into turn	steering torque	measured steering torque	†* -1.33	†* -0.68 Nm	0.155
rider lean out of turn	steering torque	measured steering torque	†* 3.98	†* 0.54 Nm	* 0.634

Note: All reported slopes (m) are significantly different than zero and all values of R^2 are significant ($\alpha = 0.05$).
* indicates that a value is significantly different than the value for the corresponding 'all' lean condition.
† indicates that a linear fit constant is significantly different from a fit to the model (m = 1.0, b = 0.0).

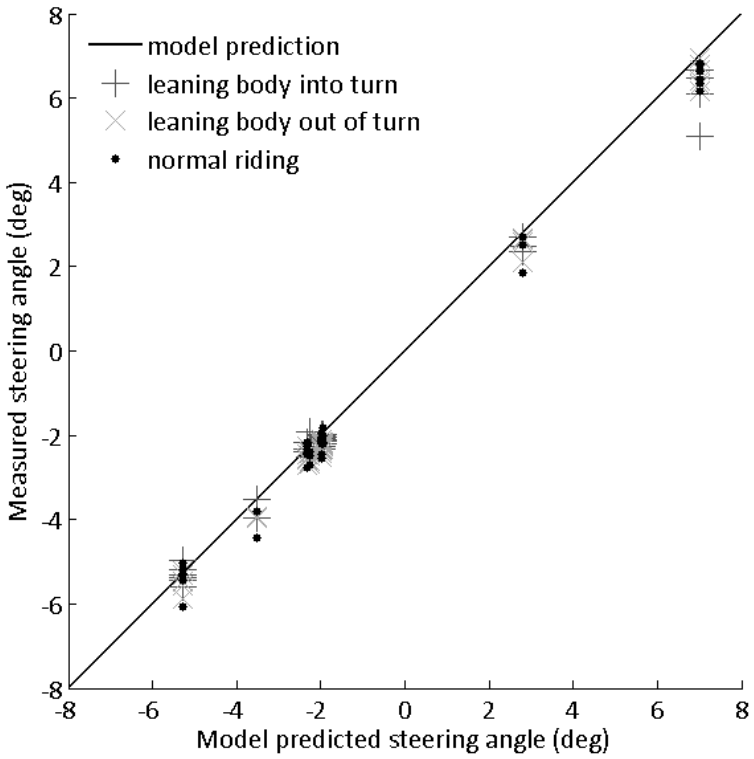

Figure 3.5. Measured steering angle versus model predicted steering angle. The experimental data are predicted well by the model (slope = 0.96, R^2 = 0.995). The clusters of data correspond to the different radii of turns tested experimentally. Scanning from left to right, the data groups correspond to: counter clockwise turning around radii of approximately 12.2, 18.3, 28.0 and 32.5 meters and clockwise turning around turns of 22.9 and 9.1 meters.

Steering torque. The steering torque for all lean conditions is not predicted well by the model, as shown in Figure 3.6. However, the model does provide a reasonable fit to the normal riding case, as evidenced by the linear fit and R^2 values reported in Table 3.2. For normal riding, the slope of the linear fit is not significantly different from 1.0, indicating that the measured steering torque is not significantly different from the model predictions. However, the model is only able to account for 56.6% of the variation in the experimental data. For the rider-lean conditions, the model is not as useful for predicting the steering torque. For the rider leaning into the turn relative to the bicycle frame, the model predicts steering torques that are in the opposite direction with magnitudes approximately 33% less than the measured steering torque. For the rider leaning out of

the turn relative to the bicycle frame, the model predicts steering torques approximately 300% less than the measured steering torques. These results highlight the fact that rider lean can have a significant effect on the steering torque required for a steady-state turn. Measured steering torque ranged in magnitude from approximately zero to 2.4 Nm; the average standard deviation for each five-second window of data was 0.74 Nm. The maximum steering torque was achieved when the rider leaned out of the turn.

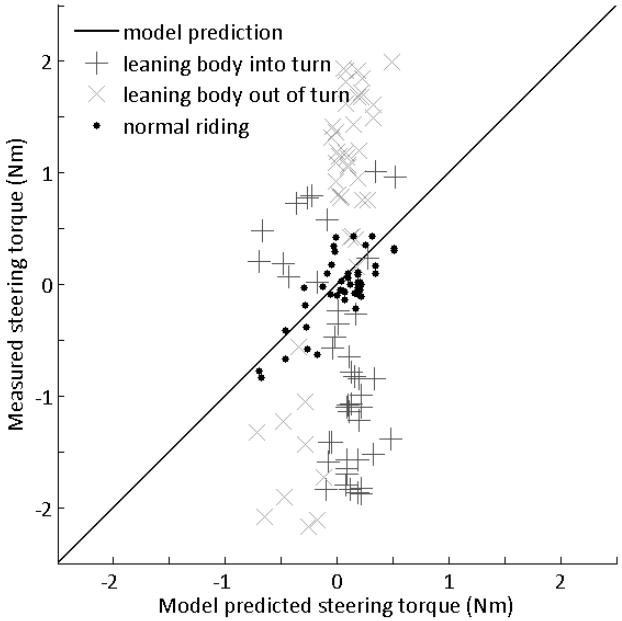

Figure 3.6. Measured steering torque versus the model predicted steering torque. The linear fit of the measured values to the model changes appreciably with different rider-lean conditions. The model provides a good fit to the 'normal riding' condition (slope = 0.86, R^2 = 0.566), but provides poor fits to the 'rider lean into turn' (slope = -1.33, R^2 = 0.155) and 'rider lean out of turn' (slope = 3.98, R^2 = 0.634) conditions.

Ratio of steering torque and steer angle. The ratio of steering torque and steer angle is plotted versus the square of the bicycle speed in Figure 3.7 for both subjects. The model predicts a linear relationship between this ratio and the square of the bicycle speed. The linear fits to the model and to each data set (combinations of subject and lean condition) are reported in Table 3.3.

For both subjects, the model predicts a positive slope of approximately 0.1 kg/radian. The linear fits to the data for Subject 1 all have negative slopes; however, only the slope of the fit to the 'normal' lean condition is significantly different from the model and significantly different from zero. By contrast, the linear fits to the data for Subject 2 all have positive slopes; none of the slopes are significantly different from the model or significantly different from zero. For both subjects, the model predicts a y-intercept of approximately -5.9 Nm. Both subjects were able to significantly change the y-intercept by leaning their bodies into or out of a turn relative to the bicycle frame. A rider leaning his/her body into a turn causes a positive steering torque/steering angle ratio, requiring a rider to apply steering torque in the same direction as the steering angle. A rider leaning his/her body out of a turn causes a negative steering torque/steering angle ratio, requiring a rider to apply steering torque in the opposite direction from the steering angle. Only one of the R^2 values for the linear fits is significantly different from zero (Subject 1, normal lean condition), which is expected from slope values not significantly different from zero. A linear model adequately predicts the data for the normal lean condition, as evidenced by the sum of squared errors (SSE) in Table 3.3.

Table 3.3. Summary of the linear fit $(T_\delta / \delta) = m(v^2) + b$.

Subject	Lean condition	Slope (m)	y-intercept (b)	R^2	SSE
model (subject 1)	--	0.097 kg	-5.986 Nm	1	0 $(Nm)^2$
subject 1	all	-0.070 kg	-0.250 Nm	* 0.008	18508 $(Nm)^2$
subject 1	normal	†* -0.088 kg	* -0.374 Nm	†* 0.202	367 $(Nm)^2$
subject 1	rider lean into turn	-0.058 kg	†* 16.490 Nm	* 0.007	4518 $(Nm)^2$
subject 1	rider lean out of turn	-0.051 kg	†* -17.238 Nm	* 0.012	1794 $(Nm)^2$
model (subject 2)	--	0.100 kg	-5.868 Nm	1	0 $(Nm)^2$
subject 2	all	0.142 kg	-7.708 Nm	* 0.015	61924 $(Nm)^2$
subject 2	normal	0.159 kg	† -9.781 Nm	* 0.127	2988 $(Nm)^2$
subject 2	rider lean into turn	0.117 kg	†* 26.432 Nm	* 0.027	7786 $(Nm)^2$
subject 2	rider lean out of turn	0.127 kg	†* -36.509 Nm	* 0.047	4060 $(Nm)^2$

Note: For the linear fits to experimental data,
* indicates that a value (m, b, or R^2) is significantly different than the model
† indicates that a value is significantly different from zero.

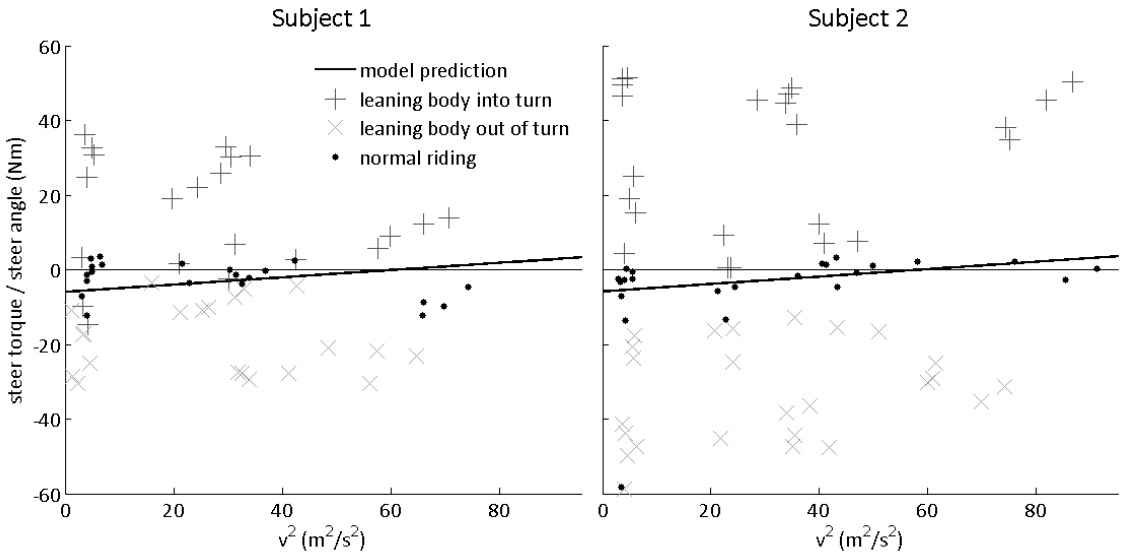

Figure 3.7. The ratio of steering torque to steer angle versus bicycle speed squared. A negative ratio means that a rider must apply a counter-clockwise (negative) steering torque when applying a clockwise (positive) steer angle, whereas a positive ratio means that a rider must apply a clockwise (positive) steering torque when applying a clockwise (positive) steer angle. Both riders were able to significantly change the ratio by leaning into or out of a turn.

Ratio of roll angle and steer angle. The ratio of the roll angle and steer angle is plotted versus the square of the bicycle speed in Figure 3.8 for both subjects. The model predicts a linear relationship between this ratio and the square of the bicycle speed. The linear fits to the model and to each data set (combinations of subject and lean condition) are reported in Table 3.4.

For both subjects, the model predicts a positive slope of approximately 0.1 s^2/m^2. Almost all of the linear fit slopes for Subject 2 are significantly different than the model, whereas only one of the linear fit slopes (rider lean out of turn) for Subject 1 is significantly different than the model. However, all of the slopes are positive, which indicates that the ratio of roll angle/steer angle increases with increasing speed. For both subjects, the model predicts a y-intercept of approximately -0.02. Both subjects were able to significantly change the y-intercept by leaning their bodies into or out of a turn relative to the bicycle frame. A rider leaning his/her body into a turn reduces the roll angle/steer angle ratio, whereas a rider leaning his/her body out of a turn increases the roll angle/steer angle ratio. For most trials and speeds, the ratio of roll angle/steer angle is positive, indicating that in a steady turn a rider must lean the bicycle in the same direction that he/she is steering. However, at low speeds and when a rider leans out of a turn, the ratio can be negative indicating that a rider must actually lean the bicycle in the opposite direction that he/she is steering. A linear model adequately predicts the data for all lean conditions, as evidenced by the R^2 values and sum of squared errors (SSE) in Table 3.4.

Table 3.4. Summary of the linear fit $(\phi/\delta) = m(v^2) + b$.

Subject	Lean condition	Slope (m)	y-intercept (b)	R^2	SSE
model (subject 1)	--	0.092 s^2/m^2	-0.024	1	0
subject 1	all	† 0.085 s^2/m^2	-0.115	†* 0.895	25.3
subject 1	normal	† 0.090 s^2/m^2	-0.164	†* 0.975	2.5
subject 1	rider lean into turn	† 0.080 s^2/m^2	†* -0.568	†* 0.894	7.3
subject 1	rider lean out of turn	†* 0.085 s^2/m^2	†* 0.429	†* 0.972	1.6
model (subject 2)	--	0.092 s^2/m^2	-0.021	1	0
subject 2	all	†* 0.080 s^2/m^2	0.103	†* 0.816	66.3
subject 2	normal	†* 0.085 s^2/m^2	-0.007	†* 0.987	1.7
subject 2	rider lean into turn	† 0.082 s^2/m^2	†* -0.977	†* 0.886	13.7
subject 2	rider lean out of turn	†* 0.072 s^2/m^2	†* 1.263	†* 0.926	5.2

Note: For the linear fits to experimental data,
* indicates that a value (m, b, or R^2) is significantly different than the model
† indicates that a value is significantly different from zero.

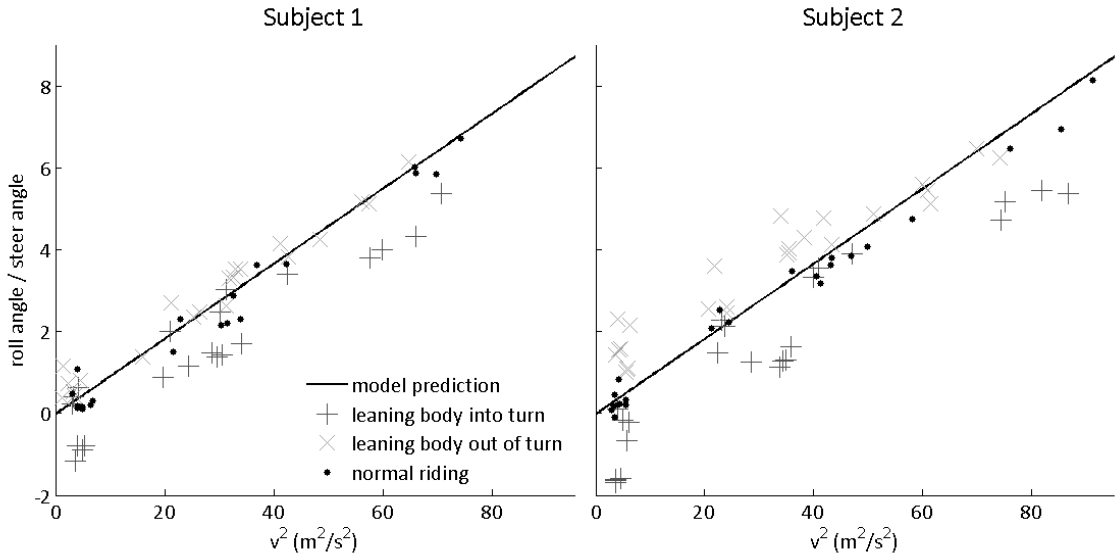

Figure 3.8. The ratio of bicycle roll angle and steering angle versus bicycle speed squared. Both subjects were able to significantly change the y-intercept of a linear fit to the data by leaning into or out of a turn.

3.5 Discussion

As illustrated in Figure 3.4, the estimated roll angle of the bicycle is predicted well by the steady-state turning model developed in Section 3.3.3. For a motorcycle in steady turning, Fu [90] showed that the roll angle is predicted best when the model includes the gyroscopic effects of the motorcycle wheels and engine, as well as tires with a circular cross-section, a conclusion also supported by Prem [45]. In contrast, we find that for a bicycle, the roll angle is predicted rather well upon considering the wheel as a thin disk with a zero-radius edge.

The above results also demonstrate that a seated rider can generate significant additional roll of a bicycle (Table 3.1) simply by leaning his/her upper body into or out of a turn relative to the bicycle frame. In fact, lean dynamics arise even while riding in a straight line as observed by riders maintaining position on a treadmill [93]. In practice, cyclists often lean their bodies into a turn relative to the bicycle frame to increase pedal clearance, such as a road cyclist racing in a criterium. As illustrated in Figure 3.4, by leaning into

the turn, the cyclist decreases the roll angle of the bicycle, and therefore gains pedal clearance. Alternatively, cyclists may lean their bodies out of a turn relative to the bicycle frame, as in the case a mountain biker leaning to avoid trees or branches lining the trail. As illustrated in Figure 3.4, by leaning out of the turn, the cyclist increases the roll of the bicycle but decreases the lateral distance of her/his body from the base of support of the bicycle.

The steer angle of the bicycle is predicted well by the model (Table 3.2 and Figure 3.5). The linear fit of the data to the model results yields values of the slope slightly less than one (Table 3.2), indicating that the model slightly over-predicts the steer angle. Similar to these results, Fu [90] and Prem [45] observed that for a motorcycle in a steady-turn, the steering angle is over-estimated by steady-state turning models. The y-intercept of the linear fit is approximately -0.3 degrees, regardless of rider lean, indicating that perhaps the method of zeroing the steering angle encoder introduced a slight systematic error.

The steady-state turning model reasonably predicts the steering torque of a bicycle when there is no exaggerated rider lean relative to the bicycle frame. The model explains 56.6% of the variation in the measured data for the normal riding condition and the slope of the linear fit to the data is not significantly different from 1.0. The discrepancies between the model and experimental data for the normal riding condition might arise from the measurement limitations of the current torque sensor. In particular, all measured steering torques were less than 10% of the full scale range of the sensor, rendering the torque measurements sensitive to both small systematic and random error sources. The steering torque required to steer a bicycle around a steady curve is substantially smaller than that for a motorcycle; we measured a maximum steering torque of 2.4 Nm for the tested

conditions, whereas Prem [45] and Bortoluzzi et al. [98] measured steering torques up to approximately 10 Nm for a motorcycle with a non-leaning rider. In addition, the steering torque during each five second window varied significantly, with an average standard deviation of 0.74 Nm. Another source of error could derive from the fact that the model predicted steering torque calculation is sensitive to the configuration of the bicycle; deviations of the measured steer angle and estimated bicycle roll angle from model predictions translate to errors in the predicted steering torque. Another possibility is that any inaccuracies in the parameters used to calculate the model predicted steering torque for the instrumented bicycle will have a larger effect on the fit when the range of steering torque is small, such as in the normal riding condition. For example: when a subject changes his/her position on the bicycle, the bicycle/rider center of mass location (x_T, z_T) changes, which alters the magnitude of the steering torque required by the rider. In addition to measurement errors, discrepancies between the data and the model could also arise from simplifications in the model. In particular, the accuracy of the model could likely be improved by allowing tires with circular cross sections, large roll angles, large steer angles, and more realistic tire parameters (particularly pneumatic trail) [6, 79, 87, 92]. The model also does not account for torque that could arise from other factors, such as the effects of the cable housing and transient dynamics.

The accuracy of the steering torque predicted by the model varies significantly depending on the rider-lean condition (Table 3.2). The model does not account for rider lean relative to the bicycle frame, which can significantly change the roll angle of the bicycle. The experimental results demonstrate that a rider can significantly change the steering torque required to negotiate a steady-turn by simply leaning into or out of the turn. Leaning into

the turn can produce a dramatic effect, namely the complete reversal of the required steering torque. If the roll of the bicycle is changed by a leaning rider, the first term of Equation (3.11) is affected, which can reverse the sign of the steering torque. Several models have been derived to explore how a rider is able to ride a bicycle with no-hands, i.e., ride with zero steering torque [5-7, 88]. These models incorporate the lean (reaction) torque that is applied between the rider's upper body and the bicycle. While lean torque is not measured herein, the results clearly demonstrate that upper body lean can control the sign and magnitude of the steering torque required to negotiate a steady-turn. Therefore, it is also possible for a rider to adjust his/her body lean to achieve zero steering torque, thereby enabling no-handed riding. Similarly, for "hands-on" riding, a rider may adjust his/her lean to control the steering torque. The discrepancies between the model and measured steering torque highlight that a rider can significantly alter the required steering torque by simply adjusting his or her lateral position on the bicycle.

The ratio of the steering torque to the steering angle is similar to the acceleration index employed in the motorcycle handling literature as a measure of maneuverability [79, 92, 99]. The steering torque/steering angle ratio represents 'steering stiffness,' which has been identified as a useful parameter for designing bicycles [100]. However, as noted by Prem [45], steady-state response parameters (including the acceleration index and steering stiffness) can vary substantially among different motorcycles with 'acceptable' handling characteristics. The acceleration index indicates the direction of the steering torque relative to the direction of the steady turn [91]. Similarly, the sign of the steering torque/steering angle ratio indicates whether steering torque must be applied in the same direction as the steer angle (usually into the turn) or in the opposite direction (usually out

of the turn). Similar to the steady turning of a motorcycle [92, 98], we find that the lateral displacement of a rider's center of mass (rider lean) relative to the bicycle frame has a significant effect on the direction of the required steering torque.

The above discussion suggests that the steering torque is not an easy quantity for a rider to predict or interpret, a conclusion also supported by Prem [45] and Watanabe and Segel [101] who noted that measured steering torque does not provide useful feedback to a motorcycle rider. For instance, a rider can simply change the required control strategy from applying a steer torque out of the turn to applying a steer torque into a turn by leaning into the turn. In addition, a dynamically leaning bicycle rider constantly changes the required steering torque when pedaling and shifting weight from side-to-side. A more predicable or useful cue is suggested by the steer angle results, which are insensitive to even exaggerated rider lean during steady-state turning.

3.6 Summary and Conclusions

Steady-state turning arises when the bicycle/rider negotiates a constant radius turn at constant speed and roll angle. This chapter examines steady-state turning using a bicycle instrumented to measure steering torque, steering angle, bicycle speed, bicycle acceleration, and bicycle angular velocity. We report data obtained from 134 trials using two subjects executing steady turns defined by nine different radii, three speeds (slow, medium, fast), and three rider lean conditions relative to the bicycle frame (normal, leaning into the turn, leaning out of the turn). We also introduce a model for the steady-state turning of the bicycle/rider system and compare the experimental data to the model predictions for the bicycle roll angle, steering angle, steering torque, steering torque/steer angle ratio, and roll angle/steer angle ratio.

The model explains 95.6% of the variability in the measured bicycle roll angle for all lean conditions, 99.5% of the variability in the measured steering angle for all lean conditions, and 56.6% of the variability in the measured steering torque for the normal riding lean condition. The experimental data demonstrate that rider lean (lateral shifting of the bicycle/rider center of mass relative to the bicycle frame) strongly influences the steering torque, suggesting that rider lean plays an important role in the control of a bicycle. By contrast, the steering angle is largely insensitive to rider lean, suggesting that using the steering angle as a cue for bicycle control is advantageous over using steering torque.

CHAPTER 4: QUANTIFYING THE PROCESS OF LEARNING TO RIDE A BICYCLE USING MEASURED BICYCLE KINEMATICS

4.1 Chapter summary

Currently, it is difficult to determine when a novice bicycle rider is ready to ride without training wheels or external assistance. It is also unclear what must be learned by a rider in order for him/her to be successful riding a bicycle. In this study, we quantify the changes that occurred as 15 children with disabilities learned to ride bicycles during a specialized bicycle training camp. These changes are revealed by three inertial measurement units (IMUs) used to measure bicycle kinematics. Out of 15 subjects, 11 were successful in riding a bicycle without assistance by the end of the camp. The peak value of the cross-correlation between steer and roll angular velocities was significantly greater for riders who ultimately succeeded in riding a bicycle without assistance. This finding suggests that rider learning can be quantified by increased correlation between bicycle steer rate and roll rate. In essence, learning to steer in the direction of lean is an essential skill in learning to ride a bicycle.

4.2 Introduction

Riding a bicycle is a skill that many people learn quite easily as reflected in the common assertion, “it’s as easy as riding a bike.” However, there is little scientific understanding about how we learn to ride and balance a bicycle. What does a new rider learn when s/he finally is able to balance on a bicycle? When is s/he ready to ride without assistance?

What underlying skills define the learning process? These questions may seem unimportant to those who have quickly learned to ride, but to those who have not succeeded in learning to ride or to those struggling to help others learn to ride, these questions remain perplexing.

Learning to ride a bicycle has many benefits, especially for populations possessing learning disabilities. For example, learning to ride increases the physical activity of children with Down syndrome [46]. Also, being able to ride a bicycle can provide those who cannot drive a car due to their disabilities with a means of efficient transportation. Understanding rider learning could improve programs that teach affected populations to ride and could also promote bicycle designs and assistive technologies that aid the learning process or help humans maintain stability when riding.

By analogy, to balance during standing or walking, a person must position their mass center above their center of pressure [47, 76]. Doing so requires significant coordination of body movements, especially in challenging balancing tasks [48]. Researchers have quantified this coordination to understand the development of mature gait [102] and to detect differences in balance performance [49, 54, 57, 68]. Unfortunately, this understanding has not yet translated to balancing a bicycle, which further requires coordination of body movements with bicycle movements.

This additional coordination of bicycle and body movements is often learned with the assistance of others and/or with training aids. However, it remains unclear what assistance works best or when a learner is ready to advance to a bicycle without training aids. Typical training aids include training wheels and balance bikes. Training wheels

significantly increase the base of support when a bicycle begins to tip. The same effect arises on pedal-less balance bikes on which a learner uses his/her feet to propel the bicycle forward. Additionally, a balance bike rider's feet can also readily stabilize the bike during incipient tipping. A relatively new training aid [103] uses a gyroscope mounted in the front wheel to augment stability. While any of these training aids can ultimately help riders learn to ride, it remains unclear what underlying skill (or set of skills) defines this learning process.

The task of human/bicycle balance is complex and not well understood. While recent studies expose the self-stability of bicycles alone [2], other studies demonstrate that humans can readily balance bicycles that lack self-stability [16, 17]. In addition, a number of proposed control systems successfully stabilize bicycle models [5, 7, 19, 30], yet they do not model or expose the human learning process. Despite our lack of understanding of this learning process, the basic strategy to keep a bicycle upright, namely steering into the lean, is well known. Schwab et al. [7] demonstrate that a simple steer-into-the-lean intuitive controller is capable of stabilizing a bicycle. Likewise, a patented training method [104] reinforces this skill. Kooijman et al. [11] further explain that the aforementioned self-stability of a bicycle results from its reaction to steer into the lean. Clearly, balancing a bicycle requires a specific relationship between steer and lean dynamics.

Doyle [16] demonstrated this relationship by measuring the cross-correlation of bicycle steer and lean (also referred to as roll) responses. In particular, the steer angle was highly correlated to the roll angle at some time shift or lag. Similar to the findings of Doyle are the findings of van Lunteren and Stassen [105] who utilized a bicycle simulator to study

human/bicycle dynamics. Their results confirm that the steer angle lags and is highly correlated to the roll angle. A human riding a bicycle represents a closed-loop system in which the rider employs sensory feedback to achieve stabilization of the bicycle/rider system. Because successful bicycle riding requires a well-defined relationship of steer and roll dynamics, we hypothesize that this relationship must also develop as a novice rider successfully learns to ride.

The objective of this study is to quantify how human subjects learn to ride a bicycle by tracking key kinematic changes in bicycle roll and steer dynamics during the learning process. The subjects for this study are children who participated in a specialized bicycle training camp called *Lose the Training Wheels*; refer to www.losethetrainingwheels.org. Children enter this camp having no ability to ride a bicycle and either acquire that ability or make significant progress towards that goal by the end of the week-long camp [46, 106]. Therefore, this camp provides an ideal setting for tracking the changes that arise as a child transitions from a non-rider to a rider. A previous analysis of pilot data [107] helped develop our hypotheses and methods. We hypothesize that the measured bicycle steer and roll angular velocities will become significantly correlated as a successful subject progresses through training. In addition, we hypothesize that the average bicycle speed, the standard deviation of the roll angular velocity, and the standard deviation of the steer angular velocity will all increase with training. We open the Methods section by summarizing the training protocol, instrumentation, experimental protocol, and data analysis methods. In the Results and Discussion section, we quantify the salient changes in the measured kinematical variables that emerge as subjects successfully learn to ride.

4.3 Methods

We measured the steer and roll dynamics bicycles ridden by 15 participants as they progressed through a bicycle training camp organized by the organization *Lose the Training Wheels*. The camp provides five consecutive days (Monday-Friday) of individual instruction for 75 minutes per day for each participant. The children (ages 8-19 years) in the camp had a range of disabilities, which included primary diagnoses of Down syndrome (n = 3), Autism Spectrum Disorder (n = 10), cerebral palsy (n = 1), and attention deficit hyperactivity disorder (n = 1); Table 4.1 reports subject details. None of the participants were able to ride/balance a bicycle prior to entering the camp. Our goal was to reveal the underlying changes in bicycle steer and roll dynamics as each participant learned to balance a bicycle, regardless of disability. The experimental protocol was approved by the University of Michigan Institutional Review Board and this included written informed consent from parents/guardians and assent from the participating subjects.

Table 4.1. Subject details.

Subject	Age (years)	Learned to ride?	Primary Diagnosis
A	19	yes	Down syndrome
B	15	yes	autism spectrum disorder
C	12	yes	autism spectrum disorder
D	14	yes	autism spectrum disorder
E	9	yes	autism spectrum disorder
F	8	no	Down Syndrome
G	18	yes	autism spectrum disorder
H	10	no	Down Syndrome
I	15	no	cerebral palsy
J	16	no	attention deficit hyperactivity disorder
K	18	yes	autism spectrum disorder
L	11	yes	autism spectrum disorder
M	14	yes	autism spectrum disorder
N	10	yes	autism spectrum disorder
O	10	yes	autism spectrum disorder

4.3.1 *Training camp program*

The training program developed by *Lose the Training Wheels* facilitates success for individuals with disabilities by taking advantage of both innovative teaching techniques and specialized equipment. An overview of the training program is given in [46].

The training camp utilizes adapted bicycles having crowned rollers in place of the rear wheel; refer to Figure 4.1 and Figure 4.2. The roller is driven by a belt from an otherwise standard bicycle transmission. Unlike training wheels, the crowned rollers allow the bicycles to roll/lean similar to traditional bicycles. As a rider demonstrates improvement, the bicycle is altered by increasing the gearing or by changing to a more crowned roller that permits greater bicycle lean (less stability) (Figure 4.2). The concept underlying the design of the adapted bicycles is explained in [18], which states that the adapted bicycles behave similar to traditional bicycles, but allow self-stabilizing behavior to be maintained

at slower speeds. During training each participant is accompanied by a trainer, who assists and protects the participant.

Participants typically begin the camp using roller number 3, which allows modest lean and substantial stability; refer to Figure 4.2. The participants ride the adapted bicycles around the perimeter of an indoor gymnasium. The floor manager at the training camp continuously observes the participants to determine which participants are ready to advance to the next roller. Rider improvement is qualitatively evaluated by the floor manager who observes rider pedaling speed, and whether the rider leans into turns, has relaxed arms, and is using the handlebars to turn and control the bicycle. After a rider demonstrates proficiency riding an adapted bicycle with a highly crowned roller (typically roller number 6 in Figure 4.2), the staff moves the rider onto a traditional bicycle. All riders, regardless of skill, are moved onto traditional bicycles on the last day of the camp.

Riders first ride traditional bikes indoors where they are ‘launched’ by the floor manager. To launch a rider, the floor manager uses the handle to push the rider up to speed and then releases the handle, allowing the rider to coast freely. During coasting, the floor manager runs alongside the rider to prevent falls. After demonstrating the ability to balance a bicycle, the participant then practices riding around the perimeter of the gymnasium, working on pedaling and turning skills. After further demonstrating the ability to turn and stop a bicycle, the rider advances to an outdoor paved closed course (paved track or parking lot) where s/he continues developing riding skills.

During training each participant is accompanied by a trainer, who helps guide and protect the participant. Handles attached to all of the bicycles (both adapted and traditional bicycles) allow the trainers to control the speed of the bicycles and allow trainers to catch riders who are in danger of tipping over. Trainers are instructed to only use the handles if their participant is in danger of falling.

Figure 4.1. An adapted bicycle. The adapted bicycles used by *Lose the Training Wheels* utilize crowned rollers in place of a rear wheel. The roller is driven by a belt, which is driven by a pulley connected to a standard bicycle transmission. In addition, the bicycles also have a handle attached to the rear of the bicycle that allows a trainer to assist the rider as needed. For this study, three wireless inertial measurement units (IMUs) were mounted the bicycles: one on the frame (frame mounted IMU), another on the handlebar stem (stem mounted IMU), and one on the spokes of the front wheel (wheel mounted IMU).

Figure 4.2. The rollers used on the adapted bicycles. A series of crowned rollers is used to modify the characteristics of the adapted bicycle. Roller number 1 (top) has the smallest crown (less lean/greater stability) while roller number 8 (bottom) has the largest crown (most lean/least stability). Participants often begin with roller number 3 and end with roller number 6 before advancing to a traditional bicycle.

4.3.2 *Instrumentation*

We employ three wireless inertial measurement units (IMUs) to measure the essential kinematics of the bicycles per Figure 4.1. We utilize two IMU designs. The first is a highly miniaturized wireless IMU developed at the University of Michigan as detailed in [108]. This design includes a 3-axis accelerometer (Analog Devices ADXL345) with a measurement range of ±157 m/s^2 and resolution of 0.038 m/s^2 and a 3-axis angular rate gyro (Invensense ITG-3200) with a measurement range of ±2000 deg/s and resolution of 0.061 deg/s. These components, along with the battery and a switch, are packaged within a small box (40x40x20 mm) yielding a total device mass of 25 grams. The embedded WiFi radio permits synchronous data collection from up to eight IMU nodes. The second IMU is a commercially available design (Yost Engineering, Inc. TSS-DL-HH-S) which includes a 3-axis accelerometer with a measurement range of ±59 m/s^2 and resolution of

0.029 m/s^2 and a 3-axis angular rate gyro with a measurement range of ±2000 deg/s and resolution of 0.070 deg/s all within a small box (35x60x15 mm) and possessing a total mass of 28 grams. This second design does not permit synchronous data collection from multiple nodes and therefore requires introducing a synchronization event (discussed below) to synchronize data during post-processing. Prior to use, all IMUs were calibrated as described in [85].

We mounted three IMU nodes on each bicycle using custom brackets (Figure 4.1). One node was fastened to either the seat tube or downtube of the bicycle (with two sense axes within the plane defined by the bicycle frame). This IMU detects the roll, yaw, and pitch rates of the bicycle frame. A second node mounted to the stem of the bicycle (with one sense axis parallel to the steering axis) detects the rotation of the front assembly, which when used in tandem with the frame mounted IMU, yields the steering rate. A third node was secured to the spokes of the front wheel to detect the angular velocity of this wheel about the front axle, hence the bicycle speed. The University of Michigan design samples the accelerometers at 800 Hz and the gyros at 256 Hz while the Yost IMUs sample the accelerometers and gyros at 1000 Hz. The data reduction section details how the recorded accelerations and angular velocities are reduced prior to analysis.

4.3.3 *Experimental protocol*

We instrumented the bicycle assigned to each participant prior to their arrival to each camp session and recorded the location and orientation of each IMU node. A high precision digital inclinometer (Dong-Do IM-2D) provided the head tube angle (or steer axis tilt) for the stem mounted IMU and the frame tube (or downtube) angle for the frame (or downtube) mounted IMU as shown in Figure 4.3. All angles were measured with the

bicycle secured in an upright position with zero steer angle. We also recorded the European Tire and Rim Technical Organization (ETRTO) tire size of the front wheel so that the circumference of the wheel could be computed. For the traditional bicycles, we also measured the roll or lean angle of the bicycles when they were resting on their kickstands so we could confirm the alignment of the IMUs with the bicycle during data reduction.

To reduce disruptions to the training sessions, no special instructions or explanations were offered to the participants. During each 75 minute session, we recorded data for four 2-minute periods of riding which essentially filled the University of Michigan IMU memory at the chosen sampling rates. For each session, we also recorded the subject identifier, the bicycle used, the roller number and gear, and the starting time for data collection. The riding task for a participant during each session depended on the participant's progress in the camp.

For trials collected using Yost IMUs, we created a synchronization event at the beginning of each trial by subjecting all three IMUs to the same oscillating angular velocity. We accomplished this by holding the handlebars fixed relative to the bicycle frame and rocking the bicycle back and forth about its roll axis. During post-processing, we used the magnitudes of the measured angular velocity vectors to synchronize the data by finding the time shifts needed to align the angular velocities measured by the steer and wheel mounted sensors with the angular velocity measured by the frame mounted sensor.

4.3.4 *Data reduction*

Our goal is to compute three things: roll rate, steer rate, and bicycle speed. The IMUs do not directly measure the quantities of interest, so we must instead use the accelerations and angular velocities measured by the IMUs to make additional calculations. First, the measured accelerations and velocities must be resolved in bicycle-fixed frames relevant to understanding bicycle dynamics (roll/lean and steer).

In order to define the orientation of each IMU relative to the bicycle, we use a combination of the measured accelerations and the frame angles that were measured with the precision digital inclinometer before each training session. First, we use the plots of accelerations versus time and angular velocities versus time for the frame mounted IMU to select a range of data to be used for determining sensor orientation. Ideally, the bicycle was at rest at some point during the trial. Because the acceleration measured by the IMU includes the acceleration of gravity, the IMU functions as an inclinometer when the bicycle is at rest, which makes it easy to extract the IMU orientation relative to the gravitational field. Due to some difficulties with wireless communication when using the custom IMUs, the bicycle was not at rest for some of the trials. For these trials, a period of straight riding at a relatively constant speed was selected to determine IMU orientation. During straight riding at a constant speed the average orientation of the bicycle is upright, so average accelerations can still be used reliably to determine the orientation of the IMU. After selecting an appropriate section of data (either when the bicycle is at rest or going straight at a relatively constant speed), we then calculate the average acceleration along each sensor axis for the selected time range. Using the average accelerations, we construct rotation matrices that allow us to resolve the accelerations and

angular velocities measured in sensor-fixed frames $(\hat{e}_1, \hat{e}_2, \hat{e}_3)$ and $(\hat{e}_4, \hat{e}_5, \hat{e}_6)$ into accelerations and angular velocities in bicycle-fixed frames $(\hat{e}_i, \hat{e}_j, \hat{e}_k)$ and $(\hat{e}_l, \hat{e}_m, \hat{e}_n)$; these frames are shown in Figure 4.3.

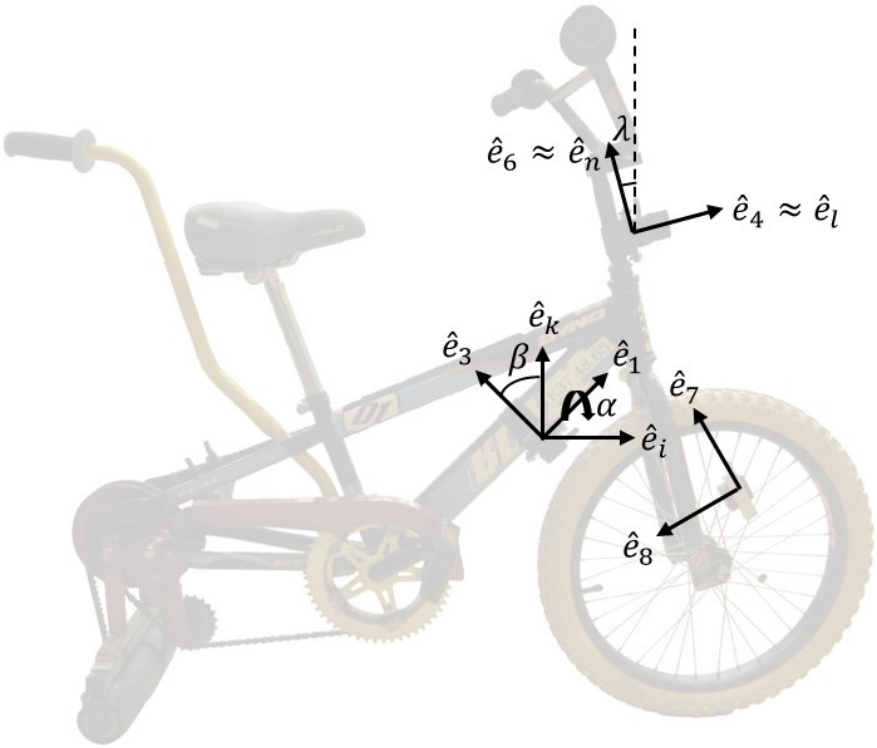

Figure 4.3. The sensor-fixed and bicycle-fixed frames. Measurements in the sensor-fixed frames $(\hat{e}_1, \hat{e}_2, \hat{e}_3)$ and $(\hat{e}_4, \hat{e}_5, \hat{e}_6)$ must be resolved in bicycle-fixed frames relevant to understanding bicycle dynamics; $(\hat{e}_i, \hat{e}_j, \hat{e}_k)$ for roll/lean motion and $(\hat{e}_l, \hat{e}_m, \hat{e}_n)$ for steer motion. The rotation angles α and β are used to align the sensor-fixed frame $(\hat{e}_1, \hat{e}_2, \hat{e}_3)$ with the bicycle-fixed frame $(\hat{e}_i, \hat{e}_j, \hat{e}_k)$. The steer axis tilt angle, λ, is used when resolving the steer rate. The frame $(\hat{e}_4, \hat{e}_5, \hat{e}_6)$ is not always exactly equal to $(\hat{e}_l, \hat{e}_m, \hat{e}_n)$ due to potential slight misalignment of the two frames.

For the frame mounted IMU, we first calculate two rotation angles (α and β) using the average measured accelerations in the frame mounted IMU sensor-fixed frame:

$$\alpha = \tan^{-1}\left(\frac{-a_2}{a_3}\right) \tag{4.1}$$

$$\beta = \tan^{-1}\left(\frac{a_1}{a_3\cos\alpha - a_2\sin\alpha}\right) \tag{4.2}$$

where a_1, a_2, and a_3 are the average measured accelerations in the frame mounted IMU sensor-fixed frame. The calculated rotation angles (α and β) are then compared to expected rotation angles, which are calculated using the known location and orientation of the IMU and the frame angles previously measured with the digital inclinometer. For example, if the IMU is mounted to the downtube of a bicycle that has been secured in an upright position (zero roll angle), we would expect one of the calculated rotation angles (β) to be equal to the angle that the downtube makes with horizontal (±5° due to misalignment or error) and the other calculated rotation angle (α) to equal approximately zero (±5° due to misalignment or error). In the case of an upright bicycle the bicycle-fixed frame is aligned with the inertial frame. The orientations of all frame mounted IMUs used for all trials were double-checked in this way. Only after confirming that the IMUs were oriented as expected did we proceed with the data processing.

For a bicycle leaning on a kickstand, one rotation angle should be equal to the previously measured roll of the bicycle on its kickstand, plus or minus some error. In this case the rotation angle needed to align the sensor-fixed frame with the bicycle-fixed frame (α) was corrected using the measured roll of the bicycle on its kickstand.

Next, the rotation matrix (${}^{ijk}R^{123}$) is defined to allow us to resolve the accelerations and angular velocities in the sensor-fixed frame to accelerations and angular velocities in a bicycle-fixed frame.

$$ {}^{ijk}R^{123} = \begin{bmatrix} \cos\beta & 0 & -\sin\beta \\ 0 & 1 & 0 \\ \sin\beta & 0 & \cos\beta \end{bmatrix} \begin{bmatrix} 1 & 0 & 0 \\ 0 & \cos\alpha & \sin\alpha \\ 0 & -\sin\alpha & \cos\alpha \end{bmatrix} \tag{4.3} $$

We then apply the rotation matrix to the time series of measured accelerations and angular velocities in the frame mounted IMU sensor-fixed frame $(\hat{e}_1, \hat{e}_2, \hat{e}_3)$, yielding measured accelerations and angular velocities in the bicycle-fixed frame $(\hat{e}_i, \hat{e}_j, \hat{e}_k)$.

$$ \begin{bmatrix} a_i \\ a_j \\ a_k \end{bmatrix} = {}^{ijk}R^{123} \begin{bmatrix} a_1 \\ a_2 \\ a_3 \end{bmatrix} \tag{4.4} $$

$$ \begin{bmatrix} \omega_i \\ \omega_j \\ \omega_k \end{bmatrix} = {}^{ijk}R^{123} \begin{bmatrix} \omega_1 \\ \omega_2 \\ \omega_3 \end{bmatrix} \tag{4.5} $$

The roll rate of the bicycle frame is the component of angular acceleration in the $\hat{e}_i$ direction measured by the frame mounted IMU:

$$ \dot{\phi} = \omega_i \tag{4.6} $$

For the stem mounted IMU, we ensured that one axis of the IMU ($\hat{e}_6$) was parallel to the steer axis of the bicycle. Similar to the frame mounted IMU, we used average measured accelerations and measured bicycle angles to check the alignment of the IMU relative to the bicycle steer axis. We define the sensor-fixed axis for the stem-mounted IMU by $(\hat{e}_4, \hat{e}_5, \hat{e}_6)$. Misalignment of the IMU axes with the steer axis was corrected using a

procedure similar to that described above for resolving measurements in the sensor-fixed frame $(\hat{e}_4, \hat{e}_5, \hat{e}_6)$ into a bicycle-fixed frame $(\hat{e}_l, \hat{e}_m, \hat{e}_n)$.

After resolving the IMU measurements in bicycle-fixed frames, we can calculate the steer rate. The stem-mounted IMU measures both the angular velocity due to rotations of the bicycle frame and due to rotations of the bicycle front assembly (handlebars, stem, and fork) relative to the bicycle frame. Steer velocity or rate is defined as the rotation rate of the front assembly relative to the bicycle frame. Therefore, the angular velocities measured by the frame mounted IMU and stem-mounted IMU must be used to resolve the steer velocity.

First the angular velocities measured by the frame-mounted IMU that are resolved the bicycle-fixed frame $(\hat{e}_i, \hat{e}_j, \hat{e}_k)$ must be resolved the bicycle-fixed frame $(\hat{e}_l, \hat{e}_m, \hat{e}_n)$:

$$\begin{bmatrix} \omega_{lf} \\ \omega_{mf} \\ \omega_{nf} \end{bmatrix} = \begin{bmatrix} \cos\lambda & 0 & -\sin\lambda \\ 0 & 1 & 0 \\ \sin\lambda & 0 & \cos\lambda \end{bmatrix} \begin{bmatrix} \omega_i \\ \omega_j \\ \omega_k \end{bmatrix} \tag{4.7}$$

where λ is the measured steer axis tilt or head angle of the bicycle. After resolving the angular velocities in the bicycle-fixed frame $(\hat{e}_l, \hat{e}_m, \hat{e}_n)$ with an axis parallel to the steering axis, the steer velocity or rate ($\dot{\delta}$) is given by:

$$\dot{\delta} = \omega_{nf} - \omega_{ns} \tag{4.8}$$

where ω_{ns} is the angular velocity in the $\hat{e}_n$ direction measured by the stem mounted IMU and ω_{nf} is the angular velocity in the $\hat{e}_n$ direction measured by the frame mounted IMU.

We calculate the speed of the bicycle by using the magnitude of the angular velocity measured by the wheel-mounted IMU (ω_{wheel}) and the estimated front wheel circumference ($2\pi r_f$). The magnitude of the angular velocity of the front wheel can be calculated by:

$$|\omega_{wheel}| = \sqrt{(\omega_7)^2 + (\omega_8)^2 + (\omega_9)^2} \tag{4.9}$$

where ω_7, ω_8, and ω_9 are the components of the angular velocity measured by the wheel mounted IMU in the wheel mounted sensor-fixed frame $(\hat{e}_7, \hat{e}_8, \hat{e}_9)$. The radius of the front wheel can be estimated using the ETRTO tire size of the front tire, which gives the tire width (w_{tire}) and inner diameter of the tire (d_{tire}) in millimeters:

$$r_f = \left(\frac{d_{tire}}{2} + w_{tire} \right) \tag{4.10}$$

Bicycle speed (v) is then calculated:

$$v = |\omega_{wheel}|(r_f) \tag{4.11}$$

Before analyzing the data, the roll rate ($\dot{\phi}$) and steer rate ($\dot{\delta}$) were low-pass filtered using a fourth-order Butterworth filter with a cutoff frequency of 5 Hz; bicycle speed (v) was low-pass filtered using a cutoff frequency of 10 Hz. After filtering, we used numerical differentiation to calculate steer acceleration ($\ddot{\delta}$) and roll acceleration ($\ddot{\phi}$) from the appropriate signals.

4.3.5 *Data analysis*

Trials with incomplete data sets were discarded resulting in a net retention of 207 out of 250 trials. In each trial retained, we selected periods of riding with approximately constant speed by visual inspection of the computed bicycle speed and the angular velocities of the frame mounted IMU and stem mounted IMU. We use bicycle speed to identify when a subject is moving. Inspection of the angular velocities helps confirm that the subject is riding without assistance, as the oscillations of the signals visibly decrease for an assisted rider. For each period of selected data, we calculated the means and standard deviations of the bicycle speed, steer angular velocity, and roll angular velocity.

We also calculated the normalized cross-correlation [15] of steer angular velocity ($\dot{\delta}$) to roll angular velocity ($\dot{\phi}$) as well as the normalized cross-correlation of steer angular acceleration ($\ddot{\delta}$) to roll angular acceleration ($\ddot{\phi}$); this was done using the *xcorr* function in the MATLAB Signal Processing Toolbox. Cross-correlation analysis is a standard system identification technique [15] that reveals relationships between system inputs and outputs. Depending on the system and experimental methods, cross-correlations may provide detailed information about the plant and/or controller transfer functions [61]. We squared the peak value of the normalized cross-correlation to yield the peak coefficient of determination, or R^2 value, between the two signals. The R^2 value provides a measure of the similarity between two signals. We recorded the time shift between the two signals required to produce the peak R^2 value; the time shift provides a measure of the lag or delay before a change in one signal is correlated to a change in the other signal. For bicycle riding, changes in steer angular velocity/acceleration typically lag changes in roll

angular velocity/acceleration. We used the time shift for peak correlation between signals to calculate the linear least-squares fits between both the steer and roll angular velocities and steer and roll angular accelerations. For these fits, we used the roll angular velocity/acceleration as the predictor. The slope of the linear fit can be thought of as a simple gain between steer and roll velocity/acceleration.

We performed our statistical analyses using an alpha level of 5% ($\alpha = 0.05$). We used mixed linear models [109] (allowing us to account for repeated measures and unequal variances) to test for the significant effects of training time. We implemented the mixed linear models using a statistics package (IBM SPSS Statistics), assuming an auto regressive covariance model with an order of one. We included a fixed effect of training time and a random effect of bicycle type (adapted bicycle roller number or traditional bicycle). Because qualitative measurements of rider improvement are used by the bicycle camp staff to determine when a rider is ready to advance to a more challenging bicycle (i.e. a more crowned roller or a traditional bicycle), bicycle type is not independent of training time and therefore we did not include bicycle type as a main effect. We used an independent samples t-test assuming unequal variances to compare the highest peak cross-correlation R^2 values from each rider that learned to ride a traditional bicycle to those who did not learn.

4.4 Results

Results for each of the 15 riders, labeled as subjects A-O, are shown in Figure 4.4 through Figure 4.8. These results include the peak cross-correlation between steer and roll angular velocity (Figure 4.4 and Figure 4.5), the slope of the fit of steer rate to roll

rate (Figure 4.6), the standard deviation of the steer angular velocity (Figure 4.7), and the standard deviation of the roll angular velocity (Figure 4.8). The results of riders who learned to ride a traditional bicycle (n = 11) are plotted in black whereas those who were not successful (n = 4) are plotted in gray. Riders that learned to ride were able to start and stop riding without assistance and were capable of riding a minimum of 30 meters independently. Dots signify trials on adapted bicycles whereas open circles signify trials on traditional bicycles. Subjects who advanced to a traditional bicycle but were not successful (subjects F, H, and J) were assisted by trainers who prevented falls. Subject I did not advance to a traditional bicycle. The pilot study [107] contains data for subjects A-J.

Observe in Figure 4.4 that the peak cross-correlation between steer and roll angular velocities increased significantly with training time for all trials ($F = 44.203$ $p < 0.001$) as well as for the subset of trials on adapted bicycles ($F = 14.861$, $p = 0.001$). Those subjects who successfully learned to ride a traditional bike also exhibited significantly higher maximum peak cross-correlation compared to those who did not learn ($t = 5.434$, $p = 0.003$) as reported in Figure 4.5. Regardless of subject, the peak cross-correlation between the steer and roll angular velocities always occurred at negative time shift values, indicating that changes in steer angular velocity always lag changes in roll angular velocity. This is consistent with the expectation that a rider must steer into the lean in order to maintain balance. Interestingly, there was no significant change in the time shift with training time ($F = 2.066$, $p = 0.157$). For all trials, the mean and standard deviation of the time shift were -90.1 ms and 32.5 ms, respectively. The slope of the linear least-squares fit of the steer angular velocity to the roll angular velocity reported in

Figure 4.6 increased significantly with training time for all trials ($F = 31.931$, $p < 0.001$) as well as for the subset of trials on adapted bicycles ($F = 27.300$, $p < 0.001$).

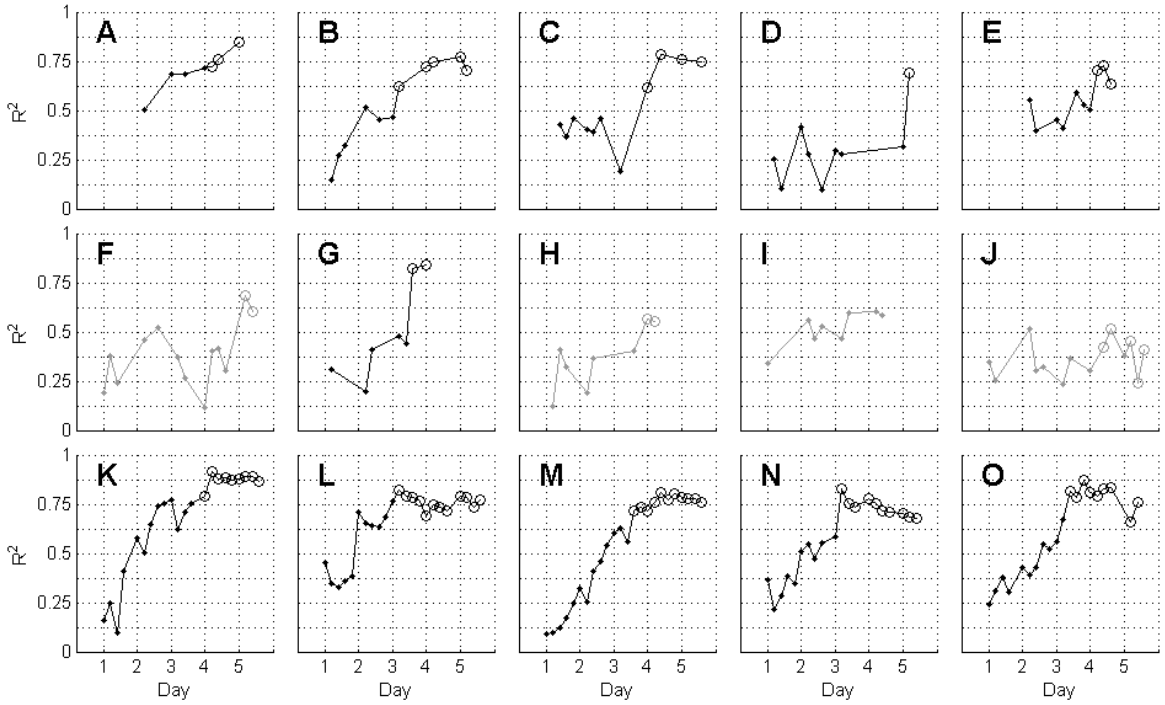

Figure 4.4. Peak cross-correlation squared (R^2) between steer and roll angular velocities versus training day/time for each subject (labeled A-O). Results of riders who learned to ride a traditional bicycle are plotted in black, whereas those who did not are plotted in gray. Dots signify trials on adapted bicycles whereas open circles signify trials on traditional bicycles. The peak cross-correlation significantly increased with training time ($F = 44.203$, $p < 0.001$).

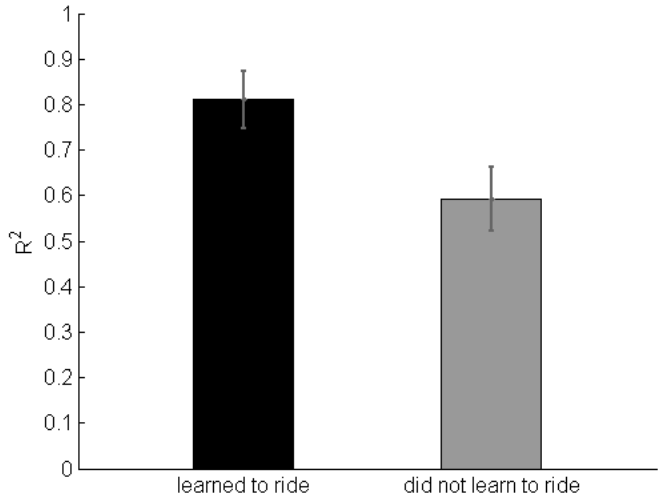

Figure 4.5. Mean peak cross-correlation squared (R^2) between steer and roll angular velocities of those who learned to ride versus those that did not. The error bars represent ± one standard deviation. Riders who learned to ride a traditional bicycle exhibited a significantly higher correlation between steer and roll angular velocities than riders who did not learn (t = 5.434, p = 0.003).

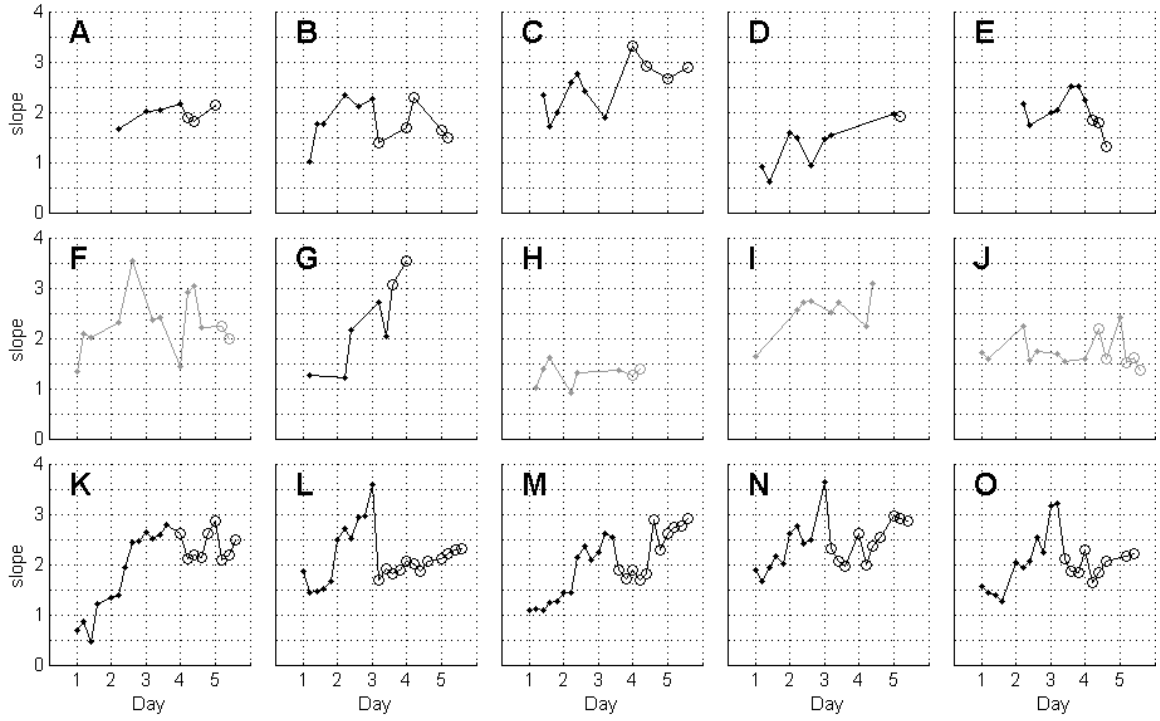

Figure 4.6. Slope of the linear fit of steer angular velocity to roll angular velocity at the time shift required for peak correlation versus training time. Plots for individual riders (labeled A-O) are provided to illustrate change as riders progressed through the camp. The results of riders who learned to ride a traditional bicycle are plotted in black, whereas the results of riders who did not are plotted in gray. Trials in which the rider rode a traditional bicycle are plotted with a circle. The slope significantly increased with training time (F = 31.931, p < 0.001).

Consistent with the peak cross-correlation between steer and roll angular velocities, the peak cross-correlation between steer and roll angular acceleration also increased significantly with training time for all trials ($F = 41.570$, $p < 0.001$) as well as for the subset of trials on adapted bicycles ($F = 8.606$, $p = 0.006$). The peak cross-correlation between the steer and roll angular accelerations occurred at negative time shift values, indicating that changes in steer angular acceleration lag changes in roll angular acceleration. There was no significant change in the time shift with training time ($F = 0.929$, $p = 0.340$). For the collected trials, the time shift had a mean of -79.2 ms with a standard deviation of 20.2 ms. The slope of the linear least-squares fit of the steer angular acceleration to the roll angular acceleration at the time shift for peak cross-correlation increased significantly with training time for all trials ($F = 36.198$, $p < 0.001$) as well as for the subset of trials on adapted bicycles ($F = 18.115$, $p < 0.001$).

The average speed of the riders increased significantly with time across all trials ($F = 27.660$, $p < 0.001$) and for the subset of trials on the adapted bicycles ($F = 6.055$, $p = 0.018$). The standard deviation of the steering rate reported in Figure 4.7 increased significantly with training time for all trials ($F = 27.579$, $p < 0.001$) and for the subset of trials on the adapted bicycles ($F = 25.196$, $p < 0.001$). Similarly, the standard deviation of the roll rate reported in Figure 4.8 increased significantly with training time for all trials ($F = 30.254$, $p < 0.001$) and for the subset of trials on the adapted bicycles ($F = 8.238$, $p = 0.008$).

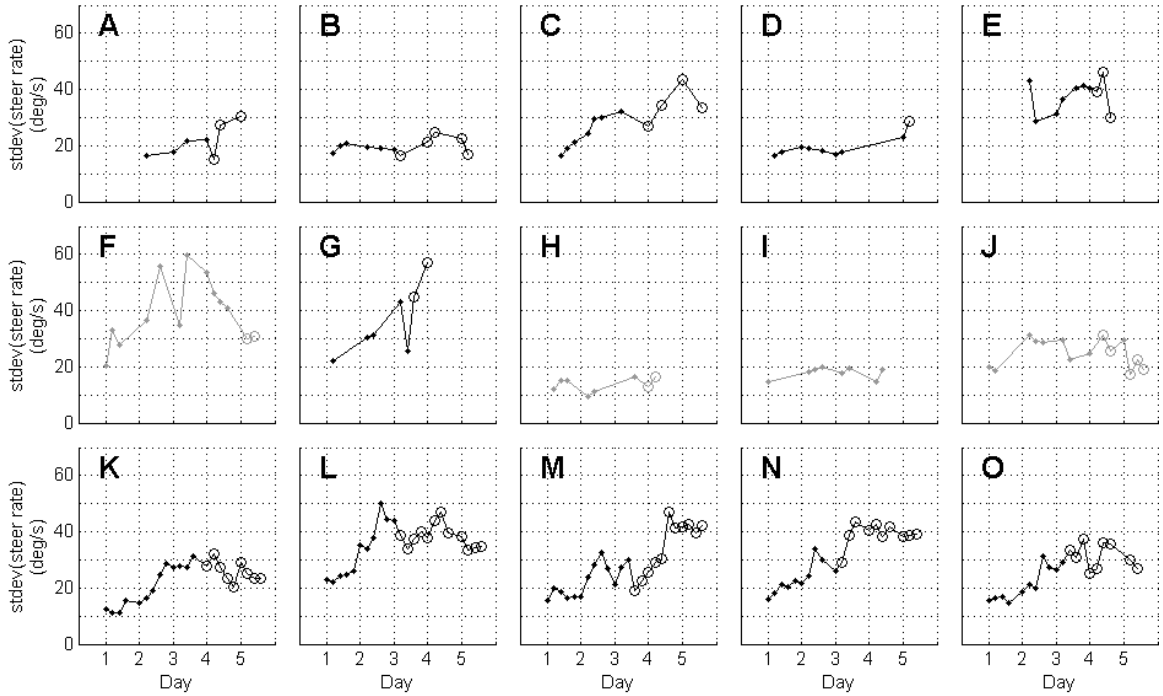

Figure 4.7. Standard deviation of the steer angular velocity versus training time. Plots for individual riders (labeled A-O) are provided to illustrate change as riders progressed through the camp. The results of riders who learned to ride a traditional bicycle are plotted in black, whereas the results of riders who did not are plotted in gray. Trials in which the rider rode a traditional bicycle are plotted with a circle. The standard deviation of the steer rate increased significantly over time for all trials ($F = 27.579$, $p < 0.001$) and for the subset of trials on the adapted bicycles ($F = 25.196$, $p < 0.001$).

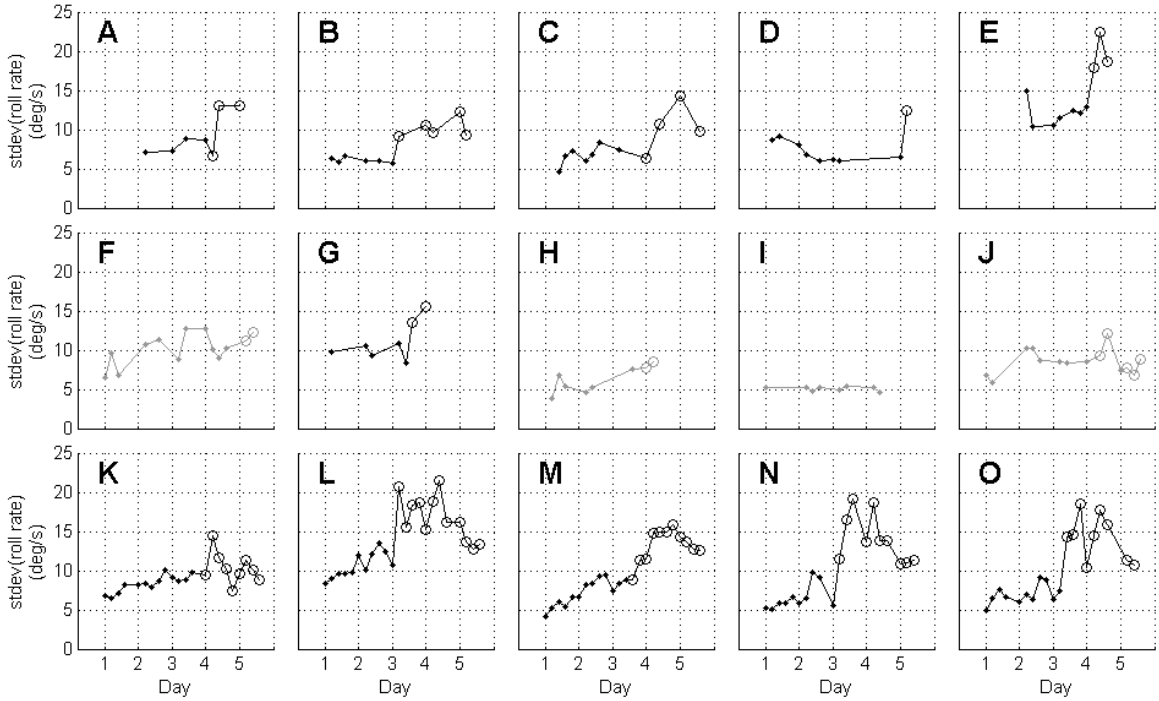

Figure 4.8. Standard deviation of the roll angular velocity versus training time. Plots for individual riders (labeled A-O) are provided to illustrate change as riders progressed through the camp. The results of riders who learned to ride a traditional bicycle are plotted in black, whereas the results of riders who did not are plotted in gray. Trials in which the rider rode a traditional bicycle are plotted with a circle. The standard deviation of the roll rate increased significantly over time for all trials ($F = 30.254$, $p < 0.001$) and for the subset of trials on the adapted bicycles ($F = 8.238$, $p = 0.008$).

4.5 Discussion

The findings reveal that rider learning can be quantified by increasing correlation between the steer and roll angular velocities (and angular accelerations). Novice riders that successfully rode unassisted on traditional bicycles achieved a high cross-correlation (mean peak $R^2 = 0.81$) between steer and roll, similar to the skilled riders of [16] and [105]. However, the peak cross-correlations did not increase similarly for all riders. For example, the peak R^2 between steer and roll velocities (Figure 4.4) for subject M increased steadily with training time, even on the adapted bicycle, whereas it increased little (or even decreased) for subjects C and D until they advanced to a traditional bicycle. Thus, the adapted bicycles appear quite effective for some riders (e.g. subjects B, K, and

M) but not for all. One explanation is that the adapted bicycles offer too much lateral stability for some riders, similar to a bicycle with training wheels, and do not promote the critical learning of steering into the lean. Thus, bicycles that specifically permit roll enhance balance skill, a conclusion that supports the use of balance bicycles and bicycles with pedals removed.

Riders who succeeded riding traditional bicycles without assistance achieved different levels of peak cross-correlation between roll and steer. The peak cross-correlations for successful riders ranged from $0.62 \leq R^2 \leq 0.91$. The mean of these values, $R^2 = 0.81$, is similar to the average value $R^2 = 0.77$ reported in [16] for riders riding a destabilized bicycle. Additionally, subject F achieved relatively high cross-correlation ($R^2 = 0.68$) but was not successful riding a traditional bicycle. Prior studies demonstrate that some riders utilize body lean in addition to steering to maintain balance. Lean control stabilizes a bicycle model [5-7] and leaning alters steer torque [82] (and therefore steer angle). Moreover, experiments utilizing a bicycle simulator [105] demonstrate negative correlation between rider lean and bicycle roll angle. Therefore, it is likely that a rider preferentially using lean control may not exhibit large correlation between steer and roll.

The mean time shift of approximately 90 ms between steer rate and roll rate is consistent with the findings of Doyle [16], who found time shifts ranging from 60 to 120 ms for riders on a destabilized bicycle. As noted by researchers in the study of human standing balance, the time shift between signals is related in a complicated way on the system parameters and on the noise in the system [61, 62]. Therefore, it seems unlikely that the magnitude of the time shift has any meaning for the experimental conditions in this study.

The slopes of the linear fit of steer angular velocity to roll angular velocity and the linear fit of steer angular acceleration to roll angular acceleration increased with training time. However, it is unclear whether this is due to the riders learning to control the bicycles to maintain balance, the increased speed that riders exhibit as they progress through the camp, or due to different dynamic properties of the adapted bicycles. Our results in Chapter 5 demonstrate that the slope decreases with increasing speed, so it is unlikely that the observed increase in this study is related to the increased speed that riders exhibit with training.

As expected, changes in the gearing and the progression from a very stable adapted bicycle to a traditional bicycle were reflected in changes in the average speed and roll rate. Higher gearing results in faster average speeds on the adapted bicycles, and the transition to a traditional bike results in even faster speeds. More crowned rollers theoretically allow the adapted bicycles to tip more, which can result in increased bicycle roll rate. Our results demonstrate that the standard deviation of roll rate does increase with training time, and therefore support the hypothesis transitioning to less stable bicycles increases the roll rates of the bicycles. However, it may be possible that the increased roll rate is an effect of the faster average speeds that riders achieve with increased training. Faster speeds make it possible for a rider to create higher lateral acceleration for a given steer angle, which would result in higher roll rates. Additionally, the standard deviation of the steer rate increased with time, suggesting that initially fearful riders learn to relax their arms and use the handlebars to control and balance the bicycles. The increased steer rates are also likely a result of the subjects responding to increased roll rates.

There are a few limitations to this study. First, the measurements were taken on a population with disabilities, which includes subjects with Down syndrome, cerebral palsy, autism spectrum disorder, and attention deficit hyperactivity disorder. It is not clear how useful the measurements will be for a non-affected population. However, the primary finding that steer must be highly correlated to roll is in agreement with past studies [16, 105, 110] on non-affected populations. Children with disabilities such as Down syndrome and autism spectrum disorder have motor deficits that may make it difficult to learn new motor skills [111, 112]. Despite learning deficits, children with disabilities must still learn the same skill as non-affected children in order to balance a bicycle. Therefore, we are confident in our conclusion that riding a bicycle requires a high correlation between steer and roll.

A second limitation is that measurements were taken on modified bicycles (the adapted bicycles) that are not available to the general public. It is not clear to what degree the adapted bicycles influence or limit performance measures or how the performance measures translate to other training techniques. The dynamics and controls approach used to develop the adapted bicycles has also been applied to develop an 'unrideable' bicycle as well as a bicycle similar to the unrideable bicycle that was made easily rideable by using a bicycle model to guide slight design modifications [18]. Therefore, all of the bicycles (adapted and traditional) have very similar dynamic properties. The main effect of the adapted bicycles seems to be that they reduce the correlation between steer and roll needed to maintain balance. The rear roller on the adapted bicycle functions similar to training wheels, providing a corrective force that allows a rider to maintain balance despite incorrect steering inputs. Unlike training wheels, the adapted bicycles maintain

the ability to roll. Our belief is that the adapted bicycles make it possible for riders to learn incrementally, which is in contrast to the typical fail/succeed nature of learning to ride a traditional bicycle. The incremental learning that riders demonstrate when using the adapted bicycles made it possible to capture the learning process.

Learning to balance a bicycle is only one part of learning to ride. Riders must also learn how to get on a bicycle, how to start pedaling/riding, how to avoid obstacles, and how to stop safely, among other skills. The primary benefit of adapted bicycles and other training aids are that they allow riders to become familiar with the controls of a bicycle and the attention and physical demands that riding a bicycle requires. Adapted bicycles and balance bikes allow riders to focus on learning the dynamics of a bicycle, whereas training wheels and tricycles allow riders to learn pedaling, steering, and traffic skills.

Our results suggest several measures that could be used to quantify the learning of novice riders—especially the peak cross-correlation between steer and roll rates and angular accelerations. Most importantly, we were able to quantify learning by measuring the kinematics of bicycles as a riders trained uninterrupted. These measures could be used to evaluate the effectiveness of existing training techniques and to help develop new training techniques.

4.6 Conclusions

We measured the essential bicycle kinematics of childern with disabilities during a specialized bicycle training camp to unravel how they learn to ride bicycles. Of the 15 subjects, 11 successfully rode a traditional bicycle without assistance by the end of the camp. Three wireless IMUs revealed the bicycle roll rate, steer rate, and speed during the

learning process. The peak value of the cross-correlation between steer and roll angular velocities was significantly greater for the 11 subjects who learned to ride compared to the 4 who did not. This finding suggests that rider learning is quantified by increased correlation between bicycle steer rate and roll rate. In essence, learning to steer in the direction of lean is an essential and quantifiable skill in learning to ride. Average speed also increased with time, likely due to the increased gearing used as a rider progressed through the camp. The standard deviation of the steer rate also increased with time, suggesting that initially fearful riders learn to relax their arms and use the handlebars to balance the bicycles. Existing and future training techniques can be systematically evaluated using this novel method.

Acknowledgements

We thank *Lose the Training Wheels* for providing access to the adapted bicycles and training program and the National Institute on Disability and Rehabilitation Research for a grant to Dr. Dale A. Ulrich that made this research possible.

CHAPTER 5: MEASUREMENT OF HUMAN/BICYCLE BALANCING DYNAMICS AND RIDER SKILL

5.1 Chapter summary

Analytical analyses of the stability of bicycle/rider systems have limited use for understanding the behavior and performance of human bicycle riders and human/bicycle systems. Experimental measurements of human/bicycle dynamics are needed to advance our understanding of how humans maintain balance of a bicycle and to identify metrics useful for quantifying rider skill. In this study, we measure the dynamics of human bicycle riding as 14 subjects ride an instrumented bicycle on training rollers mounted on a force platform at speeds ranging from approximately 1.3 to 7.2 m/s. Of the 14 riders, we classified 7 as cyclists (skilled riders) and 7 as non-cyclists (novice riders). The instrumented bicycle measures steer angle/rate, steer torque, bicycle speed, and bicycle roll rate and also enables the calculation of steering power. A motion capture system enables measurement of the roll angle of the bicycle. A force platform beneath the roller assembly measures the net force and moment that the bicycle/rider/rollers exert on the floor, which enables calculation of the lateral positions of the bicycle/rider center of mass and center of pressure. We find that the cross-correlation of the lateral position of the center of mass to the lateral position of the center of pressure quantifies balance performance, the cross-correlation of steer angle/rate to bicycle roll angle/rate quantifies steer control, and the cross-correlation of rider lean angle to the bicycle roll angle quantifies rider lean control. All riders achieved similar balance performance at the

lowest speed while utilizing similar control strategies. However at higher speeds, skilled riders (cyclists) achieved greater balance performance by employing more rider lean control and less steer control compared to novice riders (non-cyclists). In addition, skilled riders used less steer control effort (measured by average positive steering power and standard deviations of steer angle and rate) and less rider lean control effort (measured by the standard deviation of the rider lean angle) regardless of speed. The reduction in balance effort for skilled riders is not due to any reduced demands for balance. In summary, skilled riders achieve higher levels of balance performance using less effort than novice riders.

5.2 Introduction

There is little understanding of the fundamental characteristics of human bicycle riders, the types of control that humans use to balance bicycles, and the skills that distinguish riders of different ability levels. Humans have ridden bicycles (two-wheeled, single track vehicles) since the early 1800's [1], yet human/bicycle dynamics are far from well understood. Recent work [2] has established the so-called Whipple bicycle model [3] as the simplest model of a bicycle that can predict the self-stability of the bicycle alone; however the behavior of an uncontrolled bicycle provides little insight into the behavior of a bicycle controlled by a human. Identifying the types of control that humans use and differences between skilled and novice riders would simultaneously advance two uses. First, it would provide researchers with metrics to evaluate rider skill and human/bicycle stability; and second, it could provide bicycle designers with tools to objectively measure whether a specific bicycle is better or worse for a particular rider.

Bicycle riding skill or performance has previously been assessed by instructing subjects to ride around a prescribed course or to perform a prescribed task. In general, the time to complete a course/task and the number of errors committed are used to quantify performance. In the majority of studies that use these techniques, the goal has been to evaluate the performance or safety of a particular bicycle or bicycle configuration [35-40]. In a study investigating the maneuverability of children's bicycles [40], Lewis noted that there was more variation between subjects than between the use of different bicycles. The time to complete a course and number of errors were used to investigate the correlation between physical and perceptual-motor abilities and riding performance [41, 42] and to evaluate the effect of alcohol consumption on the ability to safely ride a bicycle [43]. While quantifying performance by time to complete a course/task and the number of errors is useful for the questions posed in these studies, the study results are task specific and do not translate to new tasks. In addition, the methods of quantifying performance do not allow continuous monitoring of skill because the methods rely on completion of specific courses/tasks.

Some research on motorcycles suggests that riders of different skill levels use different body lean relative to the motorcycle and steering torque. For example, Rice [44] found that riders of different skill levels phased body lean and steering torque differently when executing a lane change maneuver. Similarly, Prem [45] found that novice riders in an evasive maneuver used lean torque and steering torque differently from expert riders. Prem also used skill tests to differentiate rider ability, similar to the studies of bicycles mentioned above. However, these studies also provide little insight on how to continuously monitor skill for bicycle riders.

The ability to balance a bicycle is necessary to successfully complete any riding task. Therefore, it seems logical to investigate possible ways to quantitatively evaluate the skill of a rider to balance a bicycle. Other fields of research have investigated human balancing skills and performance and these may also provide insight into how bicycle balancing skill can be quantified. One such field is human postural control.

The tools used to evaluate human postural control are an essential part of both clinical evaluation of patients and research into how humans maintain upright posture. Some of the most basic methods to evaluate human postural control involve monitoring the location of the center of pressure (COP) and the center of mass (COM) of subjects [47]. During standing, the center of mass and center of pressure are highly correlated, with the center of pressure being below and tracking the center of mass [113]. By using an ideal inverted pendulum model of standing balance, Winter [47] explains that the (COP-COM) signal is directly related to the horizontal acceleration of the COM and can be considered to be the error signal detected by the balance control system. The assumption is that the goal of the balance control system is to maintain an upright posture and to control postural sway. While the assumption that human standing balance can be modeled effectively as an inverted pendulum, it is important to note that more complex balancing tasks require a more comprehensive model of the body [48]. Researchers have used COP measurements to investigate standing balance using a wide range of measures, including: root mean square (RMS) distance from the mean COP [49, 50], excursions of the COP [51-53], COP sway amplitude [54], velocity of the COP [55, 56], and the area enclosed by the COP trajectory [55, 57], among others. These studies represent a small sample of the extensive literature in the field of human postural control that utilize measures of

body sway, usually movement of the COP, to quantify balance performance. As a result, these types of measures are utilized by clinicians to identify patients with balance disorders [47, 63, 65].

Similar to research in the field of human postural control, our aim is to identify methods to evaluate human/bicycle control and balance. Studies of human postural control highlight the importance of the relationship between the center of mass and center of pressure. However unlike standing balance, balancing a bicycle is a highly dynamic task that also requires coordination of the human subject and the bicycle. For standing in static situations, stability requires that the vertical projection of the center of mass falls within the base of support; during more dynamic tasks, the projection of the center of mass can fall outside of the base of support, but must remain within some range of the base of the support [76]. By logical extension, it will be important to investigate the relationship of the center of mass to the center of pressure during bicycling.

Previous work highlights possible control methods that can be used by riders [82, 114], methods to quantify control [16, 105, 107], and differences between skilled and unskilled riders [115]. Lean control and steer control are effective methods to maintain stability of a bicycle model [5-7] and are observed experimentally for human riders [24, 114]. Lean control can also be used to alter steer torque [82], which can in turn alter steer angle. Both lean control and steer control can be observed by calculating cross-correlations of lean angle and steer angle/rate with bicycle roll angle/rate [16, 105]. Our pilot experiment found that skilled cyclists steer less and use less power to steer than non-skilled cyclists [115], suggesting that the effort used for control as well as variation of control can be used to distinguish rider skill.

Following from the pilot study, the objectives of this study are three-fold: to quantify 1) the relationship between center of pressure and center of mass movement of the bicycle/rider system, 2) the types of control used by riders, and 3) the differences between skilled and novice riders. We hypothesize that the lateral position of the center of mass will be highly correlated to the lateral position of the center of pressure, steer rate will be highly correlated to the roll rate of the bicycle, rider lean will be highly correlated to bicycle roll, and skilled riders will use significantly less steering effort and variation than novice riders. We open with the Methods section describing the experimental protocol, the instrumentation used to measure human/bicycle dynamics, and data analysis. In the Results and Discussion section, we present the results and quantify differences between skilled and novice riders by highlighting the relationship of the center of mass to the center of pressure, types of control used, and control effort.

5.3 Methods

We tested a total of 14 subjects (4 females, 10 males; age = 26.4 ± 6.0 years, body mass = 71.1 ± 12.8 kg; mean ± standard deviation). The University of Michigan Health Sciences and Behavioral Sciences Institutional Review Board approved the study, and all subjects gave informed consent.

We classified seven subjects as “cyclists” and seven subjects as “non-cyclists.” All cyclists go on training rides regularly, belong to a cycling club or team, compete several times per year, and have experience using rollers for training. Skilled riders often use training rollers, such as those illustrated in Figure 5.1, to practice cycling indoors. All subjects classified as cyclists identify themselves as skilled cyclists. All non-cyclists

know how to ride a bicycle but do so only occasionally for recreation or transportation and do not identify themselves as skilled cyclists.

Figure 5.1. A cyclist riding a bicycle on rollers.

To measure the dynamics of human bicycle riding, we conduct experiments indoors utilizing an instrumented bicycle, a motion capture system, and training rollers mounted on a force platform. The instrumented bicycle from Chapter 2 is again used. Recall that this bicycle has embedded sensors that measure steer angle, steer torque, bicycle speed, and bicycle frame roll rate. In addition, we calculate the steering power from the steer torque and steer angular velocity. The motion capture system measures the positions of three markers attached to the bicycle frame, which we use to calculate the roll angle of the bicycle frame. The force platform beneath the roller assembly measures the net force and moment that the rider/bicycle/rollers exert on the ground. These reactions are later used to calculate the lateral position of the bicycle/rider center of pressure and center of

mass. Utilizing the measured and calculated quantities, we examine standard deviations of signals and cross-correlations between signals to reveal differences in rider skill.

5.3.1 *Protocol*

Each subject rode in five experimental conditions distinguished by pedaling cadence (via a metronome) and bicycle speed (via gearing). The five conditions were executed in the following order: 1) cadence 80 rpm and speed 5.08 m/s, 2) cadence 80 rpm and speed 7.19 m/s, 3) cadence 80 rpm and speed 6.98 m/s, 4) cadence 80 rpm and speed 2.58 m/s, and 5) cadence 40 rpm and speed 1.29 m/s. Each subject rode for a minimum of 2 minutes in each condition until s/he could ride for at least 30 seconds without support. A platform placed over the rollers allows subjects to safely dismount the bicycle and a railing beside the rollers allows subjects to support themselves during trials (Figure 5.2). Some subjects were not able to successfully ride on the rollers at the slowest speed defined in condition 5, and instead rode with a cadence of 50 rpm and a speed of 1.61 m/s. We only instructed riders to ride on the rollers for at least 30 seconds without support and to match their pedaling rate to the beat of the metronome as closely as possible. We did not, for example, instruct riders on how to ride the rollers or what type of control to use.

Figure 5.2. A platform placed over the rollers allows subjects to safely dismount the bicycle and a railing beside the rollers allows subjects to support themselves during trials. The roller drums are mounted to a frame that is attached to a force platform near the center of the assembly.

Prior to the data collection, we allowed all subjects to practice riding the instrumented bicycle on the rollers as long as they needed to become comfortable. During this time, we also ensured that the seat height was set properly for each subject. Cyclists generally needed only a few minutes to familiarize themselves with the instrumented bicycle. Non-cyclists, all of whom had no experience riding on rollers, generally needed 10 to 15 minutes to become familiar with the bicycle and to learn how to ride on rollers.

5.3.2 *Instrumented bicycle*

The instrumented bicycle is described in detail in Chapter 2 and [81, 82]. The instrumented bicycle is a standard geometry rigid (no suspension) mountain bike equipped with slick tires. A torque sensor (Transducer Techniques SWS-20) integrated into the fork steerer tube measures the steer torque applied by the bicycle rider (T_δ) with a range of ±7.512 Nm and a resolution of 0.005 Nm. An optical encoder disk (US Digital HUBDISK-2-1800-1125-I) and encoder module (US Digital EM1-2-1800) capture the

steer angle of the bicycle (δ) with a resolution of 0.1 degrees. Numerical differentiation of the steer angle yields steer angle velocity ($\dot{\delta}$), which when multiplied by steer torque yields the instantaneous power used by the rider to steer the bicycle. Integration of steering power yields the steering work which is further decomposed into positive and negative work components. We obtain the bicycle speed (v) by using the measured circumference of the front wheel and wheel revolutions recorded using a magnetic reed switch and magnet (Cateye 169-9772 and 169-9691). A three-axis accelerometer (Analog Devices ADXL335) and three single-axis angular rate gyros (Murata ENC-03M) measure the acceleration of the bicycle frame with a range and resolution of ±29.43 and 0.067m/s^2, respectively, and the angular velocity of the bicycle frame with a range and resolution of ±300 deg/s and 3.04 deg/s, respectively. From the measured accelerations and angular velocities, we calculate the bicycle roll rate ($\dot{\phi}$) as described in Chapter 4. We sample all signals at 1000 Hz except the steer angle, which is sampled at 200 Hz.

5.3.3 *Motion capture system*

A motion capture system (Optotrak 3020, Northern Digital Inc.) measures the positions of three markers rigidly attached to the headtube of the instrumented bicycle (Figure 5.3) at a sampling rate of 750 Hz. We apply a low-pass filter with a cut-off frequency of 10 Hz to the position data. Using three markers allows us to calculate roll, pitch, and yaw of the bicycle frame relative to an inertial frame. For this study, only the roll angle is required. We calculate the roll angle of the bicycle per:

$$\phi = \sin^{-1}\left(\frac{z_3 - z_2}{|\overrightarrow{r_{23}}|}\right) - \phi_0 \tag{5.1}$$

where z_2 and z_3 are the (vertical) z-coordinates of markers 2 and 3 relative to the inertial frame (Figure 5.4), respectively, $|\overrightarrow{r_{23}}|$ is the magnitude of the position vector from marker 2 to marker 3, and ϕ_0 is the known angle that $\overrightarrow{r_{23}}$ makes with the horizontal plane when the roll angle of the bicycle is zero.

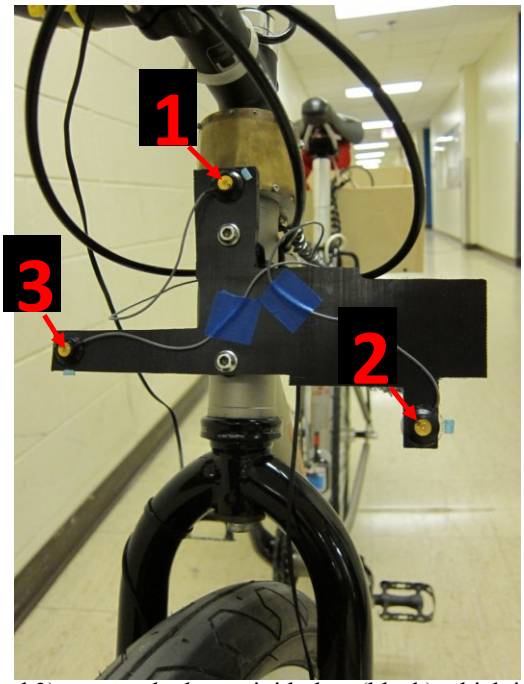

Figure 5.3. Three markers (1, 2, and 3) are attached to a rigid plate (black) which is fixed to the headtube of the bicycle.

The camera system measures the position of the markers with a maximum RMS error of 0.15mm. This RMS error in position translates to the maximum RMS error of 0.09 degrees for the bicycle roll angle.

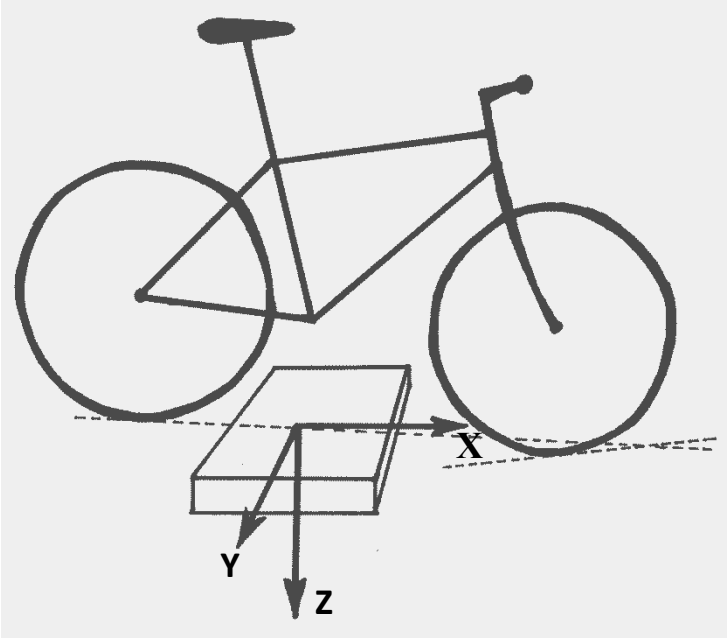

Figure 5.4. Relationship of the bicycle to the inertial frame. The inertial frame (X,Y,Z) is fixed to the force platform. The dashed line tangent to the rear wheel represents the roll axis of the bicycle.

5.3.4 *Force platform mounted rollers*

We chose to study bicycle riding on rollers to investigate the differences between cyclists and non-cyclists. As stated previously, rollers are a type of bicycle training tool that allows a rider to ride his/her bicycle indoors and with limited space. Rollers, which constrain the bicycle in the fore/aft direction but allow free lateral movement, require the rider to maintain balance of the bicycle. While riding on rollers, a rider must pedal and balance the bicycle, similar to riding outdoors. Rollers have existed since the late 1800's; the earliest US Patent for rollers that we identified was issued in 1897 [116]. The dynamics of a bicycle on rollers are similar to that of a bicycle overground [117] with the following distinctions. The cylindrical surface of rollers introduces: 1) a different shape for the tire contact patch, 2) a geometric constraint between the front wheel and front roller as the bicycle steers and yaws, and 3) moments exerted on the rear wheel from the two rollers it contacts [117]. Because the bicycle is stationary in the fore/aft direction,

riders do not experience the same visual cues riding rollers as they do when riding outdoors.

Rollers offer distinct advantages for investigating human/bicycle dynamics. Most importantly, rollers allow one to study bicycle riding in a laboratory setting. Alternatively, one could also employ a treadmill as in [24, 114, 118]. However, rollers weigh less than a treadmill which is advantageous when also mounting to a force platform, which often places strict size limits on ground reactions. In addition, riding on rollers is a safer task than riding on a treadmill. On a treadmill, a rider must carefully maintain both fore/aft and lateral positions, whereas on rollers a rider only needs to maintain lateral position. Stopping riding on rollers poses none of the risks of stopping on a (moving) treadmill. Riding a bicycle on rollers is also more challenging than riding overground, and therefore may be particularly useful in eliciting differences between skilled riders (cyclists) and less skilled riders (non-cyclists).

We designed and constructed custom rollers (Figure 5.5 and Figure 5.6) to be mounted on a force platform (OR6-5-2000, Advanced Mechanical Technology, Inc.). The custom rollers consist of commercially available drums and belt (Kreitler Challenger 4.5, Mountain Racing Products) and a frame built from aluminum T-slotted framing (15 Series T-slotted aluminum and joining plates, 80/20 Inc.). The drums selected for the custom rollers are the largest diameter commercially available. We specifically chose these rollers because larger drums produce less rolling resistance (making it easier for subjects to pedal) and are easier to balance a bicycle on than smaller drums [119]. The construction of the frame allows the rollers to be mounted to a force platform (Figure 5.7) so that the ground reactions acting on the bicycle/rider/roller system can be measured.

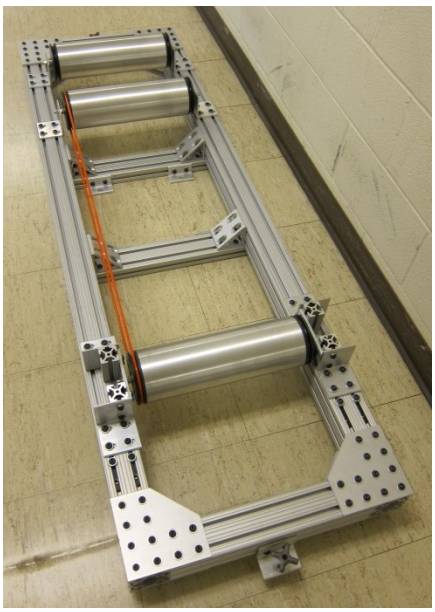

Figure 5.5. The custom rollers.

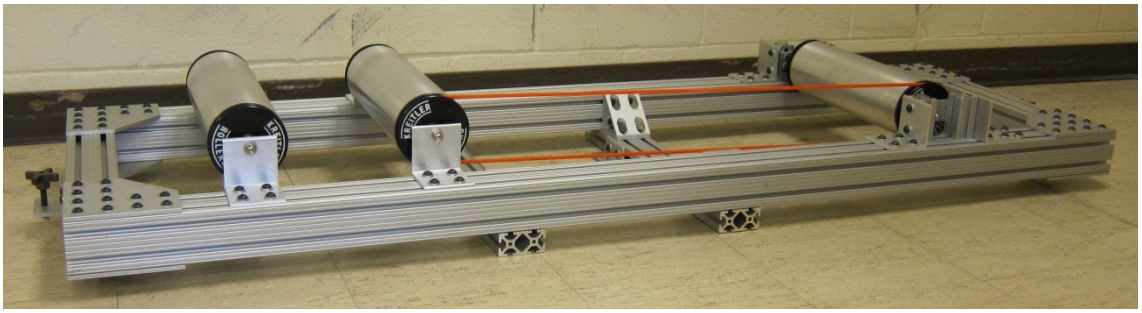

Figure 5.6. The custom rollers.

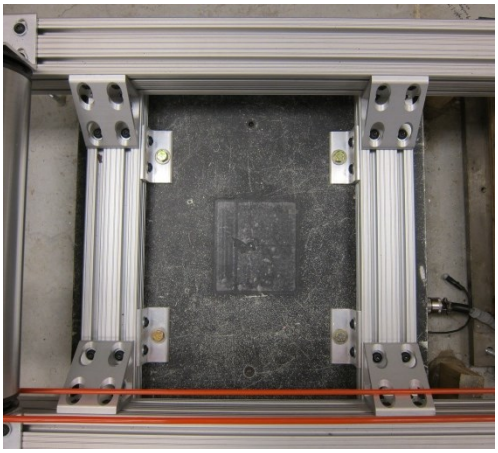

Figure 5.7. The rollers are designed to be bolted to a force platform. Four brackets on the base of the rollers are used to secure the rollers to the force platform using four bolts.

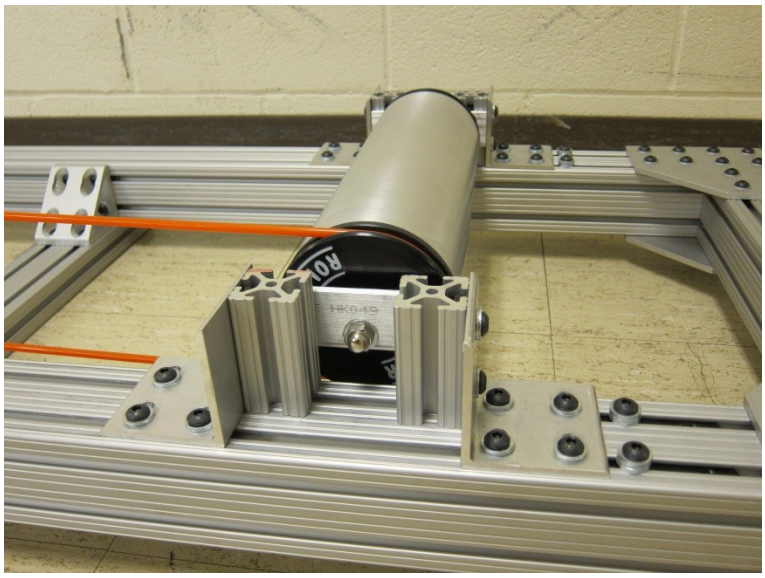

Figure 5.8. The front roller can be adjusted to ensure that the bicycle is level (adjustment up and down) and to ensure that the roller contacts the front tire appropriately (adjustment fore and aft).

Figure 5.9. A photograph of the instrumented bicycle on the custom rollers. Note that the bicycle is leaning against the wall to stay upright.

The design of the custom rollers allows adjustment of both the horizontal and vertical position of the front roller (Figure 5.8), which allows the bicycle to be level (vertical adjustment) and to allow the front roller to contact the front wheel directly below the

front axle (horizontal adjustment). When a bicycle rolls overground, the ground contacts the front wheel directly below the front axle of the wheel. Adjusting the front roller appropriately ensures that controlling the bicycle on rollers is similar to riding overground.

5.3.5 *Calculation of center of pressure and center of mass positions*

We utilize the force and moment measurements from the force platform (OR6-5-2000, Advanced Mechanical Technology, Inc.) to calculate the bicycle/rider/roller center of pressure (COP) and center of mass (COM) locations in the lateral or y-direction. We sample all six channels from the force platform at 1000 Hz. After bolting the rollers to the force platform, we zero all signals. In addition, we also include about 10 seconds of data at the beginning of each trial so that offsets can be identified and removed during post-processing. We apply a low-pass filter with a cut-off frequency of 10 Hz to the measured forces and moments.

The center of pressure is calculated as follows:

$$x_{COP} = \frac{-\left(M_y + F_x d_z\right)}{F_z} \tag{5.2}$$

$$y_{COP} = \frac{\left(M_x - F_y d_z\right)}{F_z} \tag{5.3}$$

where x_{COP} and y_{COP} are the coordinates of the center of pressure, F_x, F_y, and F_z are forces measured by the force platform, M_x and M_y are moments measured by the force platform, and d_z is the vertical distance from the origin of the force platform coordinate system to the plane representing the surface that the bicycle is riding on. The surface is

defined by a horizontal plane tangent to the top surface of front roller. Equations (5.2) and (5.3) assume that the force platform and rollers represent a single rigid body and that there is no couple applied about the x or y axis; creating a pure couple about the x or y axis would require attachment of the bicycle to the rollers. We only are interested in the lateral position of the center of pressure, y_{COP} in the subsequent analysis

To calculate the lateral position of the bicycle/rider center of mass (y_{COM}), we implement a zero-point-to-zero-point integration technique [120, 121] that is a proven for evaluating postural control [120, 122, 123]. Double integration of the bicycle/rider lateral acceleration (a_y) yields displacement of the bicycle/rider center of mass; however, the initial constants of integration (initial velocity and initial position) are not known. The zero-point-to-zero-point integration method is based on the assumption that when the lateral force is zero ($F_y = 0$), the horizontal position of the gravity line and the center of pressure coincide ($y_{COM} = y_{COP}$). By integrating from one zero point to another zero point, both the initial velocity and position can be determined. The zero-point-to-zero-point integration technique is not the only method that can be used to estimate the center of mass displacement using force platform measurements; other methods utilize dynamic models of the balancing system and specific filtering techniques [124-127].

Using force platform data to estimate the center of mass position (kinetics-based method) has several advantages over using a motion capture data (kinematic-based method). Kinematic-based methods rely on modeling the human body with a number of rigid body segments. By estimating the mass properties of each segment, usually using anthropometric data [128], the position of the total-body center of mass can be calculated if the location and orientation of each segment is known [113, 129]. Kinematic-based

methods require the use of many markers so that the location and orientation of each body segment can be measured accurately as well as a sufficient number of cameras to continuously track all markers. In addition, kinematic-based methods are more sensitive than kinetics-based methods to inaccuracies in body segment parameters, especially in regard to segment lengths and head-arms-trunk parameters [123]. By choosing a kinetics-based method to calculate center of mass displacement, we avoid inaccuracies due to errors in estimated body segment properties and, in addition, simplify the experimental setup.

To our knowledge, the zero-point-to-zero-point integration technique has not been applied to study center of mass location during cycling. Therefore, we conducted four trials in which we compared the lateral location of the center of mass calculated from force platform data using the zero-point-to-zero-point integration technique (y_{COMfp}) with that calculated using extensive motion capture data (y_{COMmc}). The kinematic method utilizes a 14-segment model to estimate the total body center of mass [113]. The motion capture system tracks markers attached to each body segment and markers attached to the bicycle frame. Using the known location of the bicycle center of mass relative to the bicycle mounted markers (Appendix A) and assumed mass fractions for each body segment [113], we calculate the center of mass location for the bicycle/rider system.

Similar to [120] and [122], we compared the center of mass location estimated using kinematic data (y_{COMmc}) to that estimated using kinetic data (y_{COMfp}) by calculating: the standard deviation (or root mean square) of each estimate [120], the standard deviation (or root mean square) of the difference between the estimates [120, 122], and the R^2

correlation between the estimates [120]. In addition, we also calculated the slope of the least squares linear fit of y_{COMfp} to y_{COMmc}. In an attempt to quantify the accuracy of the kinematic method estimate of the center of mass location, we numerically differentiated the center of mass lateral position twice to obtain the lateral acceleration of the center of mass ($\ddot{y}_{COMmc}$) and compared the result to the lateral acceleration calculated from the force platform data ($\ddot{y}_{COMfp}$, measured lateral force divided by the mass of the bicycle/rider system). Similar to the center of mass comparisons, we compared the signals by calculating the R^2 correlation and the slope of the least squares linear fit of $\ddot{y}_{COMmc}$ to $\ddot{y}_{COMfp}$. Table 5.1 summarizes the results of these comparisons.

Table 5.1. Comparison of kinematic-based and kinetics-based estimates of center of mass location and acceleration.

trial	stdev (y_{COMmc})	stdev (y_{COMfp})	stdev (y_{COMmc} - y_{COMfp})	R^2 (y_{COMmc}, y_{COMfp})	slope (y_{COMmc},y_{COMfp})	R^2 ($\ddot{y}_{COMfp}$,$\ddot{y}_{COMmc}$)	slope ($\ddot{y}_{COMfp}$,$\ddot{y}_{COMmc}$)
1	16.8 mm	26.2 mm	13.0 mm	0.825	1.41	0.387	0.36
2	17.0 mm	24.7 mm	10.5 mm	0.881	1.37	0.461	0.45
3	22.3 mm	31.5 mm	11.9 mm	0.921	1.36	0.574	0.66
4	18.1 mm	26.1 mm	10.2 mm	0.917	1.38	0.705	0.60

Similar to the findings of [120], we find that y_{COMfp} is highly correlated to y_{COMmc}. In [120], the authors report cross-correlations (R) between the kinetics-based method to the kinematic-based method ranging from 0.79 to 0.96, which translate into R^2 correlation values between 0.62 and 0.92. Therefore, the cross-correlation results indicate that utilizing the zero-point-to-zero-point integration technique for bicycle riding seems to be as good if not better than using the technique for postural analysis. As evidenced by the standard deviations of y_{COMmc} and y_{COMfp} and the slope of the linear fit of y_{COMfp} to y_{COMmc}, the kinetics-based approach results in estimates of y_{COM} approximately 40% greater than the kinematic-based approach, with an RMS difference of about 11mm;

these results suggest that perhaps using the zero-point-to-zero-point integration technique introduces some error due to the assumption that y_{COMfp} is equal to y_{COP} when the lateral force is zero. However, there is a low correlation of $\ddot{y}_{COMmc}$ to $\ddot{y}_{COMfp}$ and $\ddot{y}_{COMmc}$ is approximately 50% less than $\ddot{y}_{COMfp}$; these results suggest that using a kinematic-based approach may also be inaccurate. One explanation is that modeling the bicycle/rider as a system of rigid links does not allow small but important motions to be measured accurately during bicycle riding, which results in errors in y_{COMmc}. Using a kinematic-based approach may be inaccurate in arriving at the acceleration of the mass center due to errors introduced in successive differentiations. For our application, we believe the kinetics-based method is superior because it is not sensitive to errors in marker placement, errors in modeling the body, and errors in body segment parameters.

5.3.6 *Rider lean angle and rider lean rate*

In addition to the prior measurements and calculations, we also calculate a rider lean angle (ϕ_{lean}) and rider lean rate ($\dot{\phi}_{lean}$). We define the rider lean angle (Figure 5.10) as:

$$\phi_{lean} = \phi_{COM} - \phi \tag{5.4}$$

where ϕ is the bicycle roll angle and ϕ_{COM} is the angle formed by the line connecting the center of pressure (y_{COP}) and the center of mass (y_{COM}) with vertical; see Figure 5.10. The rider lean angle quantifies how a rider is shifting his/her center of mass relative to the bicycle. Note that a rider lean angle can be created in many ways, including: leaning the upper body, shifting laterally on the bicycle saddle, knee movements, arm movements, and head movements. We use the term “rider lean angle” for simplicity, as all of these

motions can have the effect of moving a rider's center of mass outside of the plane of the bicycle frame. The center of mass roll angle, ϕ_{COM}, is computed via

$$\phi_{COM} = \sin^{-1}\left(\frac{y_{COM} - y_{COP}}{-z_T}\right) \tag{5.5}$$

where y_{COP} is the lateral position of the center of pressure, $y_{COM}$is the lateral position of the center of mass, and z_T is the location of the bicycle/rider center of mass in the z-direction when the bicycle and rider are upright, as described and as measured in Appendix A and [82]. The rider lean rate ($\dot{\phi}_{lean}$) is calculated from the rider lean angle (ϕ_{lean}) via numerical differentiation.

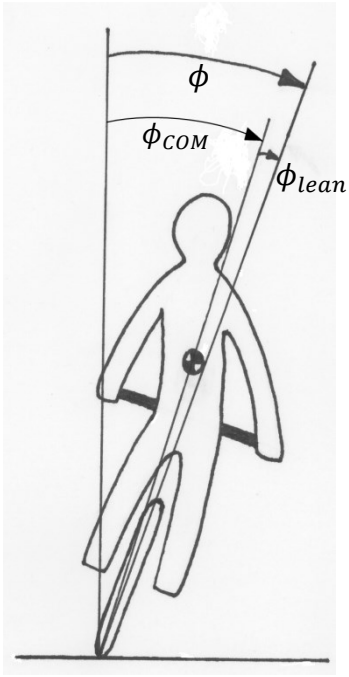

Figure 5.10. Rider lean as viewed from behind the bicycle/rider. The rider lean angle quantifies how a rider is shifting his/her center of mass relative to the bicycle. The arrows define the positive sense of all angles. Rider lean (ϕ_{lean}) is defined as the center of mass roll angle (ϕ_{COM}) minus the bicycle roll angle (ϕ). For the example illustrated, the rider lean angle is negative.

5.3.7 *Selection of data for analysis*

As discussed in Section 5.3.1, each subject rode continuously for at least 30 seconds in each trial. To identify periods of continuous riding, we examined plots of: vertical force measured by the force platform (F_z), steer torque (T_δ), and bicycle speed (v). We use bicycle speed to identify when a subject is pedaling. Inspection of the vertical force reveals when a subject is supported by the railing or platform (decrease in vertical force). Examination of the steer torque also identifies periods that a subject uses the railing for support (oscillations decrease, non-zero offset). After identifying a period of continuous riding, we use only the last 30 seconds of each period for analysis.

5.3.8 *Statistics*

In order to quantify rider skill, we looked at the standard deviations of signals, cross-correlations between signals, and linear relationships between cross-correlated signals. Normalized cross-correlations [15] are calculated using the *xcorr* function in the MATLAB Signal Processing Toolbox. For a given pair of signals, we square the peak value of the normalized cross-correlation to yield the peak coefficient of determination, or R^2 value, between the two signals. The R^2 value provides a measure of the similarity between the pair of signals. The time shift between two signals required to produce the peak R^2 value provides a measure of the lag or delay before a change in one signal is correlated to a change in the other signal. Using the time shift for peak correlation between a pair of signals, we calculate the linear least-squares fit. The slope of the linear fit can be thought of as a simple gain between signals. We use the following notation for these quantities:

- standard deviation of a signal: stdev(signal)
- peak value of the normalized cross-correlation of signal 2 to signal 1: R^2(signal 1, signal 2)
- time shift of signal 2 to signal 1: lag(signal 1, signal 2)
- slope of linear least-squares fit of signal 2 to signal 1: slope(signal 1, signal 2)

We performed our statistical analyses using an alpha level of 5% ($\alpha = 0.05$). We use mixed linear models [109] (allowing us to account for repeated measures and unequal variances) implemented using a statistics software package (IBM SPSS Statistics) to test for significant effects. We assume an auto regressive covariance model with an order of one and performed our statistical analyses using an alpha level of 5% ($\alpha = 0.05$). The models include effects of rider type (cyclist or non-cyclist), speed, and the interaction of rider type with speed. This approach yields two linear fits (one for each rider type) for each dependent variable. Including the effect of rider type allows each fit to have a different y-intercept, and including the rider type/speed interaction allows each fit to have a different slope. Therefore, significant effects of either rider type or the rider type/speed interaction indicate significant differences between cyclists and non-cyclists.

5.4 Results and Discussion

We present the experimental results in Figure 5.11 through Figure 5.23; statistical results are summarized in Table 5.2. We begin by examining the relationship of the center of mass to the center of pressure and then investigate the types of control used by riders.

After presenting these results, we discuss the differences between cyclists and non-cyclists.

Table 5.2. Summary of statistical tests. Significant effects are denoted with an asterisk (*).

Dependent Variable	Effects					
	rider type		speed		rider type*speed	
	F	*p*	*F*	*p*	*F*	*p*
stdev(δ)	13.904	*0.001	114.264	*< 0.001	2.316	0.136
stdev($\dot{\delta}$)	15.121	*< 0.001	32.223	*< 0.001	0.728	0.397
stdev(T_δ)	24.866	*< 0.001	10.870	*0.002	2.439	0.124
stdev(ϕ)	12.081	*0.001	0.650	0.800	0.813	0.372
stdev($\dot{\phi}$)	5.304	*0.027	31.998	*< 0.001	7.753	*0.007
stdev(ϕ_{lean})	19.643	*< 0.001	4.885	*0.031	0.750	0.390
stdev(ϕ_{COM})	3.106	0.086	9.013	*0.004	7.402	*0.009
stdev(y_{COP})	3.695	0.059	25.294	*< 0.001	0.037	0.848
stdev(y_{COM})	2.483	0.120	29.458	*< 0.001	0.627	0.431
$R^2(\phi, \delta)$	1.501	0.228	214.928	*< 0.001	10.951	*0.002
lag(ϕ, δ)	0.036	0.851	30.815	*< 0.001	3.617	0.063
slope(ϕ, δ)	0.632	0.432	167.203	*< 0.001	1.481	0.230
$R^2(\dot{\phi}, \dot{\delta})$	0.411	0.526	34.307	*< 0.001	4.650	*0.035
lag($\dot{\phi}, \dot{\delta}$)	0.799	0.377	10.357	*0.002	1.624	0.208
slope($\dot{\phi}, \dot{\delta}$)	0.673	0.417	142.123	*< 0.001	1.269	0.266
$R^2(\phi, \phi_{lean})$	0.182	0.672	32.948	*< 0.001	17.639	*< 0.001
lag(ϕ, ϕ_{lean})	0.015	0.902	7.973	*0.006	6.981	*0.010
slope(ϕ, ϕ_{lean})	0.017	0.896	19.220	*< 0.001	13.865	*< 0.001
$R^2(\dot{\phi}, \dot{\phi}_{lean})$	0.863	0.359	1.336	0.252	5.211	*0.026
lag($\dot{\phi}, \dot{\phi}_{lean}$)	2.457	0.125	0.069	0.793	0.969	0.330
slope($\dot{\phi}, \dot{\phi}_{lean}$)	0.852	0.362	43.120	*< 0.001	12.613	*0.001
$R^2(y_{COP}, y_{COM})$	0.041	0.841	29.113	*< 0.001	14.843	*< 0.001
slope(y_{COP}, y_{COM})	0.000	0.998	11.352	*0.001	11.263	*0.001
average positive steering power	19.213	*< 0.001	10.547	*0.002	1.743	0.194
normalized average positive steering power	25.108	*< 0.001	51.694	*< 0.001	10.612	*0.002

5.4.1 ***Relationship between the center of mass and center of pressure***

For a perfectly balanced bicycle/rider traveling in a straight line, we would expect y_{COM} to exactly equal y_{COP}. However during actual bicycle riding, similar to human standing, y_{COM} will not always be exactly equal to y_{COP}. Instead, we expect that the center of mass

will track the center of pressure. Figure 5.11 illustrates, using a representative trial, that the center of mass does indeed track the center of pressure during bicycle riding.

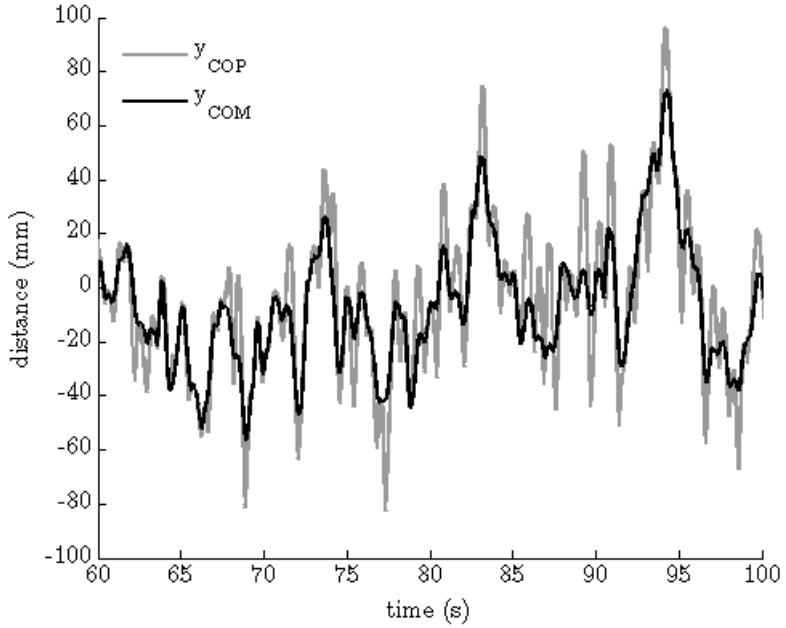

Figure 5.11. Lateral (y) center of pressure location and center of mass location versus time. Data from a representative trial (non-cyclist, v = 7.46 m/s) demonstrates the lateral center of mass location closely tracks the lateral center of pressure location during bicycle riding.

We quantify balance performance by calculating the cross-correlation (R^2) and the slope of the linear least-squares fit of the center of mass location (y_{COM}) to the center of pressure location (y_{COP}). For a perfectly balanced bicycle, both R^2 and the slope would be equal to one (1.0). For actual bicycle riding, the values are less than one. Figure 5.12 and Figure 5.13 illustrate these findings.

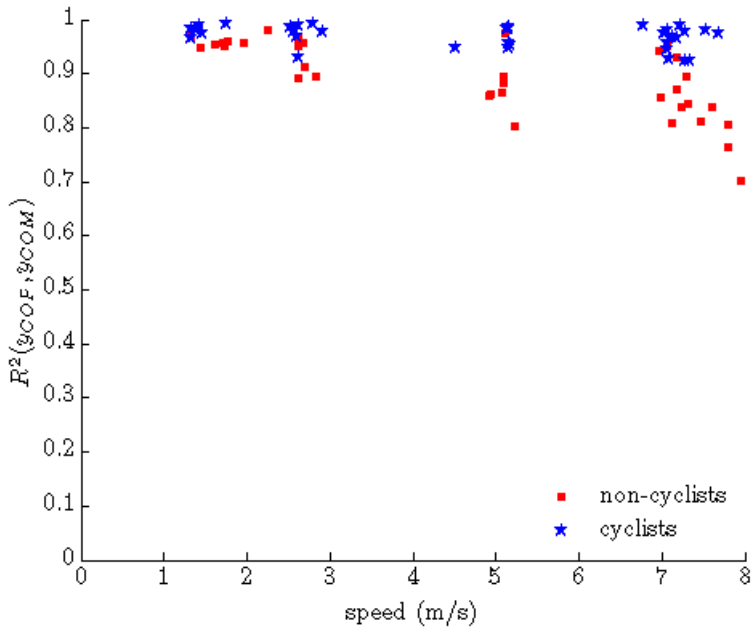

Figure 5.12. Cross-correlation of the lateral position of the center of mass to the center of pressure versus speed. The cross-correlation decreases significantly with increasing speed ($F = 29.113$, $p < 0.001$) and decreases significantly more with increasing speed for non-cyclists than cyclists ($F = 14.843$, $p < 0.001$).

As expected, the lateral positions of the center of mass and center of pressure are highly correlated during bicycle riding (Figure 5.12). Our data do not indicate a significant effect of rider type ($F = 0.041$, $p = 0.841$; see Table 5.2), but do show significant effects for both speed ($F = 29.113$, $p < 0.001$) and the rider type/speed interaction ($F = 14.843$, $p < 0.001$). All riders demonstrate high correlation at low speeds. As speed increases, cyclists maintain higher correlation than non-cyclists. Also as expected, the slope of the linear fit of y_{COM} to y_{COP} is close to one during bicycle riding (Figure 5.13). Similar to the $R^2(y_{COP}, y_{COM})$ results, the slope does not exhibit a significant effect of rider type ($F = 0.000$, $p = 0.998$) but there are significant effects of both speed ($F = 11.342$, $p = 0.001$) and the rider type/speed interaction ($F = 11.263$, $p = 0.001$). Again, cyclists and non-cyclists have slopes close to one at low speeds but the slopes for the non-cyclists diminish significantly at increased speeds. Our findings suggest that riders with higher

skill (cyclists) maintain a higher correlation between lateral center of mass and center of pressure positions than less-skilled riders (non-cyclists) across all speeds.

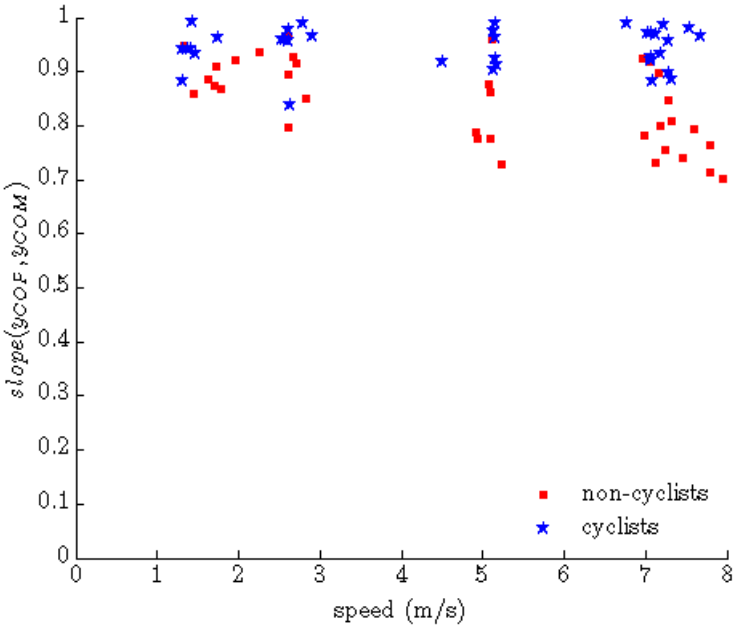

Figure 5.13. Slope of the linear fit of the lateral position of the center of mass to the center of pressure versus speed. The slope decreases significantly with increasing speed ($F = 11.352$, $p = 0.001$) and decreases significantly more for non-cyclists than cyclists ($F = 11.263$, $p = 0.001$).

5.4.2 *Steering*

Bicycle riders utilize two primary control inputs to maintain balance during riding: steering and leaning. Here we investigate how cyclists and non-cyclists utilize steering. Subsequently, we turn attention to rider lean; see Section 5.4.3. As expected, we observe that the steer angle (or steer rate) lags and is correlated to the bicycle roll angle (or roll rate) during riding (Figure 5.14). Similar to the methods used in Chapter 4, we quantify steer control by calculating the cross-correlations between steer angles/rates and bicycle roll angles/rates and the slopes of the linear fits of steer angles/rates to bicycle roll angles/rates.

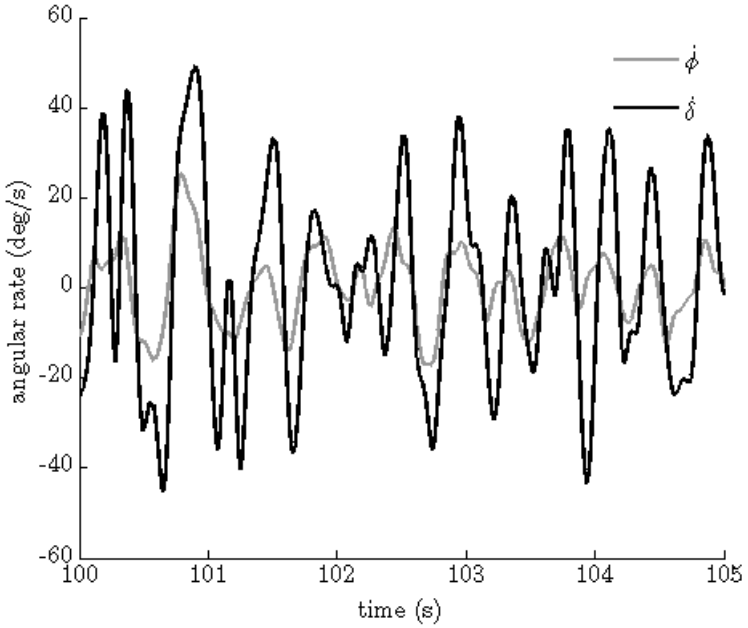

Figure 5.14. Bicycle roll rate and steer rate versus time. Data from a representative trial (non-cyclist, $v =$ 7.96 m/s) demonstrates that the steer rate ($\dot{\delta}$) lags and is correlated to the bicycle roll rate ($\dot{\phi}$) during riding.

All riders demonstrate significant correlation between steer angle and bicycle roll angle and also steer rate and bicycle roll rate; Figure 5.15 illustrates the results for the cross-correlation of steer rate to bicycle roll rate. The cross-correlation of steer rate to bicycle roll rate (Figure 5.15) decreases significantly with increasing speed ($F = 34.307$, $p < 0.001$) and decreases significantly more with increasing speed for cyclists than non-cyclists ($F = 4.650$, $p = 0.035$). The cross-correlation of steer angle to bicycle roll angle results (Table 5.2) are similar to the results for angular rates; the cross-correlation decreases significantly with increasing speed ($F = 214.928$, $p < 0.001$) and decreases significantly more for cyclists than non-cyclists ($F = 10.951$, $p = 0.002$). The peak cross-correlations between steer and bicycle roll rates for the riders in this study are somewhat less than those exhibited by riders who just learned to ride a bicycle (Chapter 4). There are no significant differences between cyclists and non-cyclists in the slope of the linear

least-squares fits of either steer angle to bicycle roll angle or steer rate to bicycle roll rate (Figure 5.16)—only speed has a significant effect (Table 5.2). The results suggest that cyclists and non-cyclists use steering similarly to control the bicycle when riding at low speeds, but then employ different control strategies at higher speeds.

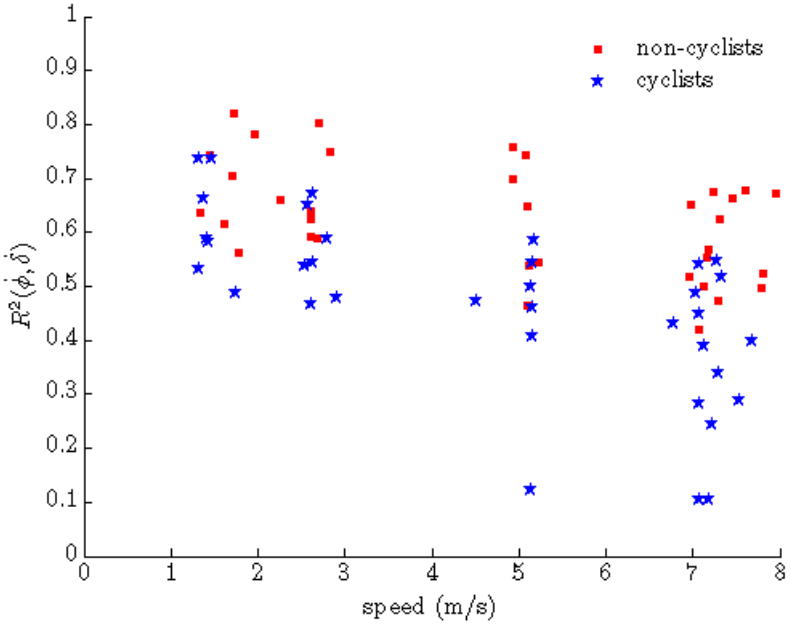

Figure 5.15. Cross-correlation of steer rate to bicycle roll rate versus speed. The cross-correlation decreases significantly with increasing speed ($F = 34.307$, $p < 0.001$) and decreases significantly more with increasing speed for cyclists than non-cyclists ($F = 4.650$, $p = 0.035$).

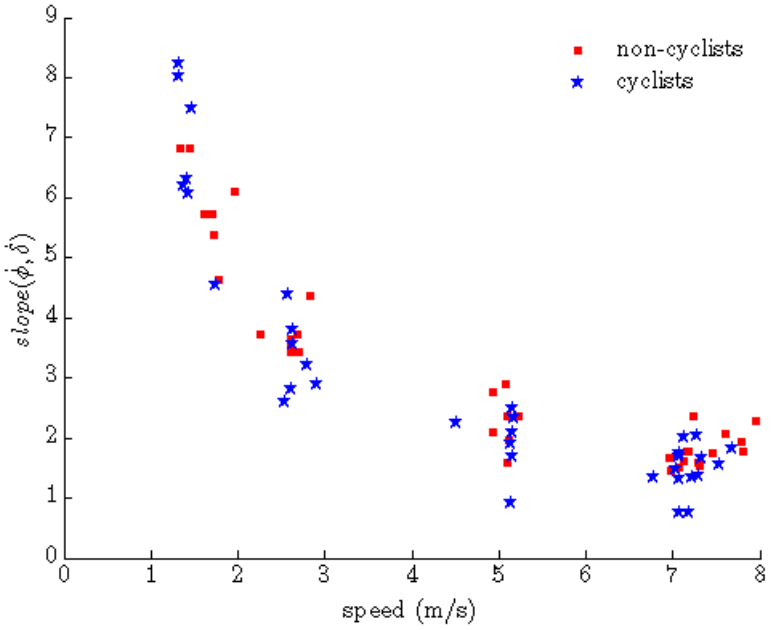

Figure 5.16. Slope of the linear least-squares fit of steer rate to bicycle roll rate versus speed. The slope decreases significantly with increasing speed ($F = 142.123$, $p < 0.001$). There are no significant differences between cyclists and non-cyclists.

To quantify the steering effort, we calculated the standard deviations of the steer angle (Figure 5.17) and steer rate (Table 5.2) and average positive steering power (Figure 5.18). The standard deviations of the steer angle and steer rate and the average positive steering power decrease significantly with increasing speed for all riders (Table 5.2). These results are consistent with subject comments that riding at higher speeds seems easier than riding at lower speeds—lower speeds require more steering effort, as measured by both the variation of the steer angle and the amount of positive power that a rider must produce for steering. Our finding that increased speed results in decreased standard deviation of steer angle is consistent with the results of Moore et al. [114], who found that the variation of the steer angle decreases with increasing speed for a bicycle ridden on a treadmill. Cyclists exhibit less variation of steer angle ($F = 13.904$, $p = 0.001$), less variation of steer rate ($F = 15.121$, $p < 0.001$), and less positive steering power ($F = 19.213$, $p <$

0.001) than non-cyclists. The higher skill level of the cyclists enables less steering effort to maintain balance of the bicycle during riding.

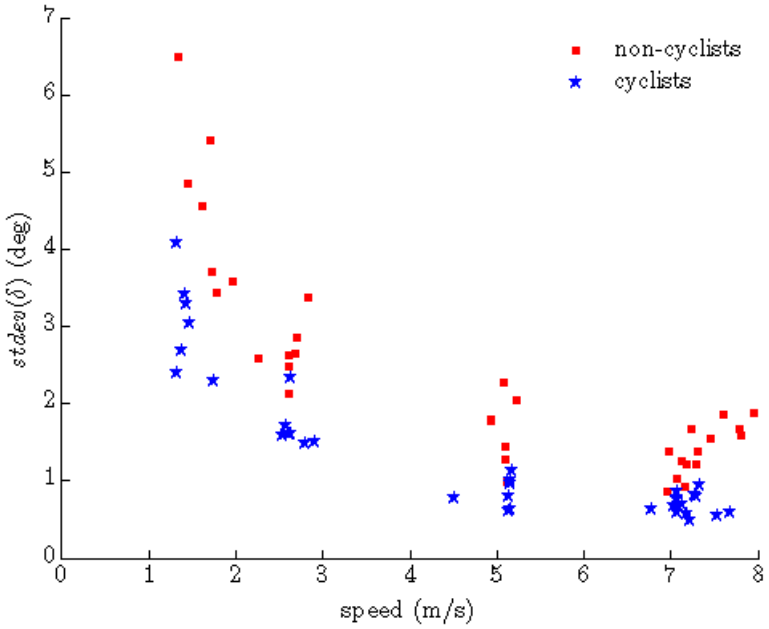

Figure 5.17. Standard deviation of steer angle versus speed. The standard deviation of steer angle decreases significantly with increasing speed ($F = 114.264$, $p < 0.001$). Cyclists exhibit significantly less steer angle variation than non-cyclists ($F = 13.904$, $p < 0.001$).

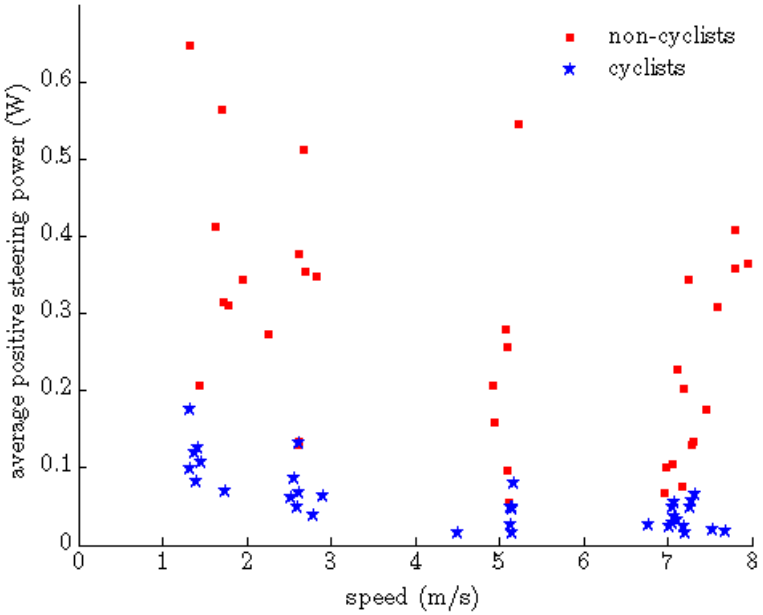

Figure 5.18. Average positive steering power versus speed. All riders produce less positive power to steer the bicycle as speed increases ($F = 10.547$, $p = 0.002$). Cyclists produce less positive power than non-cyclists ($F = 19.213$, $p < 0.001$).

5.4.3 *Rider lean*

We observed that riders utilize body movements to shift the center of mass of the bicycle/rider system outside of the plane of the bicycle frame and use the term "rider lean" to describe the effect of these movements. Refer to Figure 5.10 for definitions of rider lean and bicycle roll angles. During riding, rider lean is correlated with and opposite to the bicycle roll angle, as shown in Figure 5.19. For example, when the bicycle rolls to the left, the rider leans to the right. By leaning to the right, the rider shifts the lateral position of the center of mass of the bicycle/rider closer to the lateral position of the center of pressure. Rider lean is exaggerated and most easily observed when watching a professional road cyclist climb out of the saddle or a BMX racer sprinting—the rider's body remains primarily above the tire contact patch (i.e. center of pressure) as the bicycle rocks back and forth beneath the rider. If rider lean (ϕ_{lean}) is equal and opposite of the

bicycle roll angle (ϕ), then the lateral position of the center of mass (y_{COM}) will be equal to the lateral position of the center of pressure and the center of mass roll angle (ϕ_{COM}) will be equal to zero. If a rider is riding such that y_{COM} is always equal to y_{COP} while the bicycle is rolling, then the cross-correlation (Figure 5.20) and magnitude of the slope of the linear least-squares fit (Figure 5.21) of ϕ_{lean} to ϕ will be equal to one (1.0).

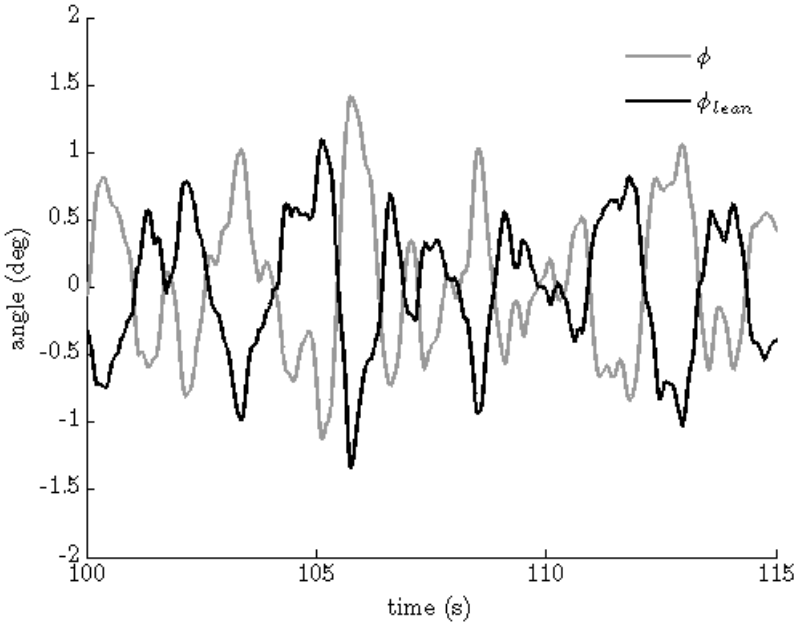

Figure 5.19. Bicycle roll angle and rider lean angle versus time. Data from a representative trial (cyclist, $v = 2.526$ m/s) demonstrates that rider lean (ϕ_{lean}) is highly correlated with and opposite to the bicycle roll angle (ϕ). Refer to Figure 5.10 for definitions of ϕ_{lean} and ϕ.

We quantify rider lean control by calculating the cross-correlations and linear fits of rider lean angle/rate to bicycle roll angle/rate. The cross-correlation of the rider lean angle to the bicycle roll angle (Figure 5.20) decreases with increasing speed for all riders ($F = 32.948$, $p < 0.001$) and decreases more for non-cyclists than cyclists ($F = 17.639$, $p < 0.001$). Similarly, the cross-correlation of rider lean rate to bicycle roll rate decreases more with increasing speed for non-cyclists than cyclists ($F = 5.211$, $p = 0.026$). As expected, rider lean is opposite to bicycle roll, as evidenced by the negative slopes of the

linear fits of rider lean angle to bicycle roll angle (Figure 5.21). Both the slopes of the fits of rider lean to bicycle roll and rider lean rate to bicycle roll rate decrease in magnitude with increasing speed and decrease in magnitude more for non-cyclists than cyclists (Table 5.2). Like the findings for steer control, these results suggest that cyclists and non-cyclists use similar rider lean strategies at low speeds, but use different strategies at higher speeds.

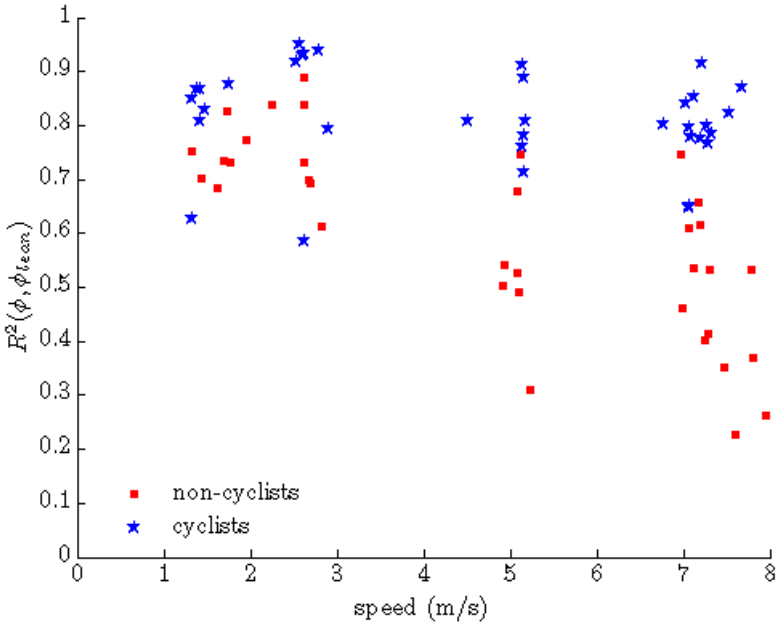

Figure 5.20. Cross-correlation of rider lean angle to bicycle roll angle versus speed. The cross-correlation decreases significantly with increasing speed ($F = 32.948$, $p < 0.001$) and decreases significantly more with increasing speed for non-cyclists than cyclists ($F = 17.639$, $p < 0.001$).

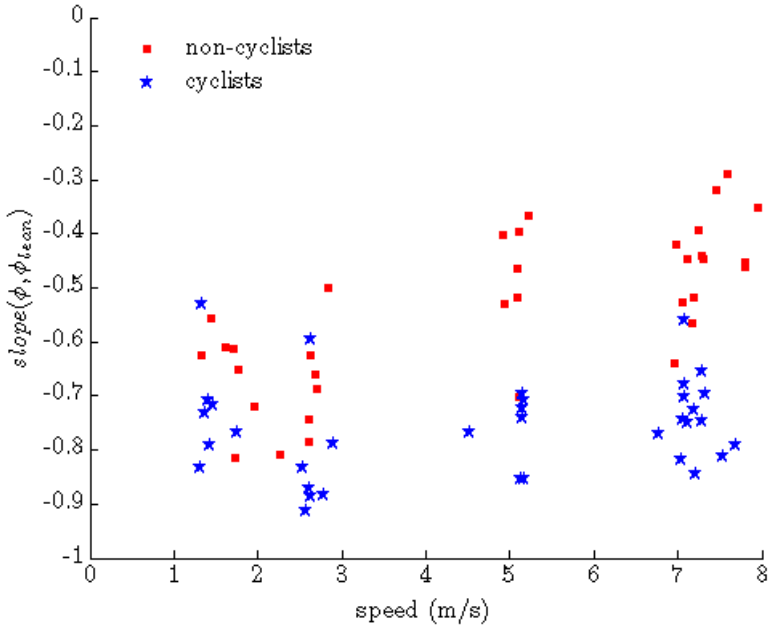

Figure 5.21. Slope of the linear least-squares fit of rider lean angle to bicycle roll angle versus speed. The magnitude of the slope decreases significantly with increasing speed ($F = 19.220$, $p < 0.001$) and decreases significantly more with increasing speed for non-cyclists than cyclists ($F = 13.865$, $p < 0.001$).

In order to gauge rider lean effort, we report the standard deviation of the rider lean angle as a function of speed in Figure 5.22. Cyclists use less rider lean than non-cyclists ($F = 19.643$, $p < 0.001$) and riders use less rider lean as speed increases ($F = 4.885$, $p = 0.031$). The results suggest that all riders use less lean effort at higher speeds and that skilled riders (i.e. cyclists) use less lean effort overall to maintain balance.

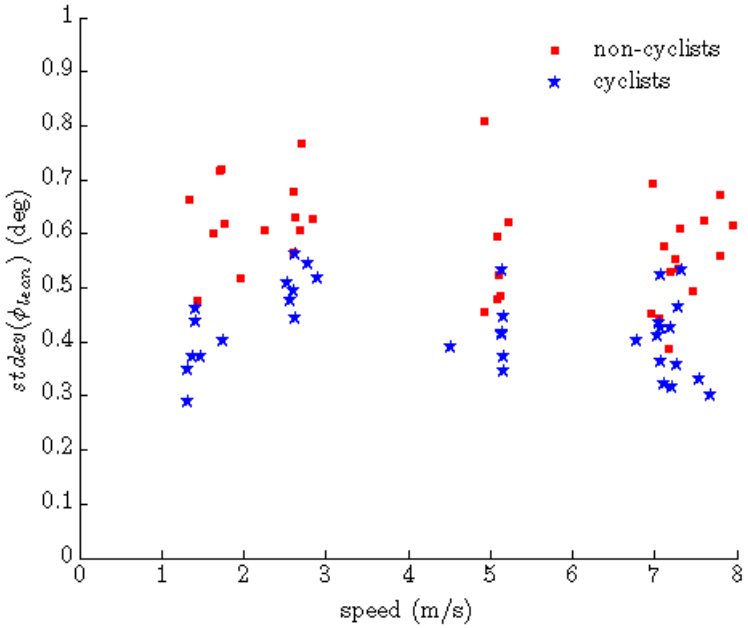

Figure 5.22. Standard deviation of rider lean angle versus speed. Cyclists exhibit significantly less rider lean than non-cyclists ($F = 19.643$, $p < 0.001$).

5.4.4 *Differences between cyclists and non-cyclists*

The above results for cyclists and non-cyclists are most similar at low speeds, but diverge as speed increased. At low speeds, all subjects commented that it is more difficult to maintain balance of the bicycle and to avoid riding off of the rollers. Therefore, it is likely that all riders had to attain similarly high levels of balance performance at the lowest speeds. At higher speeds, all subjects noted that riding on the rollers was easier. Therefore, it is possible for a rider to relax his/her balance performance at higher speeds while still maintaining balance of the bicycle on the rollers. We believe that the best measure of balance performance is the cross-correlation of the lateral center of mass location (y_{COM}) to the lateral center of pressure location (y_{COP}). At low speeds, $R^2(y_{COP}, y_{COM})$ is similar between cyclists and non-cyclists, whereas at higher speeds $R^2(y_{COP}, y_{COM})$ is significantly less for non-cyclists.

To achieve high balance performance, cyclists use a different control strategy than non-cyclists. We quantified two types of control strategies, steering and rider lean, by investigating the correlation of steer angle/rate and rider lean angle/rate to bicycle roll angle/rate. *Compared to non-cyclists, cyclists utilize greater rider lean than steering to maintain balance, especially at higher speeds*. Greater rider lean control decreases the need for additional steer control required to maintain balance. This conclusion is supported by the above observation that cyclists achieve higher balance performance than non-cyclists despite exhibiting lower cross-correlation between steer and bicycle roll rates. In Chapter 4, we hypothesized that some children were able to ride a bicycle with a lower cross-correlation between steer and bicycle roll rates than other children because they were utilizing rider lean to control balance in addition to steering; the results of this study support that hypothesis.

To assess the relative importance of steer versus lean control on balance performance, we used a mixed linear model to address whether any measures of control (i.e. cross-correlations) predict the cross-correlation of y_{COM} to y_{COP}, the adopted measure of balance performance. Again we used an alpha level of 5% and an auto regressive covariance model with order of one. The dependent variable was $R^2(y_{COP}, y_{COM})$ and the effects were $R^2(\phi, \delta)$, $R^2(\dot{\phi}, \dot{\delta})$, $R^2(\phi, \phi_{lean})$, and $R^2(\dot{\phi}, \dot{\phi}_{lean})$. Of the tested effects, only $R^2(\phi, \phi_{lean})$, the cross-correlation of rider lean to the bicycle roll angle, was a significant predictor of balance performance ($F = 84.768$, $p < 0.001$). Therefore, we conclude that rider lean is the dominant control strategy for balance performance for riding on rollers. The above results demonstrate that cyclists exploit rider lean control significantly more than non-cyclists to achieve higher balance performance.

In addition to achieving higher balance performance, cyclists also employ significantly less overall balance control effort than non-cyclists. Cyclists and non-cyclists show similar variation in the lateral position of the center of pressure during riding (Figure 5.23). Thus, cyclists are not simply riding a significantly straighter path than non-cyclists. The similar movements of the center of pressure for cyclists and non-cyclists confirm that *both groups respond to essentially the same balancing task*. In other words, not only do cyclists use less effort to maintain balance, they use less effort despite facing the same balancing task as non-cyclists.

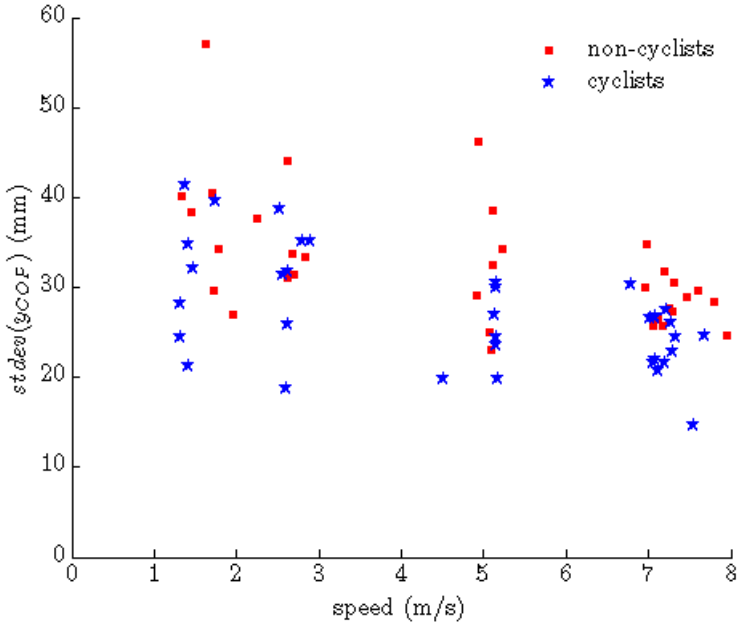

Figure 5.23. Standard deviation of the lateral position of the center of pressure versus speed. The standard deviation of the lateral position of the center of pressure decreases significantly with increasing speed ($F = 25.294$, $p < 0.001$). Although it may appear that cyclists exhibit less variation in the center of pressure position than non-cyclists, there was not a significant difference between the two groups ($F = 3.695$, $p = 0.059$).

We have identified several metrics that distinguish rider skill in balancing, and hence stabilizing, a bicycle. Skilled riders exhibit higher correlation between the lateral positions of the center of mass and center of pressure, consistently use more rider lean

than less skilled riders, and use significantly less effort than less skilled riders. While dynamic models of bicycles, such as the Whipple model [3], successfully predict the stability of an uncontrolled bicycle [12], they ignore the above stabilizing actions of the human rider. Metrics that define rider skill (such as those above) could become useful for understanding how bicycle design can influence rider balance performance. For example, any bicycle designed to help riders maintain balance at low speeds should increase the cross-correlation between the lateral positions of the center of pressure and center of mass. Metrics of balance performance could also serve to evaluate the effectiveness of bicycle training programs. For example, riders with initially poor balancing skills could undergo a training program (perhaps riding a bicycle on training rollers, as shown in Figure 5.1) to help improve their skills. By quantifying differences between skilled and novice riders, we have provided researchers and practitioners with tools to objectively measure the effects of different bicycle designs on real-life bicycle riding.

5.5 Conclusion

We measured the dynamics of human bicycle riding as 14 subjects rode an instrumented bicycle on training rollers mounted on a force platform and at speeds ranging from approximately 1.3 to 7.2 m/s. Of the 14 riders, we classified 7 as cyclists (skilled riders) and 7 and non-cyclists (novice riders). The instrumented bicycle measured steer angle/rate, steer torque, bicycle speed, and bicycle roll rate and also enabled the calculation of steering power. A motion capture system enabled the measurement of the roll angle of the bicycle. A force plate beneath the roller assembly measured the net force and moment that the bicycle/rider/rollers exerted on the floor, which also enabled calculation of the lateral position of the bicycle/rider center of mass and center of

pressure. We found that the cross-correlation of the lateral position of the center of mass to the lateral position of the center of pressure quantifies balance performance, the cross-correlation of steer angle/rate to bicycle roll angle/rate quantifies steer control, and the cross-correlation of rider lean angle to the bicycle roll angle quantifies rider lean control. All riders achieved similar balance performance at the lowest speed while utilizing similar control strategies. However at higher speeds, skilled riders (cyclists) achieved greater balance performance by employing more rider lean control and less steer control compared to novice riders (non-cyclists). In addition, skilled riders used less steer control effort (measured by average positive steering power and standard deviations of steer angle and rate) and less rider lean control effort (measured by the standard deviation of the rider lean angle) regardless of speed. The reduction in balance effort for skilled riders is not due to any reduced demands for balance. The metrics introduced herein could also quantify balance performance of the bicycle/rider system in broad contexts including 1) the analysis of bicycle designs, 2) the performance of assistive technologies, and 3) the assessment of training programs.

CHAPTER 6: SUMMARY AND CONTRIBUTIONS

The overall goal of this dissertation was to advance our understanding of how human riders control bicycles, the types of control that humans utilize to balance and steer bicycles, and the skills that distinguish human riders of different ability levels. In order to achieve this goal, we pursued the following four specific aims:

1. Design and build an instrumented bicycle that is capable of measuring the primary human control inputs (steer torque and rider lean) and fundamental bicycle kinematics.
2. Investigate human/bicycle dynamics and control during steady-state turning using experimental and analytical approaches.
3. Quantify the changes that occur as learners transition from non-riders to riders.
4. Quantify the differences between skilled and novice riders when balancing a bicycle.

Below, we discuss each specific aim by providing a brief summary, listing the main contributions and conclusions, and then discussing some limitations. Major overarching conclusions drawn from all four studies follow this discussion.

6.1 Summary, contributions, and conclusions of each study

Specific Aim 1: Design and build an instrumented bicycle that is capable of measuring the primary human control inputs and fundamental bicycle kinematics

(Chapter 2). Developing and building an instrumented bicycle was critical to the completion of this dissertation. In particular, it was important to have a bicycle and measurement techniques that could be used outside the confines a laboratory. Our instrumented bicycle measures steer angle, steer torque, angular velocity of the bicycle frame, acceleration of the bicycle frame, and bicycle speed. Through numerical differentiation, we obtain steering angular velocity or rate. Multiplication of measured steering torque by steering rate yields steering power, which quantifies rider steering effort. During steady-state turning, measurements of the acceleration of the bicycle frame and the bicycle speed provide an estimate of the bicycle roll angle, which further enables computation of rider lean angle. The battery-powered sensors and on-board data acquisition computer are self-contained, which allows the instrumented bicycle to be used in non-laboratory environments. Additionally, the design does not require any attachments or special interfaces with the rider. The rider is unconstrained and therefore free to employ the very same natural movements and control for riding any bicycle.

Specific Aim 1: Major contributions

- Designed and constructed a novel instrumented bicycle, which places no constraints on rider movement and can be used outside of laboratory environments

Specific Aim 1: Major conclusions

- The instrumented bicycle directly measures a primary human control input (steer torque) and fundamental bicycle kinematics (steer angle, roll rate, and bicycle speed)

- Additional measures of human/bicycle dynamics are calculated from the measured data including the second primary human control input (rider lean) in addition to other kinematic measures (steering angular rate, steering power, bicycle roll angle)

The instrumented bicycle is limited in that it measures rider lean and bicycle roll angles during steady-state turning, not during arbitrary or straight line riding. Conducting riding tests in a laboratory equipped with a motion capture system allowed us to overcome these limitations quite easily (Chapter 5); however, there are some elegant solutions that would allow us to measure the rider lean and bicycle roll angles outside of a laboratory environment. A simple trailer can be used to measure the roll angle of the bicycle [130]; and both [31] and [45] present simple and inexpensive methods to estimate rider lean angle using potentiometers. While the trailer would be straight forward to implement, the proposed methods to measure rider lean angle introduce limitations. Both methods require a rod to be secured to the rider and only consider rider lean developed from lateral flexion of the trunk. As demonstrated in [114] and [24], riders use many motions besides lateral flexion of the trunk to generate what we define as rider lean (lateral shifting of rider mass center). Therefore, measurements of only lateral flexion of the trunk would fail to capture many of the motions that we believe are important for maintaining balance of a bicycle. An extreme approach is to eliminate all rider motion expect for steering [118, 130].This approach includes using a body orthosis to prevent trunk movement, eliminating the task of pedaling by using an electric motor to power the bicycle, and securing the rider's feet and knees to the bicycle frame to eliminate all leg movement. Depending on the research question, eliminating all rider motions except steering may be

justified. However, our research goal was to understand the natural control humans employ while riding a bicycle and therefore it was imperative to maintain all control degrees of freedom.

Specific Aim 2: Investigate human/bicycle dynamics and control during steady-state turning using experimental and analytical approaches (Chapter 3). The steady-state turning of a bicycle arises when the bicycle/rider system negotiates a constant radius turn with constant speed and roll angle. We explored steady-state turning by employing the instrumented bicycle to measure steering torque, steering angle, and bicycle speed, acceleration, and angular velocity. We used a model for steady-state turning, based on the Whipple bicycle model [2, 3], to interpret our results.

Our experimental and analytical investigation of steady-state turning served several purposes. Consideration of the bicycle/rider system during steady-state turning was our starting point for understanding basic bicycle/rider dynamics and control. Steady-state turn testing allowed us to tightly control bicycle speed, turn radius, and rider lean to assess the effects of these variables on bicycle kinematics (roll and steer angles) and what has been considered the primary human input to the bicycle (steering torque). Additionally, because we used a steady-state formulation of the Whipple bicycle model to interpret our results, we were able to extend the utility of this commonly used model for predicting the dynamics of human bicycle riding.

In Chapter 3, we reported data obtained from 134 trials using two subjects executing steady turns defined by nine different radii, three speeds, and three rider lean conditions. A model for steady-state turning is used to interpret the experimental results. Overall, the

model explains 95.6% of the variability in the estimated bicycle roll angle, 99.4% of the variability in the measured steering angle, and 6.5% of the variability in the measured steering torque. However, the model explains 56.6% of the variability in steering torque for the subset of trials without exaggerated rider lean relative to the bicycle frame. Thus, the model, which assumes a rigid and non-leaning rider, reasonably predicts bicycle/rider roll and steering angles for all rider lean conditions and steering torque without exaggerated rider lean. The findings demonstrate that lateral shifting of the bicycle/rider center of mass strongly influences the steering torque, suggesting that rider lean plays an important role in bicycle control during steady-state turning. By contrast, the required steering angle is largely insensitive to rider lean, suggesting that the steering angle serves as a superior cue for bicycle control relative to steering torque.

Specific Aim 2: Major contributions

- Provided novel experimental data for steady-state turning that includes steer torque, steer angle, and roll angle over a wide range of turn radii, bicycle speeds, and rider lean conditions
- Adapted the Whipple bicycle model for steady-state turning.

Specific Aim 2: Major conclusions

- The model, which assumes a rigid and non-leaning rider, successfully predicts bicycle kinematics (roll and steer angles) for all rider lean conditions
- The model only reasonably predicts steering torque for normal riding (no exaggerated rider lean)

- Lateral shifting of the bicycle/rider center of mass (i.e. rider lean) strongly influences steering torque, suggesting that rider lean plays an important role in bicycle control during steady-state turning
- The required steering angle for a given turn radius is largely insensitive to rider lean, suggesting that steering angle is a better cue for bicycle control than steering torque

The steady-state turning study has the following limitations. First, we chose to compare the experimental data to a steady-state turning model based on the Whipple bicycle model. The primary shortcoming of this model is that it ignores rider lean. Nevertheless, we chose the Whipple model due to its wide use in bicycle research. As a result, our results also provide other researchers with data to evaluate the limitations of the Whipple model for understanding human bicycle riding. In an earlier study [81], we introduced an alternative, simplified steady-state turning model that explicitly incorporates rider lean. This model yields more accurate predictions of steering torque than the steady-state turning version of the Whipple model. The study is also limited because it only considers two riders and one bicycle design. A more complete study would assess several bicycle designs and riders. Different bicycle designs could arise from simply turning the fork backwards, installing different front wheels, and adding weight to different places on the bicycle to affect the mass distribution and inertia.

Specific Aim 3: Quantify the changes that occur as learners transition from non-riders to riders (Chapter 4). Riding a bicycle is a skill that many people learn quite easily as reflected in the common assertion, “it’s as easy as riding a bike.” However, there is little scientific understanding about how we learn to ride and balance a bicycle.

The objective of the study detailed in Chapter 4 was to quantify how human subjects learn to ride a bicycle by tracking key kinematic changes in bicycle roll and steer dynamics during the learning process. The subjects for this study were children who participated in a specialized bicycle training camp called *Lose the Training Wheels*; refer to www.losethetrainingwheels.org. Children enter this camp having no ability to ride a bicycle and either acquire that ability or make significant progress towards that goal by the end of the week-long camp [46, 106]. Therefore, this camp provides an ideal setting for tracking the changes that arise as a child transitions from a non-rider to a rider. A previous analysis of pilot data [107] helped develop our hypotheses and methods. We hypothesized that the measured bicycle steer and roll angular velocities would become significantly correlated as a successful subject progressed through training. In addition, we hypothesized that the average bicycle speed, the standard deviation of the roll angular velocity, and the standard deviation of the steer angular velocity would all increase with training.

We measured the fundamental bicycle kinematics of novice riders with disabilities during the specialized bicycle training camp to unravel how they learn to ride traditional bicycles. Of the 15 subjects, 11 successfully rode a traditional bicycle without assistance by the end of the camp. Three wireless IMUs revealed the bicycle roll rate, steer rate, and speed during the learning process. The peak value of the cross-correlation between steer and roll angular velocities was significantly greater for the 11 subjects who learned to ride compared to the 4 who did not. This finding suggests that rider learning is quantified by increased correlation between bicycle steer rate and roll rate. In essence, learning to steer in the direction of bicycle lean is an essential and quantifiable skill in learning to

ride. Average speed also increased with time, likely due to the increased gearing used as a rider progressed through the camp. The standard deviation of the steer rate also increased with time, suggesting that initially fearful riders learn to relax their arms and use the handlebars to balance the bicycles. As expected, the standard deviation of the bicycle roll rate also increased with time, likely due to the more crowned rollers that learners use as they progress towards riding a traditional bicycle. Existing and future training techniques can be systematically evaluated using this new skill assessment method.

Specific Aim 3: Major contributions

- We developed a novel experimental method utilizing three synchronized inertial measurement units (IMUs) to measure the bicycle kinematics critical for understanding rider learning
    - The IMUs are easily and quickly mounted to any bicycle
    - The IMUs can be reliably used in both indoor and outdoor environments

Specific Aim 3: Major conclusions

- Rider learning can be quantified by increasing correlation between the steer and roll angular velocities (and angular accelerations)
- Average speed of the riders increased with training time, likely due to increases in gearing as riders progress through the camp
- Standard deviation of the steer rate increased with time, suggesting that initially fearful riders learn to relax their arms and use the handlebars to balance the bicycles

- Standard deviation of the bicycle roll rate increased with time, likely due to the more crowned rollers that learners use as they progress towards riding a traditional bicycle
- Learning to steer in the direction of lean is an essential skill in learning to ride a bicycle

We duly note the following limitations to this study. First, the measurements were taken on a population with disabilities, which includes subjects with Down syndrome, cerebral palsy, autism spectrum disorder, and attention deficit hyperactivity disorder. It is not clear how all of the findings may translate to a non-affected population. However, the primary finding that steer must be highly correlated to roll is in agreement with past studies [16, 105, 110] on non-affected populations. Children with disabilities such as Down syndrome and autism spectrum disorder have motor deficits that may make it difficult to learn new motor skills [111, 112]. Despite learning deficits, children with disabilities must still learn the same skill as non-affected children in order to balance a bicycle. In addition, our results from Chapter 5 demonstrate that non-affected subjects (cyclists and non-cyclists) also exhibit a high correlation of steer rate to bicycle roll rate. Therefore, we remain confident in the conclusion that riding a bicycle requires a high correlation between steer and roll.

A second limitation is that measurements were taken on modified bicycles (the adapted bicycles) that are not available to the general public. It is not clear to what degree the adapted bicycles influence or limit performance measures or how the performance measures translate to other training techniques. The approach used to develop the adapted bicycles has also been applied to develop an ‘unrideable’ bicycle as well as a bicycle

similar to the unrideable bicycle that was made rideable by using a bicycle model to guide slight design modifications [18]. Therefore, we believe that all of the bicycles (both adapted and traditional) exhibit very similar dynamic properties. The main effect of the adapted bicycles is that they reduce the correlation between steer and roll needed to maintain balance. The rear roller on an adapted bicycle functions similar to training wheels, providing a corrective force that allows a rider to maintain balance despite incorrect steering inputs. Unlike training wheels, the adapted bicycles maintain the ability to roll, albeit with limits on roll. We hypothesize that the adapted bicycles make it possible for riders to learn incrementally, which is in contrast to the typical fail/succeed nature of learning to ride a traditional bicycle. The incremental learning that riders demonstrate when using the adapted bicycles made it possible to capture and study the learning process.

Specific Aim 4: Quantify the differences between skilled and novice riders when balancing a bicycle (Chapter 5). There is little understanding of the fundamental characteristics of human bicycle riders, the types of control that humans use to balance bicycles, and the skills that distinguish riders of different ability levels. Identifying the types of control that humans use and differences between skilled and novice riders would simultaneously advance two uses. First, it would provide researchers with metrics to evaluate rider skill and human/bicycle stability. Second, it could provide bicycle designers with tools to objectively measure whether a specific bicycle design enhances or diminishes the balance skill of a particular rider. The objectives of the study detailed in Chapter 5 were three-fold: to quantify 1) the relationship between center of pressure and center of mass movement of the bicycle/rider system, 2) the types of control used by

riders, and 3) the differences between skilled and novice riders. We hypothesized that the lateral position of the center of mass would be highly correlated to the lateral position of the center of pressure, that steer rate would be highly correlated to bicycle roll rate , that rider lean would be highly correlated to bicycle roll, and that skilled riders would use significantly less steering effort and variation than novice riders.

This study reports the dynamics of human bicycle riding as 14 subjects rode an instrumented bicycle on training rollers mounted on a force platform and at speeds ranging from approximately 1.3 to 7.2 m/s. Of the 14 riders, we classified 7 as cyclists (skilled riders) and 7 and non-cyclists (novice riders). The instrumented bicycle measured steer angle/rate, steer torque, bicycle speed, and bicycle roll rate and also enabled the calculation of steering power. A motion capture system enabled the measurement of the roll angle of the bicycle. A force plate beneath the roller assembly measured the net force and moment that the bicycle/rider/rollers exerted on the floor, which also enabled calculation of the lateral position of the bicycle/rider center of mass and center of pressure. We found that the cross-correlation of the lateral position of the center of mass to the lateral position of the center of pressure quantifies balance performance, the cross-correlation of steer angle/rate to bicycle roll angle/rate quantifies steer control, and the cross-correlation of rider lean angle to the bicycle roll angle quantifies rider lean control. All riders achieved similar balance performance at the lowest speed while utilizing similar control strategies. However at higher speeds, skilled riders (cyclists) achieved greater balance performance by employing more rider lean control and less steer control compared to novice riders (non-cyclists). In addition, skilled riders used less steer control effort (measured by average positive steering power and standard deviations of steer

angle and rate) and less rider lean control effort (measured by the standard deviation of the rider lean angle) regardless of speed. The reduction in balance effort for skilled riders is not due to any reduced demands for balance. In summary, skilled riders achieve higher levels of balance performance using less effort than novice riders.

Specific Aim 4: Major contributions

- Developed a novel method to measure the dynamics of human/bicycle balance that utilized custom designed rollers mounted to a force platform

Specific Aim 4: Major conclusions

- The cross-correlation of the lateral position of the center of mass to the lateral position of the center of pressure quantifies balance performance
- The cross-correlation of steer angle/rate to bicycle roll angle/rate quantifies steer control
- The cross-correlation of rider lean angle to bicycle roll angle quantifies rider lean control
- At all speeds above 1.3 m/s (the lowest speed), skilled riders (cyclists):
    - achieved higher levels of balance than novice riders (non-cyclists)
    - used more rider lean control than novice riders
    - used less steer control than novice riders
- Regardless of speed, skilled riders used less control effort than novice riders
    - Skilled riders used less positive steering power than novice riders
    - Skilled riders exhibited less steer angle/rate variation

Our investigation of human/bicycle balancing dynamics is limited by several factors. First, we chose to conduct our experiments on a custom set of bicycle training rollers. The relationship of bicycle riding on rollers to riding overground has not been quantified, and there is some disagreement about the differences and similarities between the two tasks [117, 131, 132]. Therefore, it is not yet clear if all the metrics that distinguish rider skill on rollers would also distinguish rider skill overground. We recognized this limitation before the onset of the study and decided to conduct the experiments on rollers because of several advantages they present: 1) riding on rollers is more challenging than riding overground, and therefore this task may be particularly useful in eliciting differences between skilled riders and less skilled riders, 2) rollers can be easily and securely mounted to a force platform, and 3) riding on rollers is safer than riding on a treadmill, which is the primary alternative for studying human/bicycle dynamics in a laboratory setting. We carefully designed the custom rollers to ensure that the balancing dynamics would be as similar as possible to riding overground. The adjustable front drum ensures that the bicycle is level and that the trail of the bicycle is the same on the rollers as overground. Our choice of the largest diameter drums minimizes differences between the front tire ground contact when riding on rollers versus when riding overground.

Another final limitation is that subjects were not able to ride their own bicycles—they were required to ride the instrumented bicycle. While we did adjust the seat height for each subject and allowed each subject ample time to adjust to the instrumented bicycle, the fit was not ideal for every subject. The role of bicycle fit on bicycle control has not been quantified, but it is possible that a non-ideal fit may result in diminished performance. Despite this limitation, we still were able to detect significant differences

between skilled and novice riders and believe that these differences would persist if all subjects rode their own bicycles.

6.2 Overarching conclusions

While the above studies target different aims, their results highlight two overarching conclusions.

Overarching conclusion 1: Rider lean (i.e., lateral movement of the rider relative to the bicycle frame) plays a dominant role in steering and balancing a bicycle.

Theoretical studies demonstrate that rider lean can maintain bicycle stability, even in the absence of steer control [5-7]. All three studies herein provide experimental evidence that rider lean is important for balancing and steering a bicycle. In the study on steady-state turning (Chapter 3), we conclude that lateral shifting of the bicycle/rider center of mass (i.e. rider lean) strongly influences steering torque. Because steer torque directly influences steer angle, it follows that a rider can easily influence the steer angle through leaning. In the study of rider learning (Chapter 4), results demonstrate that not all riders that learned to ride achieved similarly high levels of cross-correlation between steer and bicycle roll rates. In particular, some riders achieved very high cross-correlations (R^2 = 0.9) whereas others only achieved modest cross-correlations (R^2 = 0.7) only slightly larger than some riders that were not successful riding a bicycle. We hypothesized that a rider using lean control could reduce the otherwise required correlation between steer and roll. Our results from the study of rider balance skill (Chapter 5) confirm that a rider can indeed reduce the required correlation between steer and roll by exploiting rider lean control. In fact, we found that cross-correlation between rider lean angle and bicycle roll

angle was a significant factor in predicting balance performance (the cross-correlation between the lateral positions of the center of mass and center of pressure).

Analyses of rider movements during bicycle riding reveal a wide variety of motions [23, 24, 114], including lateral bending, leaning, and twisting of the upper body and lateral knee movements. Not surprisingly, many of these motions are not present when the rider is not required to pedal the bicycle [24]. This result has led some researchers to hypothesize that lean, bend, and twist of the upper body are not movements fundamental to balance control and are only reactions to pedaling [24]. However, as our results in Chapter 5 demonstrate, not all riders use lateral body movements in the same way. Riders that correlate rider lean to bicycle roll are able to significantly reduce the effort needed to maintain balance. Therefore, we conclude that rider lean and lateral movement of the rider relative to the bicycle frame plays an important role in controlling and balancing a bicycle.

Overarching conclusion 2: Correlating steer and rider lean (the two rider control inputs) with the bicycle roll angle/rate (the bicycle response) is essential for balance performance.

In Chapters 2 and 3, we demonstrated that steer control and rider lean control can be quantified by calculating the cross-correlations of steer angle/rate and rider lean angle/rate to the bicycle roll angle/rate. Therefore, we conclude that correlating steer and rider lean to the bicycle roll angle (and roll rate) is essential for balance performance. .

This conclusion has important implications for how we teach people to ride bicycles. Our results suggest that is crucial for the learner to experience bicycle roll and for the

learner's control actions to affect the roll of a training bicycle in a way similar to a traditional bicycle. For example, training wheels by design prevent bicycle roll, render it impossible for the learner to experience bicycle roll, and therefore impossible for the bicycle to respond similarly to one without training wheels. Without experiencing bicycle roll and how steering and rider lean affect bicycle roll, the rider has no opportunity to learn appropriate control actions. Unlike bicycles with training wheels, the adapted bicycles detailed in Chapter 4 allowed the riders to experience bicycle roll dynamics and to gradually learn distinctions between correct and incorrect control actions. Unfortunately for children that use training wheels, learning correct and incorrect control actions usually occurs only after removal of the training wheels. At that point, the penalty for a wrong control action is typically a crash. Training wheels are excellent for helping children learn pedaling and navigation skills, but they are not ideal for teaching balance skills. Fortunately, society is gradually recognizing the limitations of training wheels, as evidenced by the recent popularity of balance bikes. Balance bikes or run bikes have no pedals, drivetrain, or training wheels, and require the rider to kick his/her feet to propel the bike forward. Because balance bicycles allow bicycle roll, it is possible for the rider to learn how to correlate steer and rider lean to bicycle roll, which inevitably leads to successful riding.

APPENDIX A: MEASUREMENT OF BICYCLE PARAMETERS

The procedures used to determine the parameters of the instrumented bicycle for the steady-state turning model (Section 3.3.3) are presented below. These procedures are guided by previous studies [9, 133-135]. The measured parameters are reported in Table A.2.

A.1 Wheel base (w)

With the bicycle secured in an upright position (roll angle = 0 degrees) and with the front wheel aligned with the plane defined by the bicycle frame (steer angle = 0 degrees), we measured: the distance from the rear wheel axis to the front wheel axis on both the left and right sides of the bicycle (with a tape measure, resolution = 0.001 m), the width of the front axle, and the width of the rear axle (with calipers, resolution = 0.03 mm). We used the four measurements to define a trapezoid; solving for the height of the trapezoid yields the length of the wheel base of the bicycle, w.

A.2 Wheel radius (r_F , r_R)

Similar to [9, 133-135], we estimated the radii of the front (r_F) and rear (r_R) wheels by measuring the linear distance traveled on the ground through 14 rotations of each wheel. During each trial, a subject sat on the bicycle (tire pressure = 2.76 bar) with the seat height adjusted properly as he/she was pushed from behind while making his/her best effort to follow a straight course. We measured the distance covered in each trial using a 30 m long tape measure (resolution = 1.6 mm). We collected three trials for each wheel

for each subject. The measured distances were divided by 28π to obtain the effective rolling radius for each trial; trials were averaged to obtain values for each wheel for each subject. The effective rolling radii were not significantly different between subjects.

A.3 Steer axis tilt (λ)

We measured the steer axis tilt by securing the bicycle with each subject seated on the bicycle in an upright position (roll angle = steer angle = 0 degrees) and measuring the angle of the head tube of the bicycle using a digital inclinometer (resolution = 0.01 degrees). To account for the floor potentially being out of level, we measured the steer axis tilt with the bicycle in two configurations—the first as described above and the second simply with the bicycle facing the opposite direction. We took the average of the two measurements as the steer axis tilt of the loaded bicycle. The steer axis tilt was not significantly different between subjects.

A.4 Fork rake/offset (f_o)

We measured the fork rake (also known as fork offset) as described in [133] and found the measured fork rake to agree with the rake value provided by the manufacturer to the nearest millimeter.

A.5 Trail (c)

Instead of measuring the trail (c) of the bicycle directly, we calculated the trail using the following equation [133]:

$$c = \frac{r_F \sin\lambda - f_o}{\cos\lambda} \tag{A.1}$$

where r_F is the measured radius of the front wheel, λ is the steer axis tilt, and f_o is the fork rake or offset.

A.6 Mass

The total mass of the bicycle, including the instrumentation described in Chapter 2, was measured using a digital scale (resolution = 10 g). We measured the mass of each wheel (with the quick release skewers removed), the mass of the front assembly (handlebars, stem, fork, and front quick release skewer), and the mass of the data acquisition hardware (computer, battery, DAQ box, and cables) using a smaller digital scale (resolution = 1 g). We measured the mass of each subject using an upright physicians scale (resolution = 0.1 kg).

A.7 Center of mass location: bicycle

We estimated the location of the center of mass of the bicycle with the seat set to appropriate heights for each subject using methodology similar to [9, 134, 135], assuming the bicycle is laterally symmetric. The complete bicycle was suspended from a string, allowed to come to rest, and photographed ensuring that the plane of the bicycle defined by the wheels was perpendicular to the lens of the camera. We photographed the bicycle in four different orientations. We opened each photo in MATLAB (The MathWorks, Inc.) and used the image tools to rotate the each photograph so that the bicycle was in its normal loaded upright position. We then calculated the slope and intercept of the string in the coordinate system of the bicycle using the conventions of vehicle dynamics [94]. We calculated the meter to pixel scale factor by using 23 known dimensions of the bicycle. After finding the equation of the line defining the string in each photograph, we used the

least squares method to solve for the intersection of the four lines [133]. The intersection is the estimated center of mass location for the bicycle. The process was repeated with the seat height adjusted to the appropriate height for each subject.

A.8 Center of mass location: handlebars, stem, and fork (x_H , z_H).

We estimated the center of mass location for the handlebar, stem, and fork assembly using the methodology described for the bicycle (Section A.7). We suspended the assembly in four orientations and used nine known dimensions to calculate the meter to pixel scale factor. The center of mass location was found relative to the front fork dropout and later converted to coordinates in the bicycle coordinate system.

A.9 Center of mass location: wheels.

The centers of mass of the wheels were assumed to be at their geometrical centers.

A.10 Center of mass location: bicycle and rider (x_T , z_T)

Similar to the center of mass for the bicycle, we estimated the center of mass location for the bicycle/rider system for each subject by using photographs. We used the data of both Clauser et al. [136] and Dempster [128] to estimate the mass properties of the following 13 body segments: head and trunk, two arms, two forearms, two hands, two thighs, two legs, and two feet. For all segments except the hands, we used the data of [136] to calculate the mass of each segment (as a percentage of a subject's total weight) and the location of the center of mass (as a percentage of the limb length from one end of the segment). We chose to use the data of [136] because segment lengths are defined relative to anatomical landmarks that are easily identified by palpation. We calculated the mass of the hands using data from [136] but used data from [128] to calculate the location of the

center of mass; we made this choice because [128] found the center of mass location of hands with a similar configuration to that of a hand gripping a handlebar whereas [136] located the center of mass of hands with extended fingers. The values used to estimate segment properties as well as the landmarks used to identify each segment can be found in Table A.1.

Table A.1. Body segment properties (from Clauser et al. [136] and Dempster [128]). The mass of each segment is calculated as a fraction of the body mass and the location of the center of mass of each segment is calculated as a fraction of the segment length.

Segment	**(segment mass) / (body mass)**	**(Location of center of mass from proximal or superior end of segment) / (segment length)**	**Proximal (superior) end point**	**Distal (inferior) end point**
head and torso	0.580	0.592	vertex of head	trochanterion
upper arm	0.026	0.513	acromiale	radiale
forearm	0.016	0.390	radiale	styloid process of ulna
hand	0.007	0.506	styloid process of ulna	proximal interphalangeal knuckle of finger II
thigh	0.103	0.372	trochanterion	tibiale mediale or tibiale laterale
leg	0.043	0.371	tibiale mediale or tibiale laterale	sphyrion fibulare or sphyrion laterale
foot	0.015	0.449	dorsal surface of heel	tip of longest toe

Prior to photographing each subject on the bicycle, we used palpation to identify: the acromiale, radiale, styloid process of the ulna, trochanterion, tibiale mediale, tibiale laterale, sphyrion fibulare, and sphyrion laterale [137]. After identification, we marked the location of each landmark with small dots of tape. Each subject then sat on the instrumented bicycle with the seat height adjusted appropriately. We secured the bicycle/rider in an upright position (lean angle = steer angle = 0) and photographed the bicycle/rider from the side, ensuring that the plane of the bicycle defined by the wheels was perpendicular to the lens of the camera. We opened each photo (one for each subject)

in MATLAB and used the image tools to rotate each photograph so that the bicycle was in its normal loaded upright position. We calculated the meter to pixel scale factor by using 23 known dimensions of the bicycle. Using the dots of tape as a guide, the locations of the end points of each segment were digitized. We estimated the location of the segment centers of mass by using the ratios in Table A.1, assuming that the center of mass for a segment falls on a line connecting the two endpoints. We calculated the center of mass locations for the thigh, leg, and foot segments independently for each leg, but assumed that the left upper arm, forearm, and hand segments were symmetric to the segments on the right side of the body. Given the center of mass of the segments and the bicycle (Section A.7), we calculated the rider/bicycle center of mass:

$$x_T = \frac{1}{m_T}\sum_{i=1}^{14} m_i x_i \tag{A.2}$$

$$z_T = \frac{1}{m_T}\sum_{i=1}^{14} m_i z_i \tag{A.3}$$

where (x_T, z_T) is the location of the bicycle/rider system center of mass, i is a subscript denoting a segment or the bicycle, m_T is the total mass of the bicycle/rider system, m_i is the mass of a segment or the bicycle, and (x_i, z_i) is the center of mass location of a segment or the bicycle.

A.11 Inertia of wheels about axles (I_{Fyy}, I_{Ryy})

To measure the mass moment of inertia of a wheel about its axle, we hung the wheel as a compound pendulum by hanging the wheel from a thin horizontal rod parallel to the wheel axle [9, 133-135]. We secured a wireless angular rate gyro (InvenSense ITG-3200)

to the hub of the wheel with one axis oriented parallel to the axle of the wheel, and perturbed the wheel to oscillate about the axis of the rod. Using the measured angular rate about the axis parallel to the wheel axle, we measured the time required for the wheel to complete 35 oscillations; dividing the time by 35 yields the period (T) of oscillation. We measured the period of oscillation for each wheel in six different orientations, and used the average period for each wheel to calculate the inertia of each wheel about its axle [134]:

$$I_{iyy} = \left(\frac{T_i}{2\pi}\right)^2 \left(m_i + m_{gyro}\right) gl - \left(m_i + m_{gyro}\right) l^2 \tag{A.4}$$

where i is a subscript denoting the front (F) or rear (R) wheel, T_i is the time of one oscillation, m_i is the mass of the wheel, m_{gyro} is the mass of the angular rate gyro used for measurement (25 g), g is gravity (9.81 m/sec^2), and l is the distance from the thin rod to the center of mass of the wheel (pendulum arm length). We assumed that the distance l was equal to the inner radius of the rim, which we measured using a three-dimensional digitizing system (MicroScribe G2X, resolution = 0.23mm).

A.12 Calculation of stiffness matrices (K_0, K_2)

The terms of the two stiffness matrices that appear in our steady-state turning equations must be calculated from the measured parameters. We calculate the stiffness matrices as described in [2], and reproduce the equations here for completeness.

First, the mass properties of the front assembly (front wheel, handlebars, and fork) must be calculated:

$$m_A = m_H + m_F \tag{A.5}$$

$$x_A = \frac{x_H m_H + w m_F}{m_A} \tag{A.6}$$

$$z_A = \frac{z_H m_H - r_F m_F}{m_A} \tag{A.7}$$

Next, we calculate the perpendicular distance between the center of mass of the front assembly and the steering axis:

$$u_A = (x_A - w - c)\cos\lambda - z_A \sin\lambda \tag{A.8}$$

The ratio of the mechanical trail to the wheel base is given by:

$$\mu = \frac{c\cos\lambda}{w} \tag{A.9}$$

The gyrostatic coefficients are given by:

$$S_R = \frac{I_{Ryy}}{r_R} \tag{A.10}$$

$$S_F = \frac{I_{Fyy}}{r_F} \tag{A.11}$$

$$S_T = S_R + S_F \tag{A.12}$$

A frequently appearing static moment term is defined as:

$$S_A = m_A u_A + \mu m_T x_T \tag{A.13}$$

Finally, we can calculate the gravity-dependent stiffness terms:

$$K_{0\phi\phi} = m_T z_T \tag{A.14}$$

$$K_{0\phi\delta} = K_{0\delta\phi} = -S_A \tag{A.15}$$

$$K_{0\delta\delta} = -S_A \sin\lambda \tag{A.16}$$

and the velocity-dependent stiffness terms:

$$K_{2\phi\phi} = K_{2\delta\phi} = 0 \tag{A.17}$$

$$K_{2\phi\delta} = \frac{(S_T - m_T z_T)\cos\lambda}{w} \tag{A.18}$$

$$K_{2\delta\delta} = \frac{(S_A + S_F \sin\lambda)\cos\lambda}{w} \tag{A.19}$$

which form the stiffness matrices:

$$\mathbf{K_0} = \begin{bmatrix} K_{0\phi\phi} & K_{0\phi\delta} \\ K_{0\delta\phi} & K_{0\delta\delta} \end{bmatrix} \tag{A.20}$$

$$\mathbf{K_2} = \begin{bmatrix} K_{2\phi\phi} & K_{2\phi\delta} \\ K_{2\delta\phi} & K_{2\delta\delta} \end{bmatrix} \tag{A.21}$$

Table A.2. Bicycle parameters for use in the model.

Parameter	Symbol	value for subject 1	value for subject 2
Wheel base	w	1.060 m	1.060 m
Steer axis tilt	λ	0.3307 rad	0.3307 rad
Fork rake/offset	f_o	0.045 m	0.045 m
Trail	c	0.064 m	0.064 m
Gravity	g	9.81 m/sec^2	9.81 m/sec^2
Rear wheel radius	r_R	0.322 m	0.322 m
Rear wheel mass	m_R	2.420 kg	2.420 kg
Rear wheel mass moment of inertia about axle	I_{Ryy}	0.127 kgm^2	0.127 kgm^2
Front wheel radius	r_F	0.326 m	0.326 m
Front wheel mass	m_F	1.885 kg	1.885 kg
Front wheel mass moment of inertia about axle	I_{Fyy}	0.128 kgm^2	0.128 kgm^2
Bicycle/rider system total mass	m_T	85.400 kg	89.400 kg
Bicycle/rider system center of mass location	(x_T, z_T)	(0.383, -0.996) m	(0.355, -1.053) m
Front handlebar and fork assembly mass	m_H	2.442 kg	2.442 kg
Front handlebar and fork assembly center of mass location	(x_H, z_H)	(0.890, -0.765) m	(0.890, -0.765) m
Gravity-dependent stiffness matrix	$\mathbf{K_0} = \begin{bmatrix} K_{0\phi\phi} & K_{0\phi\delta} \\ K_{0\delta\phi} & K_{0\delta\delta} \end{bmatrix}$	$\begin{bmatrix} -85.050 & -2.028 \\ -2.028 & -0.659 \end{bmatrix}$ kgm	$\begin{bmatrix} -94.156 & -1.969 \\ -1.969 & -0.639 \end{bmatrix}$ kgm
Velocity-dependent stiffness matrix	$\mathbf{K_2} = \begin{bmatrix} K_{2\phi\phi} & K_{2\phi\delta} \\ K_{2\delta\phi} & K_{2\delta\delta} \end{bmatrix}$	$\begin{bmatrix} 0 & 76.606 \\ 0 & 1.924 \end{bmatrix}$ kg	$\begin{bmatrix} 0 & 84.733 \\ 0 & 1.872 \end{bmatrix}$ kg

REFERENCES

[1] Herlihy, D. V., 2004, *Bicycle: The history* Yale University Press, New Haven.

[2] Meijaard, J. P., Papadopoulos, J. M., Ruina, A., and Schwab, A. L., 2007, "Linearized dynamics equations for the balance and steer of a bicycle: A benchmark and review," *Proc. R. Soc. London, Ser. A*, **463**(2084), pp. 1955-1982.

[3] Whipple, F. J. W., 1899, "The stability of the motion of a bicycle," *The Quarterly Journal of Pure and Applied Math*, **30**, pp. 312-348.

[4] Meijaard, J. P., and Schwab, A. L., 2006, "Linearized equations for an extended bicycle model," *III European Conference on Computational Mechanics: Solids, Structures, and Coupled Problems in Engineering*, C. A. M. Soares, ed., Lisbon, Portugal.

[5] Sharp, R. S., 2008, "On the stability and control of the bicycle," *Appl. Mech. Rev.*, **61**(6), pp. 060803-060801 - 060803-060824.

[6] Peterson, D. L., and Hubbard, M., 2008, "Yaw rate and velocity tracking control of a hands-free bicycle," *ASME Conference Proceedings*, **2008**(48630), pp. 447-454.

[7] Schwab, A. L., Kooijman, J. D. G., and Meijaard, J. P., 2008, "Some recent developments in bicycle dynamics and control," *4th European Conf. on Structural Control*, A. K. Belyaev, and D. A. Indeitsev, eds., St. Petersburg, Russia, pp. 695–702.

[8] Schwab, A. L., and Kooijman, J. D. G., 2010, "Lateral dynamics of a bicycle with passive rider model," *The 1st Joint International Conference on Multibody System Dynamics*, Lappeenranta, Finland.

[9] Kooijman, J. D. G., Schwab, A. L., and Meijaard, J. P., 2008, "Experimental validation of a model of an uncontrolled bicycle," *Multibody System Dynamics*, **19**, pp. 115-132.

[10] Kooijman, J. D. G., and Schwab, A. L., 2009, "Experimental validation of the lateral dynamics of a bicycle on a treadmill," *ASME 2009 International Design Engineering Technical Conferences and Computer and Information in Engineering Conference*, San Diego, CA, USA.

[11] Kooijman, J. D. G., Meijaard, J. P., Papadopoulos, J. M., Ruina, A., and Schwab, A. L., 2011, "A bicycle can be self-stable without gyroscopic or caster effects," *Science*, **332**(6027), pp. 339-342.

[12] Moore, J., and Hubbard, M., 2008, "Parametric study of bicycle stability (p207)," The engineering of sport 7, M. Estivalet, and P. Brisson, eds., Springer Paris, pp. 311-318.

[13] Tak, T.-O., Won, J.-S., and Baek, G.-Y., 2010, "Design sensitivity analysis of bicycle stability and experimental validation," *Bicycle and Motorcycle Dynamics 2010*, A. L. Schwab, and J. P. Meijaard, eds., Delft, The Netherlands.

[14] Zinn, L., 2005, *Zinn's cycling primer: Maintenance tips and skill building for cyclists*, Velopress.

[15] Sheridan, T. B., and Ferrell, W. R., 1974, *Man-machine systems: Information, control, and decision models of human performance*, The MIT Press, Cambridge, MA.

[16] Doyle, A. J. R., 1987, "The skill of bicycle riding," Ph.D. thesis, Department of Psychology, University of Sheffield, Sheffield, England, UK.

[17] Jones, D. E. H., 1970, "The stability of the bicycle," *Phys. Today*, **23**(4), pp. 34-40.

[18] Astrom, K. J., Klein, R. E., and Lennartsson, A., 2005, "Bicycle dynamics and control: Adapted bicycles for education and research," *IEEE Contr. Syst. Mag.*, **25**(4), pp. 26-47.

[19] Sharp, R. S., 2007, "Optimal stabilization and path-following controls for a bicycle," *Proc. Inst. Mech. Eng., Part C*, **221**, pp. 415-428.

[20] Weir, D. H., 1972, "Motorcycle handling dynamics and rider control and the effect of design configuration on response and performance," Ph.D. thesis, Engineering, University of California, Los Angeles, Los Angeles, CA, USA.

[21] Sharp, R. S., 1971, "The stability and control of motorcycles," *Journal of Mechanical Engineering Science*, **13**(5), pp. 316-329.

[22] Eaton, D. J., 1973, "Man-machine dynamics in the stabilization of single-track vehicles," Ph.D. thesis, Mechanical Engineering, The University of Michigan, Ann Arbor, MI.

[23] Kooijman, J. D. G., and Schwab, A. L., 2008, "Some observations on human control of a bicycle," *11th mini Conference on Vehicle System Dynamics, Identification and Anomalies*, Budapest, Hungary.

[24] Moore, J. K., Kooijman, J. D. G., Schwab, A. L., and Hubbard, M., 2011, "Rider motion identification during normal bicycling by means of principal component analysis," *Multibody System Dynamics*, **25**, pp. 225-244.

[25] Tanaka, Y., and Murakami, T., 2009, "A study on straight-line tracking and posture control in electric bicycle," *IEEE Transactions on Industrial Electronics*, **56**(1), pp. 159-168.

[26] Tanaka, Y., and Murakami, T., 2004, "Self sustaining bicycle robot with steering controller," *The 8th IEEE International Workshop on Advanced Motion Control*, pp. 193-197.

[27] Yamakita, M., Utano, A., and Sekiguchi, K., 2006, "Experimental study of automatic control of bicycle with balancer," *2006 IEEE/RSJ International Conference on Intelligent Robots and Systems*, Beijing, China.

[28] Iuchi, K., Niki, H., and Murakami, T., 2005, "Attitude control of bicycle motion by steering angle and variable cog control," *Industrial Electronics Society, 2005. IECON 2005. 31st Annual Conference of IEEE*.

[29] Beznos, A. V., Formal'sky, A. M., Gurfinkel, E. V., Jicharev, D. N., Lensky, A. V., Savitsky, K. V., and Tchesalin, L. S., 1998, "Control of autonomous motion of two-wheel bicycle with gyroscopic stabilisation," *Proceedings of the 1998 IEEE International Conference on Robotics and Automation* pp. 2670-2675.

[30] Hess, R., Moore, J. K., and Hubbard, M., 2012, "Modeling the manually controlled bicycle," *Systems, Man and Cybernetics, Part A: Systems and Humans, IEEE Transactions on*, **42**(3), pp. 545-557.
[31] Roland, R. D., 1973, "Computer simulation of bicycle dynamics," Mechanics and sport, J. L. Bleustein, ed., ASME, pp. 35-83.
[32] Getz, N. H., 1994, "Control of balance for a nonlinear nonholonomic non-minimum phase model of a bicycle," *American Control Conference*, Balitmore, MD.
[33] Lunteren, A. v., and Stassen, H. G., 1970, "On the variance of the bicycle rider's behavior," *6th Annual Conference on Manual Control*, Wright-Patterson Air Force Base, Ohio, USA, pp. 419-437.
[34] Moore, J. K., 2012, "Rider control variation," Sports Biomechanics Lab Blog, University of California Davis, Jan 22, 2012. Web. February 14, 2012. <http://biosport.ucdavis.edu/blog/2012/01/22/rider-controller-variation>.
[35] Rice, R. S., and R. Douglas Roland, J., 1970, "An evaluation of the performance and handling qualities of bicycles," Cornell Aeronautical Laboratory, Inc., Vehicle Research Department, Buffalo, NY.
[36] Mortimer, R. G., Domas, P. A., and Dewar, R. E., 1973, "The relationship of bicycle maneuverability to handlebar configuration," Highway Safety Research Institute, University of Michigan, Ann Arbor, MI.
[37] Mortimer, R. G., Domas, P. A., and Dewar, R. E., 1976, "The relationship of bicycle manoeuvrability to handlebar configuration," *Applied Ergonomics*, **7**(4), pp. 213-219.
[38] Arnberg, P. W., and Tyden, T., 1974, "Stability and manoeuvrability performance of different types of bicycles," National Swedish Road and Traffic Research Institute, Stockholm.
[39] Godthelp, J., and Buist, M., 1975, "Stability and manoeuvrability characteristics of single track vehicles," Institute for Perception TNO.
[40] Lewis, G. D., 1973, "The manoeuvrability and braking performance of small-wheeled bicycles when ridden by childern," Transport and Road Research Laboratory, Department of the Environment, Crowthorne, Berkshire.
[41] Daniels, E. B., Zajkowski, M. M., and Drury, C. G., 1976, "Bicycle riding performance," *Proceedings of the Human Factors and Ergonomics Society Annual Meeting*, **20**(18), pp. 410-414.
[42] Drury, C. G., and Daniels, E. B., 1980, "Predicting bicycle riding performance under controlled conditions," *Journal of Safety Research*, **12**(2), pp. 86-95.
[43] Schewe, G., Knoss, H.-P., Ludwig, O., Schaufele, A., and Schuster, R., 1984, "Experimental studies on the question of the marginal value of alcohol-induced unfitness to operate a vehicle in the case of bicyclists," *Blutalkohol*, **21**(2), pp. 97-109.
[44] Rice, R. S., 1978, "Rider skill influences on motorcycle maneuvering," *Motorcycle Dynamics and Rider Control, SAE Congress and Exposition*, Detroit, MI, pp. 79-90.
[45] Prem, H., 1983, "Motorcycle rider skill assesment," Ph.D. thesis, Department of Mechanical and Industrial Engineering, University of Melbourne, Melbourne, Victoria, Australia.

[46] Ulrich, D. A., Burghardt, A. R., Lloyd, M., Tiernan, C., and Hornyak, J. E., 2011, "Physical activity benefits of learning to ride a two-wheel bicycle for childern with down syndrome: A randomized trial," *Phys. Ther.*, **91**(10), pp. 1463-1477.

[47] Winter, D. A., 1995, "Human balance and posture control during standing and walking," *Gait and Posture*, **3**(4), pp. 193-214.

[48] Otten, E., 1999, "Balancing on a narrow ridge: Biomechanics and control," *Philosophical Transactions of the Royal Society of London. Series B: Biological Sciences*, **354**(1385), pp. 869-875.

[49] Maki, B. E., Holliday, P. J., and Topper, A. K., 1994, "A prospective study of postural balance and risk of falling in an ambulatory and independent elderly population," *Journal of Gerontology*, **49**(2), pp. M72-M84.

[50] Geraldine L, P., 2003, "Postural sway increases with attentional demands of concurrent cognitive task," *Gait and Posture*, **18**(1), pp. 29-34.

[51] Daley, M. L., and Swank, R. L., 1981, "Quantitative posturography: Use in multiple sclerosis," *Biomedical Engineering, IEEE Transactions on*, **BME-28**(9), pp. 668-671.

[52] Masani, K., Vette, A. H., Abe, M. O., Nakazawa, K., and Popovic, M. R., 2011, "Smaller sway size during quiet standing is associated with longer preceding time of motor command to body sway," *Gait and Posture*, **33**(1), pp. 14-17.

[53] Scholz, J., Schöner, G., Hsu, W., Jeka, J., Horak, F., and Martin, V., 2007, "Motor equivalent control of the center of mass in response to support surface perturbations," *Experimental Brain Research*, **180**(1), pp. 163-179.

[54] Jeka, J. J., and Lackner, J. R., 1994, "Fingertip contact influences human postural control," *Experimental Brain Research*, **79**(2), pp. 495-502.

[55] Lichtenstein, M. J., Burger, M. C., Shields, S. L., and Shiavi, R. G., 1990, "Comparison of biomechanics platform measures of balance and videotaped measures of gait with a clinical mobility scale in elderly women," *Journal of Gerontology*, **45**(2), pp. M49-M54.

[56] Jeka, J., Kiemel, T., Creath, R., Horak, F., and Peterka, R., 2004, "Controlling human upright posture: Velocity information is more accurate than position or acceleration," *Journal of Neurophysiology*, **92**(4), pp. 2368-2379.

[57] Prieto, T. E., Myklebust, J. B., Hoffmann, R. G., Lovett, E. G., and Myklebust, B. M., 1996, "Measures of postural steadiness: Differences between healthy young and elderly adults," *IEEE Transactions on Biomedical Engineering*, **43**(9), pp. 956-966.

[58] Masani, K., Popovic, M. R., Nakazawa, K., Kouzaki, M., and Nozaki, D., 2003, "Importance of body sway velocity information in controlling ankle extensor activities during quiet stance," *Journal of Neurophysiology*, **90**(6), pp. 3774-3782.

[59] Masani, K., Vette, A. H., Kawashima, N., and Popovic, M. R., 2008, "Neuromusculoskeletal torque-generation process has a large destabilizing effect on the control mechanism of quiet standing," *Journal of Neurophysiology*, **100**(3), pp. 1465-1475.

[60] Peterka, R. J., 2002, "Sensorimotor integration in human postural control," *Journal of Neurophysiology*, **88**(3), pp. 1097-1118.

[61] van der Kooij, H., van Asseldonk, E., and van der Helm, F. C. T., 2005, "Comparison of different methods to identify and quantify balance control," *J. Neurosci. Methods*, **145**(1–2), pp. 175-203.
[62] Kohn, A., 2005, "Cross-correlation between emg and center of gravity during quiet stance: Theory and simulations," *Biological Cybernetics*, **93**(5), pp. 382-388.
[63] Visser, J. E., Carpenter, M. G., Kooij, H. v. d., and Bloem, B. R., 2008, "The clinical utility of posturography," *Clinical Neurophysiology*, **119**, pp. 2424-2436.
[64] Horak, F. B., Henry, S. M., and Shumway-Cook, A., 1997, "Postural perturbations: New insights for treatment of balance disorders," *Physical Therapy*, **77**(5), pp. 517-533.
[65] Monsell, E. M., Furman, J. M., Herdman, S. J., Konrad, H. R., and Shepard, N. T., 1997, "Computerized dynamic platform posturography," *Otolaryngology - Head and Neck Surgery*, **117**(4), pp. 394-398.
[66] McGeer, T., 1990, "Passive dynamic walking," *The International Journal of Robotics Research*, **9**(2), pp. 62-82.
[67] Kuo, A. D., 1999, "Stabilization of lateral motion in passive dynamic walking," *The International Journal of Robotics Research*, **18**(9), pp. 917-930.
[68] Bauby, C. E., and Kuo, A. D., 2000, "Active control of lateral balance in human walking," *Journal of Biomechanics*, **33**(11), pp. 1433-1440.
[69] Donelan, J. M., Shipman, D. W., Kram, R., and Kuo, A. D., 2004, "Mechanical and metabolic requirements for active lateral stabilization in human walking," *Journal of Biomechanics*, **37**(6), pp. 827-835.
[70] Maki, B. E., 1997, "Gait changes in older adults: Predictors of falls or indicators of fear?," *Journal of the American Geriatrics Society*, **45**(3), pp. 313-320.
[71] Hausdorff, J. M., Edelberg, H. K., Mitchell, S. L., Goldberger, A. L., and Wei, J. Y., 1997, "Increased gait unsteadiness in community-dwelling elderly fallers," *Archives of Physical Medicine and Rehabilitation*, **78**(3), pp. 278-283.
[72] Hausdorff, J. M., Rios, D. A., and Edelberg, H. K., 2001, "Gait variability and fall risk in community-living older adults: A 1-year prospective study," *Archives of Physical Medicine and Rehabilitation*, **82**(8), pp. 1050-1056.
[73] Chang, C.-L., and Ulrich, B. D., 2008, "Lateral stabilization improves walking in people with myelomeningocele," *Journal of Biomechanics*, **41**(6), pp. 1317-1323.
[74] Domingo, A., and Ferris, D. P., 2009, "Effects of physical guidance on short-term learning of walking on a narrow beam," *Gait and Posture*, **30**(4), pp. 464-468.
[75] Domingo, A., and Ferris, D., 2010, "The effects of error augmentation on learning to walk on a narrow balance beam," *Experimental Brain Research*, **206**(4), pp. 359-370.
[76] Hof, A. L., Gazendam, M. G. J., and Sinke, W. E., 2005, "The condition for dynamic stability," *Journal of Biomechanics*, **38**(1), pp. 1-8.
[77] Pai, Y.-C., and Patton, J., 1997, "Center of mass velocity-position predictions for balance control," *Journal of Biomechanics*, **30**(4), pp. 347-354.
[78] Lugade, V., Lin, V., and Chou, L.-S., 2011, "Center of mass and base of support interaction during gait," *Gait and Posture*, **33**(3), pp. 406-411.
[79] Cossalter, V., Doria, A., and Lot, R., 1999, "Steady turning of two-wheeled vehicles," *Vehicle System Dynamics*, **31**(3), pp. 157-182.

[80] Winter, D. A., Prince, F., Frank, J. S., Powell, C., and Zabjek, K. F., 1996, "Unified theory regarding a/p and m/l balance in quiet stance," *Journal of Neurophysiology*, **75**(6), pp. 2334-2343.

[81] Cain, S. M., and Perkins, N. C., 2010, "Comparison of a bicycle steady-state turning model to experimental data," *Bicycle and Motorcycle Dynamics 2010: Symposium on the Dynamics and Control of Single Track Vehicles*, A. L. Schwab, and J. P. Meijaard, eds., Delft, The Netherlands.

[82] Cain, S. M., and Perkins, N. C., 2012, "Comparison of experimental data to a model for bicycle steady-state turning," *Vehicle Syst. Dyn.*, **50**(8), pp. 1341-1364.

[83] Jackson, A. W., and Dragovan, M., 1998, "An experimental investigation of bicycle dynamics," unpublished work. Available at http://www2.bsn.de/Cycling/articles/dynamics.doc and http://www2.bsn.de/Cycling/articles/dynamics_fig.doc.

[84] Cheng, K. Y., Bothman, D., and Astrom, K. J., 2003, "Bicycle torque sensor experiment," University of California, Santa Barbara.

[85] King, K. W., 2008, "The design and application of wireless mems inertial measurement units for the measurement and analysis of golf swings," Ph.D. thesis, Mechanical Engineering, University of Michigan, Ann Arbor, MI.

[86] Basu-Mandal, P., Chatterjee, A., and Papadopoulos, J. M., 2007, "Hands-free circular motions of a benchmark bicycle," *Proceedings of the Royal Society A*, **463**(2084), pp. 1983-2003.

[87] Peterson, D. L., and Hubbard, M., 2009, "General steady turning of a benchmark bicycle model," *the ASME 2009 International Design Engineering Technical Conferences and 7th International Conference on Multibody Systems, Nonlinear Dynamics, and Control*, San Diego, USA.

[88] Franke, G., Suhr, W., and Riess, F., 1990, "An advanced model of bicycle dynamics," *European Journal of Physics*, **11**(2), pp. 116-121.

[89] Man, G. K., and Kane, T. R., 1979, "Steady turning of two-wheeled vehicles, sae paper 790187," *Dynamics of Wheeled Recreational Vehicles*, Detroit, MI, pp. 55-75.

[90] Fu, H., 1966, "Fundamental characteristics of single-track vehicles in steady turning," *Bulletin of the Japan Society of Mechanical Engineers*, **9**(34), pp. 284-293.

[91] Cossalter, V., 2006, *Motorcycle dynamics*, Lulu Press, Inc., Raleigh, North Carolina.

[92] Bortoluzzi, D., Doria, A., and Lot, R., 2000, "Experimental investigation and simulation of motorcycle turning performance," *3rd International Motorrad-konferenzen*, Monaco.

[93] Moore, J. K., Kooijman, J. D. G., and Schwab, A. L., 2009, "Rider motion identification during normal bicycling by means of principal component analysis," *MULTIBODY DYNAMICS 2009, ECCOMAS Thematic Conference*, K. Arczewski, J. Fraczek, and M. Wojtyra, eds., Warsaw, Poland.

[94] SAE, 2008, "Vehicle dynamics terminology," Document Number J670, SAE International.

[95] Pacejka, H. B., 2002, *Tyre and vehicle dynamics*, Butterworth-Heinemann, Oxford.

[96] Wong, J. Y., 1993, *Theory of ground vehicles*, J. Wiley, New York, N.Y.
[97] Gillespie, T. D., 1992, *Fundamentals of vehicle dynamics*, Society of Automotive Engineers, Warrendale, Pa.
[98] Bortoluzzi, D., Lot, R., and Ruffo, N., 2001, "Motorcycle steady turning: The significance of geometry and inertia," *FISITA 7th International Conference - The Role of Experimentation in the Automotive Product Development Process*, Firenze, Italy.
[99] Zellner, J. W., and Weir, D. H., 1978, "Development of handling test procedures for motorcycles," Technical Paper No. 780313, SAE.
[100] Patterson, W. B., and Leone, G. L., 2010, "The application of handling quanlities to bicycle design," *Bicycle and Motorcycle Dynamics 2010*, A. L. Schwab, and J. P. Meijaard, eds., Delft, The Netherlands.
[101] Watanabe, Y., and Segel, L., 1980, "Comparison of linear analysis with experiment for a single-track vehicle in a steady turn.," *International Motorcycle Safety Conference*, Washington, D.C.
[102] Brenière, Y., and Bril, B., 1998, "Development of postural control of gravity forces in children during the first 5 years of walking," *Experimental Brain Research*, **121**(3), pp. 255-262.
[103] Murnen, H., Niles, A., Sigworth, N., and Sperling, D., 2009, "System and method for providing gyroscopic stabilization to a two-wheeled vehicle." U.S. Patent 7597337 B2.
[104] Joules, R. G., 1999, "Method for teaching an individual to operate a bicycle." U.S. Patent 5887883.
[105] Lunteren, A. v., and Stassen, H. G., 1969, "Investigations of the characteristics of a human operator stabilising a bicycle model," *Symposium on Ergonomics in Machine Design*, Prague, pp. 349-369.
[106] Burt, T. L., Porretta, D. L., and Klein, R. E., 2007, "Use of adapted bicycles on the learning of conventional cycling by childern with mental retardation," *Educ. Train. Dev. Disab.*, **42**(3), pp. 364-379.
[107] Cain, S. M., Ulrich, D. A., and Perkins, N. C., 2012, "Using measured bicycle kinematics to quantify increased skill as a rider learns to ride a bicycle," *2012 ASME Dynamic Systems and Control Conference and 2012 Motion & Vibration Conference*, Fort Lauderdale, FL.
[108] McGinnis, R. S., and Perkins, N. C., 2012, "A highly miniaturized, wireless inertial measurement unit for characterizing the dynamics of pitched baseballs and softballs," *Sensors*, **12**(9), pp. 11933-11945.
[109] Wolfinger, R., Tobias, R., and Sall, J., 1994, "Computing gaussian likelihoods and their derivatives for general linear mixed models," *SIAM Journal on Scientific Computing*, **15**(6), pp. 1294-1310.
[110] Doyle, A. J. R., 1988, "The essential human contribution to bicycle riding," Training, human decision making and control, J. Patrick, and K. D. Duncan, eds., Elsevier Science Publishers B.V. (North-Holland), pp. 351-370.
[111] Jansiewicz, E., Goldberg, M., Newschaffer, C., Denckla, M., Landa, R., and Mostofsky, S., 2006, "Motor signs distinguish children with high functioning autism and asperger's syndrome from controls," *Journal of Autism and Developmental Disorders*, **36**(5), pp. 613-621.

[112] Latash, M. L., 1993, *Control of human movement*, Human Kinetics Publishers, Chicago, Ill.
[113] Winter, D. A., Patla, A. E., Prince, F., Ishac, M., and Gielo-Perczak, K., 1998, "Stiffness control of balance in quiet standing," *Journal of Neurophysiology*, **80**(3), pp. 1211-1221.
[114] Moore, J. K., Hubbard, M., Schwab, A. L., Kooijman, J. D. G., and Peterson, D. L., 2010, "Statistics of bicycle rider motion," *Procedia Engineering*, **2**(2), pp. 2937-2942.
[115] Cain, S. M., and Perkins, N. C., 2011, "Human stabilization of a bicycle on rollers," *35th Annual Meeting of the American Society of Biomechanics*, Long Beach, CA.
[116] Sturgis, S. A., 1897, "Bicycle training device." U.S. Patent 581835.
[117] Dressel, A., and Papadopoulos, J. M., 2012, "Comment on 'on the stability of a bicycle on rollers'," *European Journal of Physics*, **33**(4), p. L21.
[118] Schwab, A. L., Lange, P. D. L. d., and Moore, J. K., 2012, "Rider optimal control identification in bicycling," *ASME 2012 5th Annual Dynamic Systems and Control Conference joint with the JSME 2012 11th Motion and Vibration Conference*, Fort Lauderdale, Florida, USA.
[119] "Kreitler's guide to choosing rollers," Mountain Racing Products. Web. 11/6/2012. <http://www.mountainracingproducts.com/kreitler/kreitlers-guide-to-choosing-rollers-step-2/>.
[120] Zatsiorsky, V. M., and King, D. L., 1998, "An algorithm for determining gravity line location from posturographic recordings," *Journal of Biomechanics*, **31**(2), pp. 161-164.
[121] Zatsiorsky, V. M., and Duarte, M., 2000, "Rambling and trembling in quiet standing," *Motor control*, **4**(2), pp. 185-200.
[122] Lafond, D., Duarte, M., and Prince, F., 2004, "Comparison of three methods to estimate the center of mass during balance assessment," *Journal of Biomechanics*, **37**(9), pp. 1421-1426.
[123] Lenzi, D., Cappello, A., and Chiari, L., 2003, "Influence of body segment parameters and modeling assumptions on the estimate of center of mass trajectory," *Journal of Biomechanics*, **36**(9), pp. 1335-1341.
[124] Morasso, P. G., Spada, G., and Capra, R., 1999, "Computing the com from the cop in postural sway movements," *Human Movement Science*, **18**(6), pp. 759-767.
[125] Zok, M., Mazzà, C., and Della Croce, U., 2004, "Total body centre of mass displacement estimated using ground reactions during transitory motor tasks: Application to step ascent," *Medical Engineering & Physics*, **26**(9), pp. 791-798.
[126] Shimba, T., 1984, "An estimation of center of gravity from force platform data," *Journal of Biomechanics*, **17**(1), pp. 53-60.
[127] Hof, A. L., 2005, "Comparison of three methods to estimate the center of mass during balance assessment," *Journal of Biomechanics*, **38**(10), pp. 2134-2135.

[128] Dempster, W. T., 1955, "Space requirements of the seated operator: Geometrical, kinematic, and mechanical aspects of the body with special reference to the limbs," WADC Technical Report 55-159, Wright Air Development Center, Air Research and Development Command, United States Air Force, Wright-Patterson Air Force Base, Ohio.

[129] Hasan, S. S., Robin, D. W., Szurkus, D. C., Ashmead, D. H., Peterson, S. W., and Shiavi, R. G., 1996, "Simultaneous measurement of body center of pressure and center of gravity during upright stance. Part i: Methods," *Gait and Posture*, **4**(1), pp. 1-10.

[130] Moore, J. K., 2012, "Human control of a bicycle," Ph.D. thesis, Mechanical and Aerospace Engineering, University of California Davis, Davis.

[131] Patricia, A. C., and Pirooz, M., 2011, "On the stability of a bicycle on rollers," *European Journal of Physics*, **32**(5), p. 1293.

[132] Patricia, A. C., and Pirooz, M., 2012, "Reply to 'comment on "on the stability of a bicycle on rollers"'," *European Journal of Physics*, **33**(4), p. L25.

[133] Moore, J. K., Hubbard, M., Schwab, A. L., and Kooijman, J. D. G., 2010, "Accurate measurement of bicycle parameters," *Bicycle and Motorcycle Dynamics*, A. L. Schwab, and J. P. Meijaard, eds., Delft, The Netherlands.

[134] Kooijman, J. D. G., 2006, "Experimental validation of a model for the motion of an uncontrolled bicycle," MSc thesis, Delft University of Technology, Delft, The Netherlands.

[135] Moore, J. K., Hubbard, M., Kooijman, J. D. G., and Schwab, A. L., 2009, "A method for estimating physical properties of a combined bicycle and rider," *ASME 2009 International Design Engineering Technical Conference & Computers and Information in Engineering Conference*, San Diego, California, USA.

[136] Clauser, C. E., McConville, J. T., and Young, J. W., 1969, "Weight, volume, and center of mass of segments of the human body," Aerospace Medical Research Laboratory, Aerospace Medical Division, Air Force Systems Command, Wright-Patterson Air Force Base, Ohio.

[137] Eston, R. G., and Reilly, T., 2009, *Kinanthropometry and exercise physiology laboratory manual: Tests, procedures and data*, Routledge, Abingdon, Oxon, New York.